UNIVERSITEIT VAN PRETORIA
UNIVERSITY OF PRETORIA
YUNIBESITHI YA PRETORIA

Structural geological controls on the flow and occurrence of groundwater in the basement lithologies of the Limpopo Province, South Africa

By

KONSTANT JOHANNES PETZER

Submitted in partial fulfilment of the requirements for the degree

MSc. Geology

in the Faculty of Natural and Agricultural Sciences,
University of Pretoria

PRETORIA

June 2009

UNIVERSITEIT VAN PRETORIA
UNIVERSITY OF PRETORIA
YUNIBESITHI YA PRETORIA

Structural geological controls on the flow and occurrence of groundwater in the basement lithologies of the Limpopo Province, South Africa

By Konstant Johannes Petzer

Supervisor: Dr. Adam J. Bumby

Co-supervisor: Dr. K. T. Witthüser

Department: Geology

University: University of Pretoria

Degree: M.Sc. Geology

ABSTRACT

The work for this thesis was conducted on the basement lithologies of the Limpopo Province in South Africa. An investigation into the correlation between structural geology and the flow/occurrence of groundwater was conducted on these lithologies. Field measurements of geological structures were recorded and compared graphically and statistically to existing groundwater borehole data. Data analysis revealed that the structural geology in the basement lithologies of the Limpopo Province of South-Africa does not have a clearly identifiable influence in terms of spatial patterns in groundwater flow and occurrence at a regional scale. Groundwater targets created through weathering rather than tectonics were evidently more easily recognized. Structural controls on groundwater in the granitic aquifers from this specific area are not totally negligible, although it is believed that such influences will be better identified through intensive local scale investigations. As drilling for groundwater is an expensive practice, the knowledge gained through this study and the possibility of a correlation between groundwater flow/occurrence compared to structural geology might improve the odds of finding groundwater for the communities and farmers in the area.

UNIVERSITEIT VAN PRETORIA
UNIVERSITY OF PRETORIA
YUNIBESITHI YA PRETORIA

Die struktuurgeologiese kontrole op die vloei en voorkoms van grondwater in die vloergesteentes van die Limpopo Provinsie, Suid-Afrika

Deur Konstant Johannes Petzer

Studieleier/mentor: Dr. Adam J. Bumby

Sub-mentor: Dr. K. T. Witthüser

Departement: Geology

Universiteit: Universiteit van Pretoria

Graad: M.Sc. Geologie

OPSOMMING

Hierdie tesis se veldwerk was uitgevoer op die vloergesteentes van die Limpopo Provinsie in Suid-Afrika. ‘n Ondersoek rakende die verwantskap tussen struktuurgeologie en die vloei/voorkoms van grondwater was geloods op die bogenoemde litologieë. Veldopnames en meetings van geologiese strukture was grafies en statisties vergelyk met grondwaterdata van bestaande boorgate. Data-analise het bewys dat die struktuurgeologie van die vloergesteentes in die Limpopo Provinsie van Suid-Afrika nie ‘n duidelik-identifiseerbare invloed i.t.v. geografiese verspreidingspatrone van grondwater op ‘n streekskaal het nie. Potensiële grondwaterteikens wat deur verwering veroorsaak is was makliker identifiseerbaar uit die ingesamelde data. Nietemin kan die invloed van geologiese strukture op die grondwater in die granitiese waterdraers van die area nie geïgnoreer word nie, alhoewel daar geglo word dat sulke verwantskappe beter geïdentifiseer kan word deur intensiewe kleinskaalse ondersoeke. Aangesien boorkostes vir grondwatereksplorasie uiters hoog is, kan die kennis wat uit hierdie studie opgedoen is, asook die moontlike korrellasie tussen die vloei/voorkoms van grondwater en struktuurgeologie die kanse op suksesvolle boorgate in die toekoms verbeter vir die boere en gemeenskappe van die area om sodoende minder geld te vermors op die boor van droë gate.

I hereby declare that this thesis is my own unaided work except where referenced otherwise. It is being submitted for the degree M.Sc. Geology at the University of Pretoria, Pretoria. It has not been submitted before for any degree or examination in any other University.

_____ Signature of author

Date _____

ACKNOWLEDGEMENTS

Eerstens wil ek dankie se vir my Hemelse Vader vir die voorreg wat ek gehad het om hierdie studie te doen. Ek het pragtige dele van Sy skepping gesien en Hy het my soos Dawid in die veld beskerm tydens my avonture. God is immers die skepper van grondwater wat by Horeb vir Moses en die volk water uit 'n klip laat vloei het (Eks. 17:5-7). Verder gee Hy ook vir ons Sy lewende water (Joh. 4:13-14).

Thank you very much Adam for your guidance and friendship throughout this study. It was a real honour to work with you.

Baie dankie vir almal by die Tukkies se Geologiedepartement, veral aan Theo vir die lekker ekskursies en grappies wat ons deur al die werk gekry het! Aan my familie en vriende, baie dankie vir julle ondersteuning deur my hele lewe, maar veral tydens my M.Sc. Laaste maar nie die minste nie wil ek dankie sê vir my meisie, Carina. Dankie vir jou hardwerkende voorbeeld en jou bemoediging tydens my projek. Ek is baie lief vir julle almal!

TABLE OF CONTENTS

Page

LIST OF FIGURES

Page

LIST OF TABLES

Page

1. INTRODUCTION:

1.1 Study area background:

This thesis focuses on the structural geological controls of groundwater in a portion of the Limpopo Province of South Africa which falls within the north-eastern section of the Kaapvaal Craton and is underlain almost entirely by Archaean-aged basement lithologies (granite, gneiss and greenstone). More specifically, the study area roughly forms a 100km x 200km rectangle which is bordered to the south by the Thabazimbi-Murchison Lineament (TML). In the east, basement lithologies are bounded by the Drakensberg Group volcanic rocks (Karoo Supergroup) of the Lebombo Mountains associated with the eastern margin of the Kaapvaal craton. The northern margin is bound by the Palala Shear Zone and Central Zone of the Limpopo Belt and the western margin is delineated by intrusive rocks of the northern lobe (Potgietersrus Limb) of the Bushveld Igneous Complex (refer to Figure 1).

The north-eastern section of the Kaapvaal Craton mainly consists of Palaeo-, Meso- and Neoarchaean intrusions with later supracrustal rocks covering some of the edges of the study area. Due to its old age, this part of the continent has existed long enough to experience numerous geological events which, when combined, results in a complex structural character of the geology in the area. Semi-arid regions of the Limpopo Water Management Area (WMA1) characterize the eastern section of the study area; whereas subtropical conditions with higher rainfall are found west of the northern escarpment in the Levuvu/Letaba Water Management Area (WMA2) (refer to Figure 2).

According to the national census of 2001, the Limpopo Province is home to about 11.8% of South Africa's total population (refer to Figure 3). The national census of 1996 states that 89% of Limpopo's inhabitants live in non-urban areas and many of those people make a living through subsistence farming. Apart from subsistence farming, a large part of the Limpopo Province's income comes from agriculture. Citrus, tomatoes, table grapes, sunflowers, maize, cotton, peanuts, bananas, litchis, pineapples, mangoes, paw paws, tea and coffee are grown on a commercial basis (GCIS 2004). Furthermore, cattle farming, game ranching and game hunting also contribute to the commercial agricultural activities of the province (GCIS 2004). Evidently a lot of water is necessary to run all of the agricultural activities in the area. 78% of the households in the Limpopo Province have piped water, but often only from a communal tap (SSA 2003). The need for irrigation and household water has placed a greater demand on groundwater resources and further groundwater exploration is required in this area.

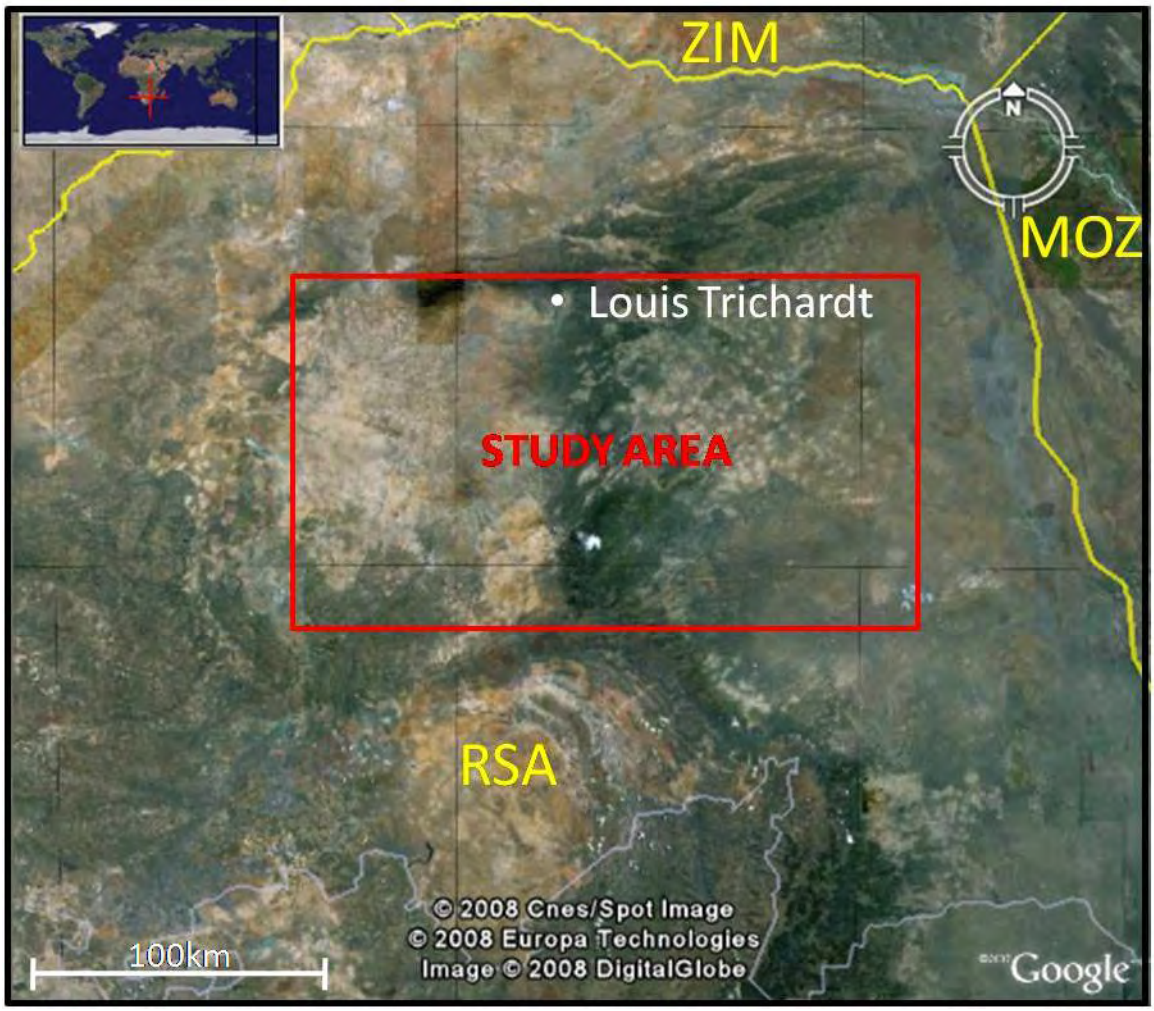

Figure 1: A Google Earth© image indicating the location of this project's study area.

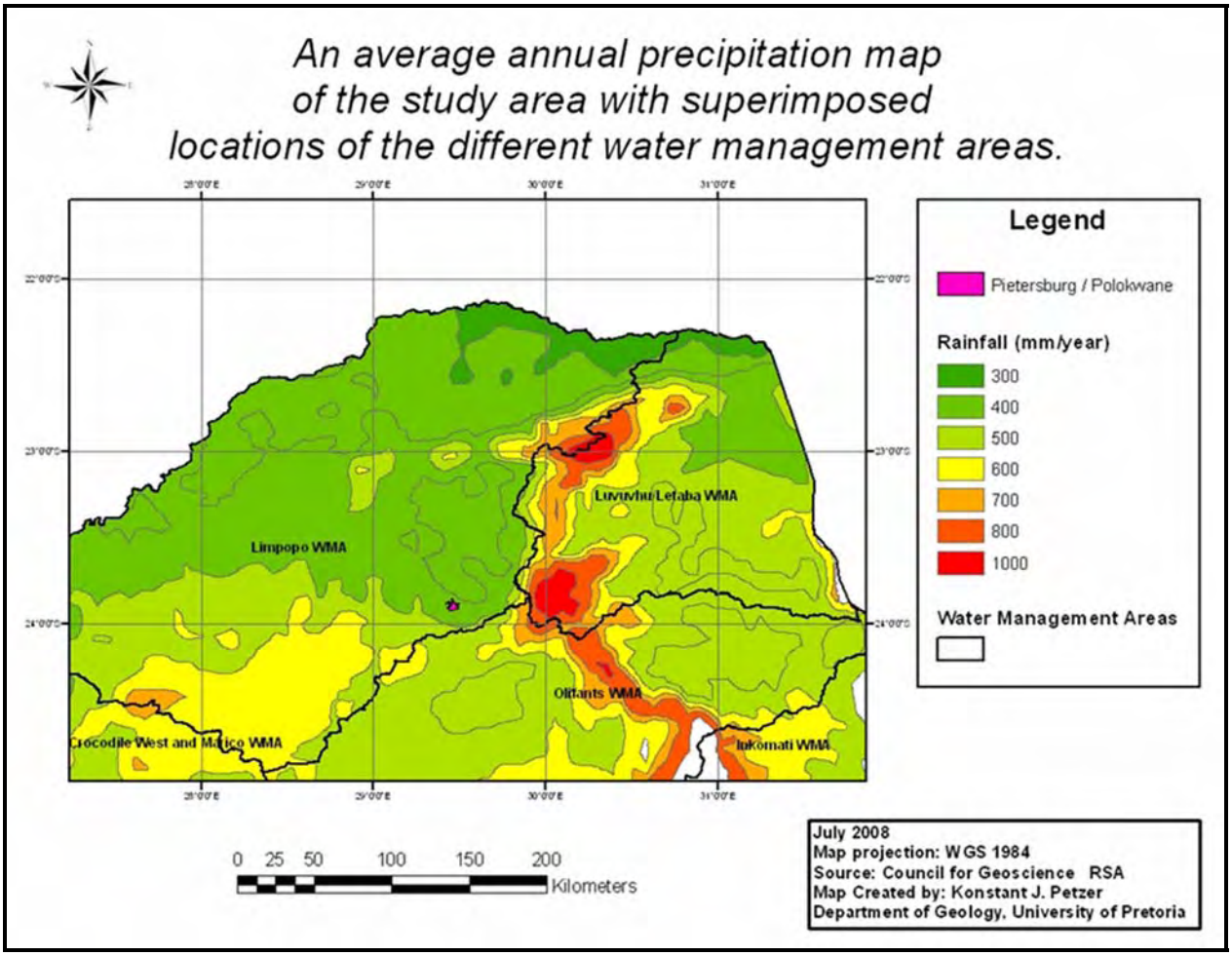

Figure 2: An average annual precipitation map of the study area, which falls within the Limpopo- (WMA1) and Levuvu/Letaba- (WMA2) water management areas.

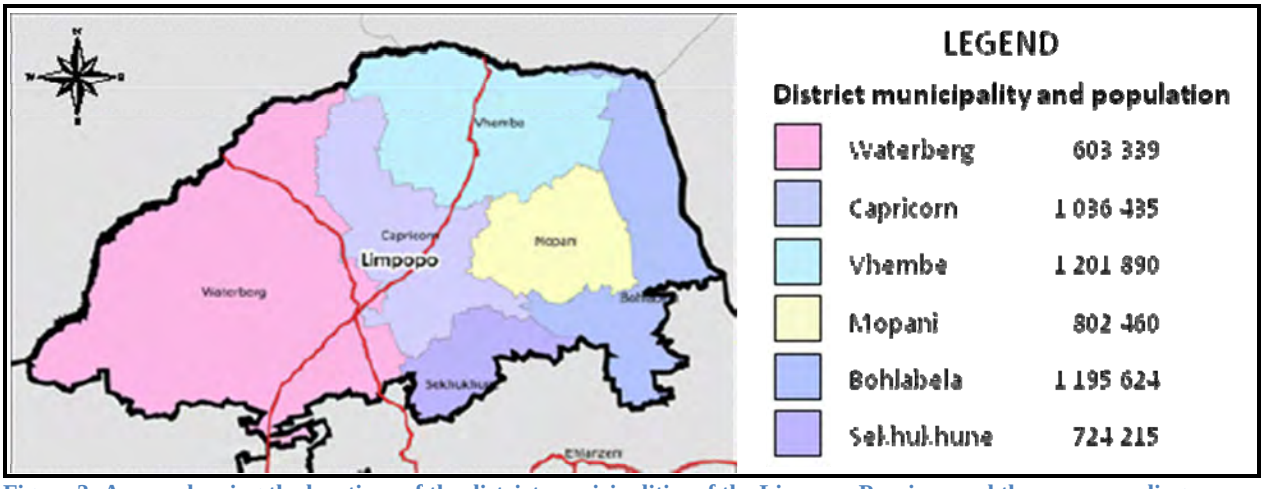

Figure 3: A map showing the locations of the district municipalities of the Limpopo Province and the corresponding population of each. Source: The South African Demarcation Board and Statistics South Africa, 2000.

1.2 Problem statement:

An investigation into the correlation between structural geology and the flow/occurrence of groundwater in the basement lithologies of the Limpopo Province in South Africa.

1.3 Objectives:

Primarily, this investigation aims to examine the structural geology of the Limpopo basement lithologies. Once the structural interpretations have been made, the investigated structures will be compared to the groundwater data in order to determine whether or not there exists a spatial correlation between the structural elements and the flow or presence of groundwater in different parts of the basement aquifers. Since drilling for groundwater is an expensive practice, the knowledge gained through this study and the possible correlation between groundwater flow/occurrence compared to structural geology, might improve the odds of finding groundwater and save a lot of money. Moreover, the discovery of groundwater could improve the living conditions of some of the inhabitants of the Limpopo Province and help to boost the province's economic growth through enhanced productivity of commercial agriculture.

1.4 Scope and limitations of the study:

Although the study area is extremely large (~ 20 000km^2), the extent of outcrops are remarkably limited in some of the regions due to weathering and soil cover. This makes it difficult to trace structures from one area to the next with a lack of intervening outcrop. The sheer size of the study area limits the amount of detail with which the total area could be mapped. Due to the long geological history and relatively small amount of outcrops, it is difficult to accurately recreate an exact geochronological timeline of the numerous events that took place by using relative age relationships only. Therefore, the focus of this study is more on understanding the orientation of structures presently in the rocks (as this is what influences the flow of groundwater) than it is on interpreting a detailed tectonic history. Nevertheless, where possible, geochronology was taken into consideration and related to isotopic and relative ages described in literature. However, literature on the structural geology of the basement lithologies is very limited. Lastly, the author had to rely heavily on interpolated data between existing boreholes instead of drilling precisely on structures recognized in the field.

1.5 Methodology:

Relevant literature was collected and studied in order to have a thorough understanding of the field area. As the study progressed and new ideas came to mind, more sources of literature were consulted. The information gathered from this stage of the project was compiled into the literature review found below (Chapter 2).

As in most exploration projects, remote sensing was used during the early stages of this project. Aerial photographs of one area in WMA1 and a N-S line through WMA2 were studied stereoscopically in order to gain a three-dimensional view of the topography and the regional structures in the area. Observed structures were then compared to structures described in the literature study and marked as targets for field investigation. For a more regional survey, satellite images from Google Earth were also viewed for a preliminary regional structural interpretation. Aeromagnetic data from the study area was also acquired from the Council for Geoscience of South Africa, which mainly indicated the presence of dolerite dykes and major faults.

A number of field excursions were undertaken to cover the study area as thoroughly as possible with available time, finances and access to property all playing a constraining role. Large areas without measurable outcrops, as well as areas with structureless outcrops (usually post tectonic) were also unfortunately encountered. At each location with measurable structures, a waypoint was marked with a GPS. A compass-clinometer was then used to measure dips and strikes of planes (mostly joint planes, but also fault planes, foliation planes, fold axial planes, bedding planes and contacts). Trends and plunges of lineations such as the traces of veins, hinge lines, sense of fault/shear movements (including slickenside lineations), traces of dykes and the trend of rivers were also measured using the compass. All the measurements were initially recorded in a field notebook and were later transferred to a computer database. Sketches were drawn in the field notebook of some of the more interesting/involved structures to help solve the complex nature of the structural geology. Many scaled photographs were also taken of the structures found in the field to serve as visual aids during data interpretation. The emplacement sequences and relative age relationships of rocks and structures were recorded where possible, but as mentioned before, geochronology was not the main focus of this study.

The computer database was then analyzed further. Structural measurements from the database were stereographically projected, using Spheristat 2.2 software. Poles to planes were plotted and density distributions of these poles were also created in order to find

preferred orientations of structures. Coordinates from the GPS were plotted onto an ArcGIS geology base map of the study area. The orientations of the structures were then related to their GIS coordinates in order to identify the spatial relationships of the structures and to identify possible dominant orientations. Since brittle structures (such as joints) with different three-dimensional orientations don't all form under the same stress-strain conditions, such structures were subdivided into groups. Each group of structures was then analyzed based on its orientation, distribution and possible relationship to the lithologies in which it occurs.

A database containing groundwater data of most of the boreholes in the area was obtained from (Groundwater Resources Information Project "GRIP"). Each of the boreholes was also plotted on the GIS map. Special attention was paid to the transmissivity and yield values from each borehole. In simple terms, transmissivity is defined as the ability of an aquifer to transmit water. More specifically, transimissivity is the rate at which water of the prevailing kinematic viscosity is transmitted through a unit width (i.e. 1 meter) of an aquifer under a unit *hydraulic gradient.* Transmissivity is equal to an integration of the hydraulic conductivities across the saturated part of an aquifer, perpendicular to the flow paths and is measured in cubic meters per day (Horton, 1999).

$$T = Kb$$

Where T = Transmissivity, K = Hydraulic Conductivity and b = the saturated thickness of the aquifer.

Yield is defined as the quantity of water from a groundwater source, expressed as a rate of flow (m^3/s) in this case, that can be collected for a given use (adapted from Willmitzer, 2008). Transmissivity- and yield values of the boreholes were spatially interpolated through inverse distance weighting (see appendix for explanation) to see if any spatial patterns or trends could be identified. Although the interpolated maps still appear quite random, better correlation between inverse distance weighted interpolations and geological features were observed than when other geostatistical methods such as kriging were used. The spatial trends in water occurrence and flow were then related to the lithologies and geological structures at the boreholes' locations to determine whether or not any correlations exist.

2. LITERATURE REVIEW:

2.1. Regional Geology:

2.1.1. General:

Although Archaean crystalline basement rocks characterize the study area, other lithologies which outcrop locally and in adjacent areas will also be considered in this thesis, as many of the post-Archaean geological structures are not limited to the basement rocks alone, and often cross-cut younger strata preserved nonconformably above the basement rocks. Since the supracrustals have undergone less weathering and erosion than their basement predecessors, tectonic events that occurred during or after supracrustal formation are often better preserved in these younger rocks.

Unfortunately the extremely large area covered by the basement rocks alone influenced the author to only include previous supracrustal data found in existing literature. One of the main aims of this study is to identify structures in the basement rocks that could influence the occurrence and movement of groundwater. Below is a geological map of the area and a timeline of emplacement events to familiarise the reader with the area.

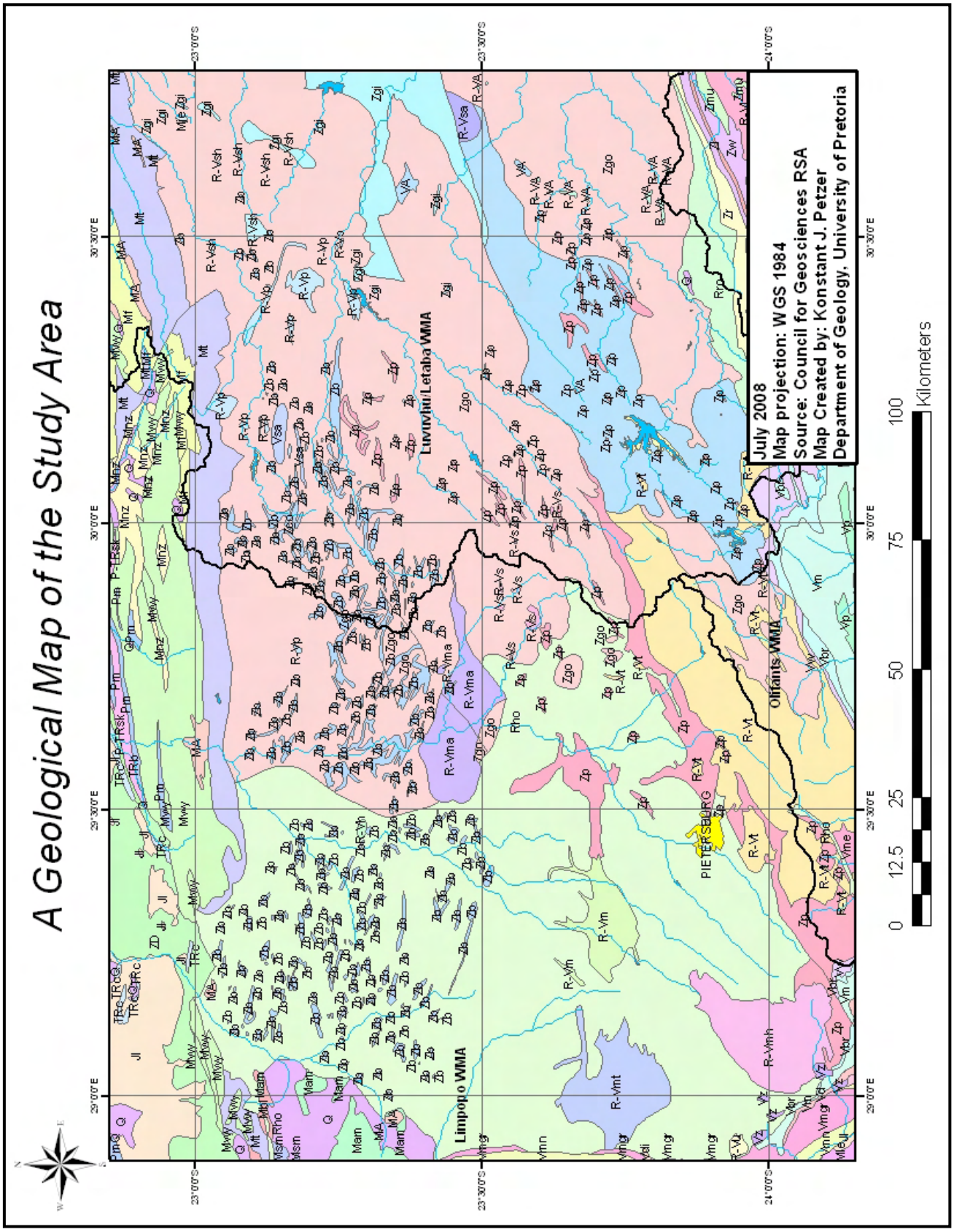

Figure 4: A Geological Map of the Study Area. Refer to legend on next page.

Stratigraphic Units and Legend for Geology Map

Table 1: Geological timeline of igneous/metamorphic lithological emplacements/events (Modified after Robb et al., 2006)

Unit/locality	Sample nature	Age in Ma. (method if available)	Ref.
Goudplaats-Hout River Gneiss	Migmatitic tonalite gneiss	3333 ± 5 (C)	1
Goudplaats-Hout River Gneiss	Tonalite gneiss	3282.6 ± 0.4 (C)	2
Goudplaats-Hout River Gneiss	Tonalite gneiss	3274 +56/-45 (A)	2
Makhutswi Gneiss	Trondhjemite and Tonalite gneiss	3228 ± 12 (A)	3
Giyani Greenstone Belt	?	3202.3 ± 2 (?)	10
Central KV Craton stable	----------	3100	10
Harmony Granite	Trondhjemite gneiss	3091 ± 5 (A)	4
Murchison Greenstone Belt	----------	3090 - 2970	3, 11
Makhutswi Gneiss	Tonalite gneiss	3063 ± 12 (A)	4
Baderoukwe Gneiss	Trondhjemite gneiss	3018 ± 15 (A)	5
Discovery Granite	Granite	2969 ± (A)	5
Gneisses in the Matlala and Moletsi vicinity	Migmatitic and non-migmatitic biotite gneisses	2940-2870 (C)	Unp ubl.
Melkboomfontein Granite	Granite	2853 +19/-18 (A)	2
Gravelotte area	Pegmatite	2848 ± 58 (A)	4
Willie Granite	Porphyritic granite	2820 ±38 (A)	5
Cunning Moor Tonalite	Massive, homogenous tonalite	2784 ± 53 (Rb-Sr whole rock)	12
Turfloop Granite	Porphyritic granodiorite	2777 ± 10 (A)	6
Turfloop Granite	Monzogranite	2765 ± (A)	2
Turfloop Granite	Porthyritic granodiorite	2763 ± 15 (A(T))	6
Rooiwater Complex	Hornblende tonalite	2740 ± 4 (A)	3
Dolerite dykes (Ventersdorp related)	Dolerite	2.7 Ga.	13
Limpopo orogeny	Bulai Gneiss	2.57 – 2.66 Ga. Minimum age	14
Mashishimale Suite	Peraluminous granite	2698 ±21(A)	5
Lekkersmaak Granite	Porphyritic granite	2690 ± 65 (A)	7
Uitloop Granite	Granite	2687 ± 2 (A)	8
Matok Granite	Charno-enderbite	2671 ± (C(?))	9
Palmietfontein Granite	Granite	2456 ± 78 (Rb-Sr whole rock)	13
Reactivation of Palala	------	2.0 Ga.	15

Unit/locality	Sample nature	Age in Ma. (method if available)	Ref.
Bushveld Igneous Complex	-------	2.06 Ga.	
Blouberg Fm.	Alluvial sandstones	2.0 – 1.9 Ga.	
Waterberg Gp.	Sedimentary	>1.85 Ga.	
Soutpansberg Gp.	sst	1.85 Ga.	
Extrusion of Drakenberg Flood Basalts	Basalt	180 Ma.	

Methods: **A = U-Pb ID-TIMS; C = Pb-Pb zircon evaporation; (T) = Titanite. Mineral analyse zircon, unless otherwise mentioned.**
References: **1. Brandl and Kröner (1993); 2. Kröner et al. (2000); 3 Poujol et al. (1996); 4. Poujol and Robb (1999); 5 Poujol (2001); 6. Henderson et al. (2000); 7. Walraven (1989); 8. De Wit et al (1993); 9. Barton et al. (1992); 10. Kröner et al. (2000); 11. Brandl et al. (1996); 12. Robb et al. (2006), 13. Uken & Watkeys (1997); 14. McCourt & Armstrong, (1998); 15. Bumby et al. (2004).**

2.1.2. Kaapvaal Craton:

The Kaapvaal Craton formed and stabilized between 3.7 - 2.7 Ga. and covers about 1.2 $x10^6$ km^2 (de Wit et al., 1992). Growth of the craton during this time was achieved by processes of initial separation of continental lithosphere from the mantle, followed by tectonic accretion of crustal fragments to form the various granite-greenstone subdomains (de Wit et al., 1992). The oldest Kaapvaal rocks are preserved in the Barberton area, in the eastern domain of the craton. Growth of the Kaapvaal Craton likely took place by accretion onto its northern edge, as recorded by a series of ENE-trending subdomains, and on the western edge of the craton (NNW-trending subdomains).

The northern domain (ca. 3.25 – 2.7 Ga.) of the Kaapvaal Craton (the focus of this study) is thus younger than the eastern domain (ca. 3.6 – 3.1 Ga.) (Poujol et al., 2003). Accretion along the northern edge of the growing Craton most likely caused deformational structures within the basement lithologies that could subsequently influence groundwater movement. Furthermore, the northern domain of the Kaapvaal Craton also experienced magmatic activity during early Neoarchaean times, including the emplacement of largely post-tectonic granitoids in the Pietersburg and Murchison areas (Poujol et al., 2003). The following sections consider the various Archaean subdomains within the study area, and then consider some of the supracrustal successions which are preserved above these basement rocks, and which border the study area.

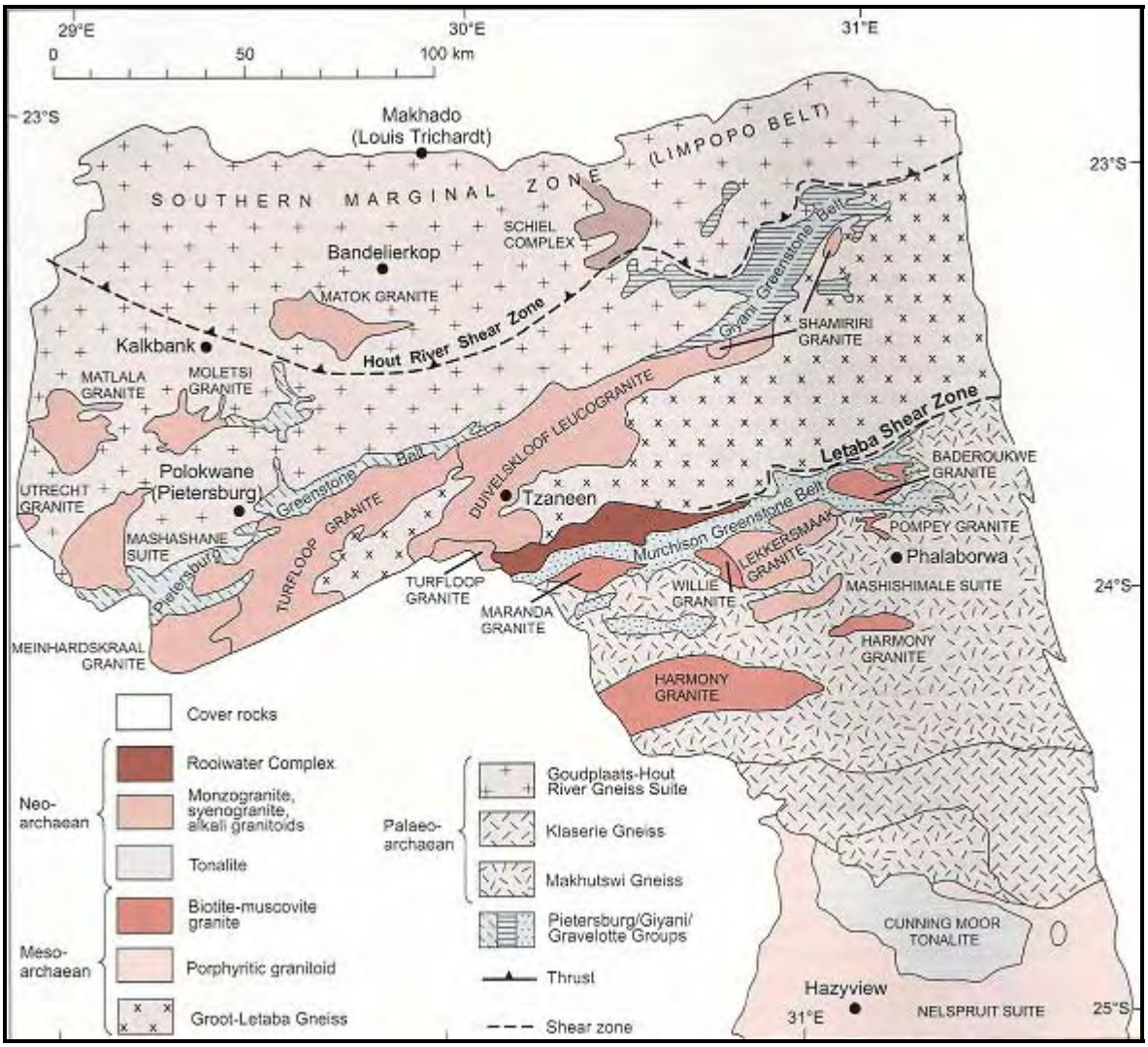

Figure 5: Map of the northern and north-eastern sectors of the Kaapvaal Craton and their different granitoid occurrences (from Robb, et al., 2006)

2.1.3. Paleoarchaean Intrusions (3600 – 3200 Ma) and the Pietersburg- and Giyani Greenstone Belts:

The Pietersburg and Giyani Granite-Greenstone Belts extend parallel to, and to the south of the Southern Marginal Zone (SMZ) of the Limpopo Belt and are separated by a 60km wide zone of intensely migmatised rock. Anhaeusser (1992) suggests that these two belts are actually parts of the same Granite-Greenstone Belt, with their tectono-thermally reworked equivalents and associated granitoids between them. Kröner et al. (2000) on the other hand, regard the Giyani and Pietersburg Granite-Greenstone Belts as two separate crustal units, which were originally in close proximity to one another, but were later displaced by strike-slip movement.

The NE-trending Pietersburg Greenstone Belt (PGSB) is made up of two well-defined tectonostratigraphic units that are separated by an unconformity (De Wit et al., 1992). Locally, evidence for northwest-verging thrust movement between these two units has also been found. The lower unit is a typical greenstone sequence with a Pb/Pb age of 2.4 Ga. (Barton, 1990), whereas the upper unit, called the Uitkyk Formation, is an arenaceous to rudaceous unit that can be correlated with the Central Rand Group of the Witwatersrand Basin (de Wit et al., 1992). Terrain accretion along the northern margin of the Mid-Archaean protocraton resulted in northward-verging thrusts along the PGSB (de Wit et al., 1993). The 3203,3 Ma ± 2,0 Ma Giyani Greenstone Belt also trends NE, and is surrounded by pre-3200Ma polydeformed gneisses (Kröner et al., 2000).

Apart from the greenstone belts, the northeastern section of the Kaapvaal Craton (North of 25°S) consists of various other Archaean subdomains. Of importance to the present study are the Paleoarchaean intrusions (3600 – 3200 Ma) that underlie a large part of the study area. Dominating the northern half of the study area is the Goudplaats-Hout River Gneiss Suite (GHGS). A wide variety of granitoid gneisses varying in type and composition belong to this suite which is found both north and south of the Hout River Shear Zone. Most of the phases of the GHGS have emplacement ages of around 2900Ma and seem to have been generated by dehydration melting of amphibolites and biotite gneiss protoliths (Robb et al., 2006).

Throughout this major magmatic period, various gneiss precursors extensively pervaded an older granitoid crust, of which only minor leftovers in the form of *c.*3300 Ma dark grey gneisses remain today. This crustal material also yields an age older than its neighbouring greenstone belts, which suggests that it served as a basement for the greenstone belts or represents a separate crustal block adjacent to the greenstones. Two main types of gneiss are found in the Lowveld, South of the Murchison Greenstone Belt (MGSB). Firstly, the layered composite Makhutswi Gneiss extends for 60km south of the MGSB and also south of the Klaserie Gneiss. Karoo and Transvaal sediments cover the Makhutswi Gneiss in the east and west respectively. The Makhutswi Gneiss is complexly folded, and in some areas intruded by a younger, unmigmatised biotite gneiss of tonalitic composition. These younger local intrusions are Mesoarchaean in age. At the northern boundaries of the Cunning Moor Tonalite and the Nelspruit suite lies a 30km wide E-W stretching strip of “homogeneous” gneiss called the Klaserie Gneiss. Mineralogically, the Klaserie gneiss is similar to the Makhutswi Gneiss, but appears to be relatively younger than the latter. Furthermore, the Klaserie Gneiss is well foliated.

2.1.4. Mesoarchaean Intrusions (3200 – 2800 Ma) and the Murchison Greenstone Belt (MGSB):

The Murchison Greenstone Belt exists along a major ENE-WSW crustal lineament that can be traced all the way to Thabazimbi, known as the Thabazimbi-Murchison Lineament (TML). This is a 400km+ long, poly-deformational zone with a width of about 25km (Vearncombe et al., 1991). The TML was an important control on the spatial deposition or emplacement of later successions such as the Wolkberg Group, Transvaal Supergroup, the Bushveld Igneous Complex and the Waterberg Group. Because of the sub-parallel orientation of the TML and the Limpopo Belt, one expects a number of geological structures in the study area to be parallel to this ENE-WSW trend. Vearncombe et al. (1992) interpreted the MGSB as the deformed remnants of five distinct domains that have been tectonically juxtaposed. Two of these domains were Archaean island arcs which obducted onto the proto-Kaapvaal Craton (Vearncombe et al. 1991). The MGSB is bounded by granitic gneisses, migmatites and pegmatites (discussed below). Dating of the MGSB revealed an age of 3090-2970 Ma. (Brandl et al., 1996; Poujol et al., 1996).

The oldest magmatic event in the vicinity of the MGSB led to the formation of a batholith-shaped intrusion called the Harmony Granite. This poorly exposed intrusion is mainly made up of light-grey, coarse-grained granite with a locally developed porphyritic variety (Poujol and Robb, 1999). On the eastern side of the MGSB lies the Baderoukwe Granite. Although various phases exist within the Baderoukwe Granite, its main phase has a granodioritic character and is slightly peraluminous. Both the Baderoukwe- and the Willie Granites show signs of strong marginal deformation orientated parallel to the MGSB contact, which might indicate a late solid-state rise of granite juxtaposed against the denser greenstone lithologies (Annaeusser, 1992). It is believed that granite magmatism was associated with volcanism at about 2970 Ma., since the Discovery Granite on the southern edge of the MGSB yielded an age of 2969 ± 14 (Poujol, 2001). Another relatively small Mesoarchaean intrusion adjacent to the southern edge of the MGSB is the Willie Granite. This medium-grained granite is grey, with microcline megacrysts of 3cm and longer and formed at a time of major felsic magmatism on the Kaapvaal Craton between 2820 and 2880 Ma (Robb et al., 2006).

Groot Letaba Gneiss is a collective term, which refers to all the granitoid gneisses between the MGSB and the Pietersburg-Giyani greenstone belts (Brandl and Kröner, 1993). The Groot Letaba Gneiss includes a wide variety of closely fused gneisses including fine- to medium-grained tonalite, coarse-grained trondhjemite and minor banded and linear gneisses. The rocks have a massive appearance in some cases, but are well- to weakly-foliated and strongly folded for the most part, though the

orientation of folds is not mentioned in literature. Gneisses belonging to this unit are generally migmatised with leucosome bands belonging to distinct generations of magma. Small inclusions of mafic to ultramafic greenstone are found in some areas, implying the intrusive nature of the gneiss protolith with the greenstone belt. Various generations of gneisses are represented by the Groot Letaba Gneiss, one of which is the gneiss near Tzaneen and further west, which yielded Pb-Pb ages of *c.* 3100-3000 Ma (Robb et al., 2006). The Pietersburg Greenstone Belt is intruded by two strongly foliated granitoid bodies. Firstly, by the trondhjemitic Melkboomfontein Gneiss which represents one of the youngest, strongly foliated granitoids at *c.* 2853 Ma. and secondly by the tonalitic Mosokgome Gneiss (Kröner *et al*., 2000).

2.1.5. Neoarchaean Intrusions (2800 – 2500 Ma):

During Early Neoarchaean times magmatic activity caused largely post-tectonic granitoid emplacements in the Pietersburg and Murchison areas. Neoarchaean granites generally form prominent topographic features in the study area, relative to the older granitoid gneisses (Robb et al., 2006). The ages of these intrusions range from 2800 Ma (upper limit dated from regional deformation of surrounding rocks upon emplacement) and 2650 Ma (lower age limit of Transvaal Supergroup strata that overlie the intrusions) (Kröner *et al*., 2000).

Of the Neoarchaean intrusions associated with the Pietersburg and Giyani Greenstone Belts, the Turfloop Granite is the largest and best studied. The Turfloop Granite trends roughly NE-SW along the southern border of the PGSB and ranges in composition from granodioritic to monzogranitic, which might be an indication that it is composed of a number of smaller plutons (Henderson *et al.*, 2000; Kröner *et al*., 2000). The Meinhardskraal Granite has intruded to the southwestern side of the Turfloop Granite. Compositionally, the different phases of the Meinhardskraal Granite vary between monzogranites, syenogranites and alkali granites (with alkali feldspar megacrysts showing a strong north-easterly preferred orientation) (Robb et al., 2006).

At the south-western end of the PGSB the Mashashane Suite batholith intrudes the Goudplaats-Houtriver Gneiss Suite. The Mashashane suite consists of three distinct phases, called the Lunsklip, Uitloop and Uitvlugt Granites (Brandl, 1985, 1986, in press). All three of these phases contain blue opalescent quartz (De Villiers and Brandl, 1977). The Uitvlugt Granite is the oldest of these three intrusions, while the Lunsklip Granite is the dominant phase. Uitvlugt and Lunsklip Granites are both metaluminous, whereas the Uitloop Granite is slightly peraluminous (Robb et al., 2006). Due to the distribution of its three phases, the Mashashane Suite could represent a large sheet-like intrusion with a shallow southwesterly dip.

One of the few S-type Neoarchaean granites in the northern part of the Kaapvaal Craton is the Utrecht Granite. This tabular sheet that tilts gently to the west is a medium to fine-grained, pink, leucocratic rock with a local pink pegmatoidal variety. It is believed that the Utrecht Granite formed by partial melting of a largely pelitic protolith under granulite grade conditions (Robb et al., 2006).

North of the Mashashane Suite lies the Matlala Granite, an almost circular batholith composed of various phases (Brandl, 1986). The two most common phases include a fine-grained, pink granite and a medium-grained porphyritic, pink granite. A prominent off-shoot of the Matlala Granite, called the Chloe Dyke, possibly formed in a pre-existing zone of weakness in the country rock.

East of the Matlala Granite Lies a batholith of similar size called the Moletsi Granite, which is made up of three phases (Brandl, 1985, 1986, in press). In the core of the body, a coarse-grained pinkish to pinkish-grey rock occurs. Around the central phase is a younger, grey to pinkish grey, coarse-grained variety. Both of these phases contain rafts of the initial fine-grained, dark grey, tonalitic granite. Analogous to the Matlala Granite, the Moletsi granite also has prominent off-shoots trending in a northerly direction (Robb et al., 2006).

Just north of the Hout River Shear Zone (in the Southern Marginal Zone of the Limpopo Belt) the Matok Granite is located (Brandl, 1985, 1986). The Matok Granite is unique amongst granitic bodies in the northern part of the Kaapvaal Craton in that it contains a large charnockitic component (mainly found in the northern part of the Matok Granite). Several NE-trending shear zones run through the Matok Granite. The older charnockitic suite contains enderbite and charno-enderbite, whereas the younger granitic suite comprises up to eleven different phases (Barton et al., 1992; Bohlender, 1992). Roughly 20km northwest of the Matok Pluton is the Hugomond Granite. This relatively small granite from *c.* 2658 ± 2 Ma is coarse-grained grey biotite granite which is porphyritic in areas and cut by tourmaline-bearing pegmatite veins (Robb et al., 2006).

Two distinct intrusive stocks on the southern and eastern side of the Giyani Greenstone Belt are referred to as the Shamiri Granite (Vorster, 1979; Brandl, 1987). At both localities, the Shamiri Granite is a grey, medium-grained rock, which can grade into a coarse porphyritic phase with microcline megacrysts of up to 6cm. Since rotated rafts of Shamiri Granite are found within the Duiwelskloof Leucogranite, the former predates the latter. The Duiwelskloof Leucogranite is a large, northeast-trending, elongate intrusion that stretches from the southeastern boundary of the Giyani Greenstone Belt to the Turfloop Granite. The northern boundary of the Duiwelskloof Leucogranite is

fairly linear (same orientation as the two adjacent greenstone belts) and may exploit a tectonic lineation. Dehydration melting of a pelitic source at a relatively shallow crustal level is believed to have been the method of formation of this peraluminous S-type granite (Robb et al., 2006).

Small plutons and dykes of the Palmietfontein Granite probably represent the youngest granitic rocks north of the Pietersburg Greenstone Belt in South Africa, with a Rb-Sr whole rock age of 2456 ± 78 Ma (reported by Barton *et al.*, 1983). Palmietfontein Granites are unfoliated and mainly fine- to medium-grained pinkish grey granodiorites.

There are a number of Neoarchaean granitoids south of the Murchison Greenstone Belt. First of all, the Vorster Suite is emplaced along the southern Boundary of the MGSB in an area where many ovoid granite bodies form an intricate pattern with intervening greenstone nodules (Brandl, 1987; Walraven, 1989; Vearncombe *et al.*, 1992). Originally, the suite was defined as comprising the following four phases: Lekkersmaak-, Willie-, Pompey- and Baderoukwe Granites. Of these four granites, the Lekkersmaak Granite has the largest aerial extent. The Lekkersmaak granite is a grey, medium-grained rock, which becomes coarser towards its centre and also contains common porphyritic types. Recently, the Willie Granite yielded a Mesoarchaean age older than 2800 Ma (Poujol and Robb, 1999; Poujol, 2001) and is therefore no longer considered a part of the Vorster Suite magmatic event. Contacts between the Willie- and Lekkersmaak Granites that outcrop are sheared and therefore relative age relationships are hard to determine. Several small stock-like bodies away from the main batholith make up the Pompey Granite. This medium-grained granite varies from light grey to pink and can be classified as a syenogranitic rock.

Slightly south of the Vorster Suite a narrow northeast-trending intrusion called the Mashimale Suite occurs (Brandl, 1987; Walraven, 1989; Vearncombe *et al*., 1992). The Hoed-, Lillie- and Transport Granites are the three phases of this suite. Lillie- and Transport Granites are medium- to coarse-grained stock-like intrusions. The Hoed Granite is a fine-grained, locally porphyritic biotite granite that is intruded by the other two minor phases. A ductile shear zone with apparent sinistral displacement exists near the northern margin of this intrusion.

Apart from the Duiwelskloof Leucogranite and the Utrecht Granite, the other massive granites are regarded as I-type granites (based on the limited geochemistry), which formed in subduction collision-related settings. However, one could argue that these granites actually represent A-type anorogenic granites, as they are not foliated nor

metamorphosed. Heat necessary for such granites to form could have been supplied by under- and intraplating of mantle-derived gabbroic magmas (Robb et al., 2006). Bordering the Murchison Greenstone Belt to the north is a layered mafic igneous body called the Rooiwater Complex. This complex is capped by a 2740 ± 4 Ma (Poujol *et al*., 1996) hornblende tonalitic rock. Rooiwater Complex rocks mainly consist of albite and large, opalescent blue quartz grains. Furthermore, minor opaque minerals and secondary blue-green hornblende, chlorite, epidote, piemontite and muscovite are also present. Van Eeden *et al.* (1939) believed that the Rooiwater Complex is the late-stage differentiate of underlying gabbro-anorthosite of the Novengilla Suite.

The only tonalitic "late" pluton in Mpumalanga is the Cunning Moor Tonalite, which intrudes gneisses and migmatites of the Nelspruit Suite. It is a 50km-long oval shaped body, consisting predominantly of grey, medium-grained, massive, homogenous tonalite (Robb, 1978; 1994).

2.1.6. The Limpopo Belt (LB):

The Limpopo Belt (LB) in the northern part of South Africa may be the oldest example of a Himalayan-type continent-continent collisional orogeny between large cratons. This granulite-grade metamorphic belt has an ENE trend and stretches for approximately 550km with a width of 250km (Bumby & van der Merwe, 2004). Although there is some dispute over the timing of the Limpopo orogeny, a general consensus has been reached by most geologists over its formation mechanism. The orogenic event occurred as an oblique collision between the northern edge of the Kaapvaal Craton and the southern edge of the Zimbabwe Craton, with a third exotic terrain encorporated into the orogen, preserved between the two cratons. The combination of the Kaapvaal and Zimbabwe cratons is referred to as the Kalahari Craton.

The resulting LB consists of three main crustal zones, namely the Northern Marginal Zone (NMZ), the Central Zone (CZ) and the Southern Marginal Zone (SMZ), which lie parallel to one another in an ENE direction (refer to Figure 6). The NMZ represents the metamorphosed southern margin of the Zimbabwe Craton. To the north, the NMZ is bounded by the Northern Marginal Shear Zone, whereas the shallow south-dipping Triangle and Magogaphate Shear Zones separate the NMZ from the CZ in the south. At the southern boundary of the CZ lies the Palala Shear Zone and Tshipise Straightening Zone, which dip steeply to the north. The Triangle and Palala shear zones have dextral and sinistral senses of shear respectively (McCourt & Vearncombe 1987), suggesting that the CZ may have been emplaced as a westwards-vergent nappe. South of the Palala Shear Zone lies the SMZ, that in turn is bounded further south by the northwards-dipping Hout River Shear Zone. The Hout River Shear Zone incorporates the ortho-

amphibole isograd in its hanging wall, so that relatively low-grade basement rocks to the south are separated from higher amphibole- and granulite-grade rocks in the SMZ hanging wall. A large part of the area investigated in this study falls within the SMZ, which can be readily recognized by the presence of several ultramafic bodies, which are absent in the Kaapvaal Craton lithologies in the footwall.

When viewed in a N-S cross section, the LB appears to be a very symmetrical feature, apart from the fact that the Palala Shear Zone dips much steeper than the Triangle Shear Zone. Another symmetrical pattern within the LMB is indicated by metamorphic grades that show a general increase from the marginal zones (amphibolite facies) towards the CZ (granulite facies).

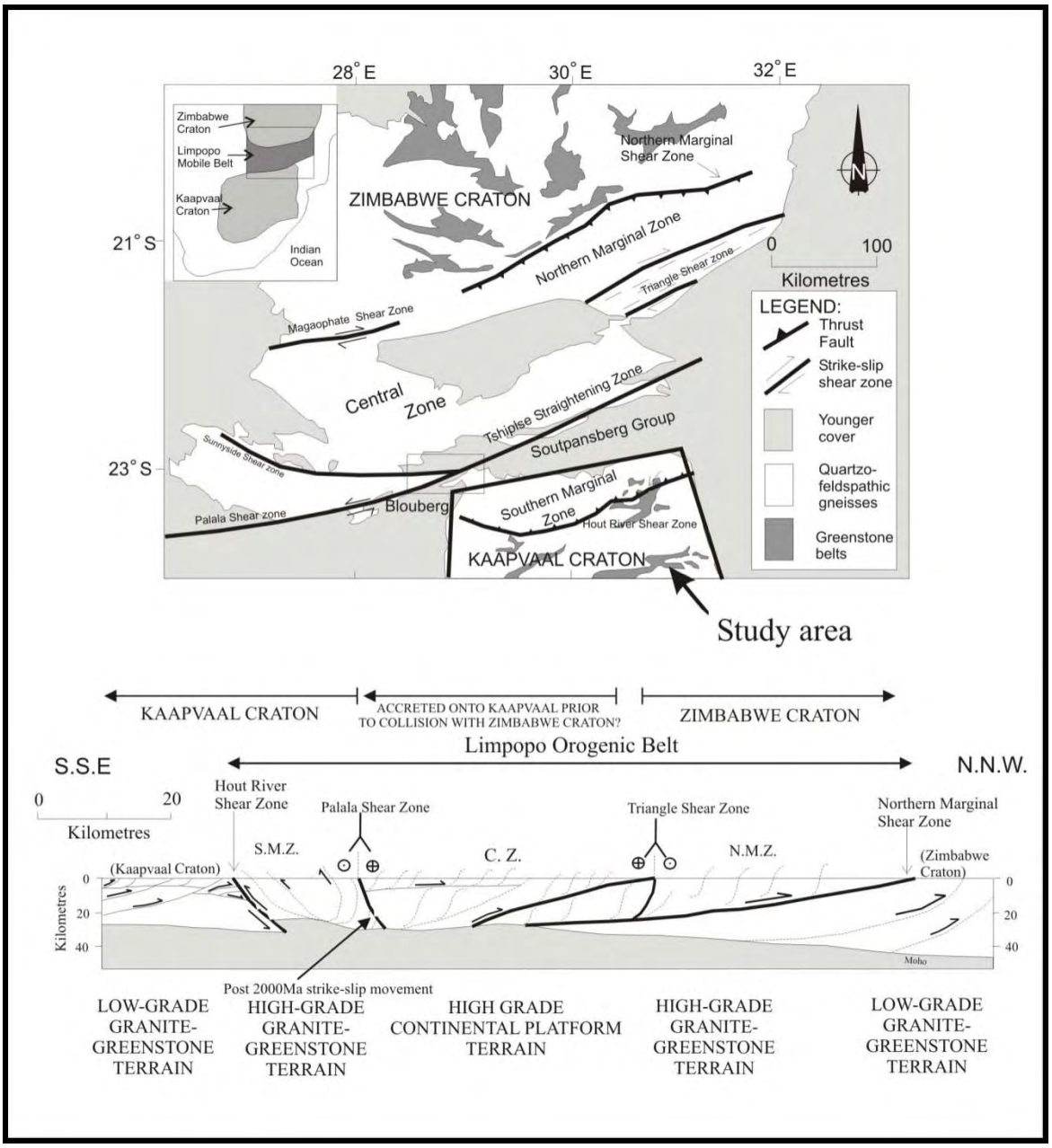

Figure 6: Regional geological map and cross section through the Limpopo Belt, showing the subdivisions, major shear zones and location of northern part of the study area (modified after Bumby & van der Merwe, 2004).

2.1.7. Timing of the Limpopo Orogeny:

Two main interpretations concerning the timing of the Limpopo Orogeny have been made in the past. The first interpretation focuses on the age of granitic gneiss bodies within the CZ. These granitic bodies, such as the Bulai Gneiss, are believed to have intruded into the Beit Bridge Complex as a result of decompression melting during exhumation, following the Limpopo collisional event (Bumby & van der Merwe, 2004). Dating of the Bulai Gneiss gives an indication of the minimum age of the collision at about 2.57 – 2.66 Ga. (McCourt & Armstrong, 1998). Further studies have been done

around the Blouberg area (e.g. Bumby et al., 2004), which is located along the projected strike of the Palala Shear Zone. In this area, lithologies from the Blouberg Formation, Waterberg and Soutpansberg Groups are found above a nonconformity with the granulite-grade gneiss of the LB and are separated from one another by angular unconformities. Due to this long tectono-sedimentary record in the Blouberg area (from the Limpopo collisional event up to the deposition of the Soutpansberg strata 1.97 - 1.8 Ga.) an Archaean-aged (ca. 2.6 - 2.7 Ga.) collision is favoured. Structures recorded by Bumby et al. (2004) in the Blouberg area reflect a southward-vergent tectonic event at ca. 2.0 Ga. According to this model, the ca. 2.0 Ga. event is interpreted as a reactivation of the Palala Shear Zone, rather than the primary Limpopo collision itself.

A second model concerning the timing of the Limpopo Orogeny deals with dates derived from metamorphic silicates found in the Triangle and Palala Shear Zones, as well as anatectic melts from the CZ. According to Holzer et al. (1998) and Schaller et al. (1999), these silicates and melt components represent times of peak metamorphism, thus implying the actual time of the collision between the KVC and the ZC. According to this model, a Proterozoic (ca. 2.0 Ga.) primary collision is suggested.

2.1.8. The Hout River Shear Zone (HRSZ):

One of the potential structural targets for groundwater in the study area is the Hout River Shear Zone (HRSZ). The HRSZ is located on the southern side of the Limpopo Belt (LB) and forms the boundary between the low grade basement lithologies of the Kaapvaal Craton (KC) and the higher grade rocks of the Southern Marginal Zone (SMZ). A lot of similarities exist between the HRSZ and its northern counterpart, the Northern Marginal Shear Zone (NMSZ), which separates the Zimbabwe Craton (ZC) from the Northern Marginal Zone (NMZ). However, the HRSZ is generally more steeply inclined than the NMSZ (Smit et al., 1992). In general the HRSZ comprises E-W striking, steeply northward-dipping thrusts and reverse faults, as well as several NE-SW striking strike-slip faults (Smit et al., 1992). The strike-slip faulting on the eastern part of the HRSZ changes to a system of frontal and lateral ramps as one move to the western section (refer to Figure 6). Geothermobarometric studies have shown that the vertical displacement of the HRSZ was of the order of 15km (Miyano et al., 1992; Perchuk et al., 1996).

Prior to the formation of the HRSZ, north-vergent thrusting ($\mathbf{D_1}$) took place along moderately southward-dipping thrusts in the northern margin of the KC. Through lead stepwise leaching (PbSL) of titanite from the Renosterkoppies Greenstone Belt in the KC, Passeraub et al. (1999) have shown that this initial event ($\mathbf{D_1}$) took place between 2760 and 2710 Ma. This first event was followed by amphibolite facies southward-vergent

thrusting ($\mathbf{D_2}$) along the newly formed HRSZ. The $\mathbf{D_2}$ event is characterized by cooling and decompression to amphibolite facies conditions. Such conditions led to the exhumation of the charno-enderbitic rocks of the ($\mathbf{D_2}$) Matok Pluton along the Matok Shear Zone, which forms part of the HRSZ. Ductile reactivation of the Matok Shear Zone postdates the emplacement of granodioritic members of the Matok Pluton, which implies that $\mathbf{D_2}$ thrusting continued after the exhumation to mid-crustal levels. According to Kreissig et al. (2001), the geochronology of the HRSZ stretches over ~90Ma (c. 2690 until 2600 Ma.) of episodic shearing. Lastly, strike-slip shear zones parallel to $\mathbf{D_2}$ structures may indicate a continuous transition from high grade $\mathbf{D_2}$-shearing to mylonitic $\mathbf{D_3}$. Metapelites of the Bandelierkop Formation are only found in the SMZ, north of the HRSZ. Furthermore, the distribution of swarms of dolerite dykes also seem to be influenced by the HRSZ, as these are more densely populated south of the HRSZ, in low-grade rocks of the KC, and are less common within the SMZ.

The mylonitic rocks which occupy the HRSZ are likely to be more highly weathered than the adjacent gneisses and granites of the area. Such predicted deep weathering profiles along the HRSZ are expected to have a strong positive influence on the hydraulic conductivity parallel to the strike of the shear zone. Unfortunately, faults can also lower an area's water table by acting as drainage pathways (Mulwa *et al*., 2005).

2.1.9. Dolerite dykes:

Dyke swarms outcrop more densely in the north-eastern domain of the Kaapvaal than elsewhere on the craton and northeast-striking diabase dykes are dominant in the study area. From their orientation and age, these northeast-striking dykes are associated with 2.7 Ga. Ventersdorp Supergroup trends (Uken & Watkeys, 1997), which formed either in response to the Limpopo orogeny (Burke et al., 1985) or by crustal extension due to mantle plume activity (Hatton, 1995). Later Karoo dolerites sporadically cut through the older dykes but usually follow the same intrusion paths as their Archaean predecessors. One of the possible controls of the dyke emplacement in the studied area is the Hout River Shear Zone (HRSZ), because many more dykes are observed north of the HRSZ (in the SMZ) than south of it.

In groundwater exploration one should not only consider the orientations of dykes, but also their thickness. Pumping tests in Botswana revealed that dolerite dykes thicker than 10m serve as groundwater barriers, whereas those that are narrower tend to be permeable due to the fact that cooling joints and fractures are developed in them (Bromley *et al*., 1994). Geometry, grain size and the degree of weathering are other factors which, through a complex interplay, affect the hydraulic conductivity of dolerites. However, due to the structural geological nature of this thesis, the author

largely focussed on the orientation and distribution of dolerites and their associated joints. Stettler *et al*. (1989.) divided the northern part of South Africa into six domains based on the character and orientation of their magnetic lineaments. Domains A, C and E are similar in character in that they have the highest frequency of magnetic lineations and a high degree of NE-SW to ENE-WNW orientation. Domains B and D on the other hand have more randomly orientated magnetic lineations (refer to Figure 7).

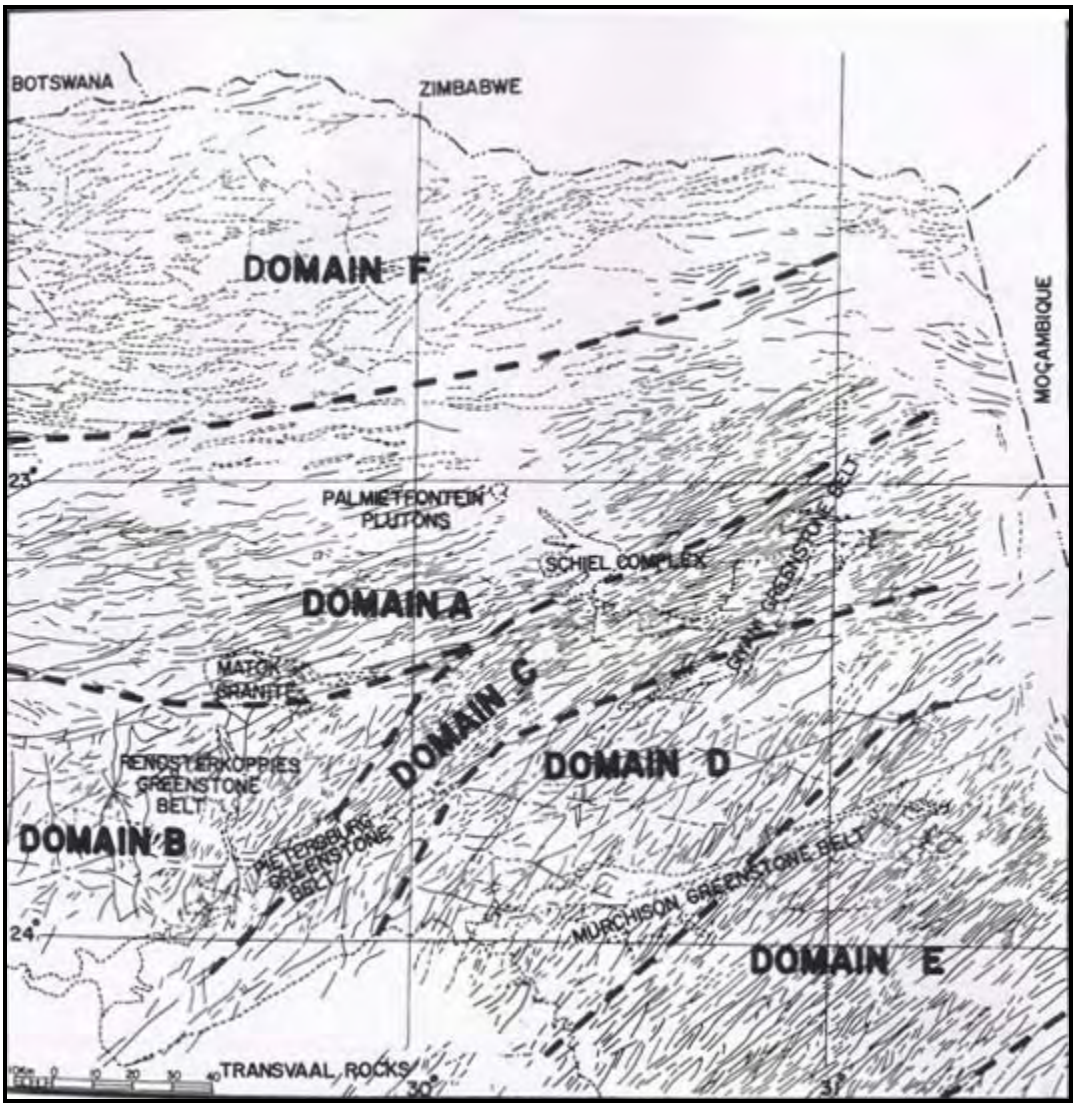

Figure 7: Aeromagnetic lineament map of the northern part of South Africa an interpreted lineament domains (after Stettler et al., 1989).

2.1.10. Wolkberg Group:

The Wolkberg Group is an up to 2000m thick sedimentary succession (Button, 1973, Bosch, 1992), which outcrops along the southern border of the study area. It consists of alternating feldspathic quartzites and argillaceous sedimentary rocks, coarse quartz arenites, some conglomerates, basaltic lava and minor stromatolitic carbonate beds

(Button, 1973; Bosch 1992). The Wolkberg Group comprises, from the base upwards, the Sekororo, Abel Erasmus, Schelem, Selati, Mabin and Sadowa formations (Button, 1973; Bosch, 1992). The basal Sekororo Formation nonconformably overlies Archaean basement of the Kaapvaal craton (Button, 1973).

2.1.11. Bushveld Igneous Complex:

The western edge of the study area is bound by the northern limb of the c. 2.06 Ga. Bushveld Complex. This is a large economically important layered intrusive complex, comprises of the lower Rustenburg Layered Suite which underlies the Lebowa Granite Suite and the Rashoop Granophyre Suite, which intruded into the basement gneiss. The northern edge of the northern limb of the Bushveld Complex appears to abut against the HRSZ and the extent of intrusion may thus, in part, be controlled by such pre-existing structures.

2.1.12. Blouberg Formation:

The Blouberg Formation is a clastic sedimentary sequence that was deposited nonconformably over the granulite-grade gneisses of the LB in the far north-west of the study area. Outcrops of the Blouberg Formation are found on the eastward extension of the Palala Shear Zone, WSW of the Soutpansberg. According to Bumby et al. (2002) the depositional environment of the Blouberg Formation was most likely a deep, localized pull-apart basin caused by strike-slip reactivation along the Palala Shear Zone. Other features, like the ENE-trending Melinda Fault also affected the geometry of the Blouberg Formation. The maximum thickness of the Blouberg Formation is about 1400m (Bumby et al., 2001) of which the lower member makes up about 600m.

Lower member lithologies of the Blouberg Formation vary from coarse arkosic sandstone and channel fills of arkosic granulestone (presumably from braided streams). According to Bumby et al. (2001), the sizes of lower member sets of trough cross bedding decrease upward. Upper member lithologies of the Blouberg Formation were deposited in alluvial fans, and consist of feldspathic sedimentary breccia and conglomerate. Syn-sedimentary tectonism recorded in the Blouberg Formation is thought to reflect a 2.0 Ga. southward-verging reactivation event of the Palala Shear Zone (Bumby et al., 2004). This same southward-verging compressional event caused E-W-trending folds and locally overturned strata with reverse faults that dip to the north.

2.1.13. Waterberg Group:

The Waterberg Group similarly outcrops along the north-western margin of the study area, and consists of the Setlaole, Makgabeng and Mogalakwena formations. The basal Setlaole Formation rests nonconformably on the basement rocks, and is composed of

coarse granulestone and is locally conglomeratic. This formation is interpreted to have been deposited in a fluvial, braided river environment. The Makgabeng Formation was likely to have been deposited conformably on the Setloale Formation, and consists of large-scale trough and planar cross-bedded fine- to medium-grained sandstone, which is interpreted as an aeolianite (Bumby, 2000). The Mogalakwena Formation, in contrast, lies disconformably above the Makgabeng Formation, and further to the north rests on the Blouberg Formation on a sharp angular unconformity. These strata consist of interbedded sheets of granulestone and conglomerate in proximal areas, grading into trough cross-bedded granulesotnes and sandstones in distal areas to the SW (Bumby, 2000).

Disputes have occurred in the past over the relative age relationship between the Waterberg and Soutpansberg Groups. Basement-derived clasts were observed in the basal Tshifhefhe Formation of the Soutpansberg Group, but not in the Waterberg strata and therefore Brandl (1987) believed that the Soupansberg Group predates the Waterberg Group. However, more recent studies (Bumby, 2000; Bumby et al., 2001) showed the opposite relationship between the Soutpansberg and Waterberg Groups in the vicinity of the Blouberg Formation. Bumby (2000) and Bumby et al. (2001) found that the Soutpansberg clastic strata rest unconformably on the Mogalakwena Formation of the Waterberg Group.

2.1.14. Soutpansberg Group:

Strata from the Soutpansberg Group presently outcrop in a continuous linear escarpment stretching ENE-WSW from Punda Maria in the east to Vivo in the west, and form the northern border of the present study area. Outliers of Soutpansberg rocks also outcrop further to the west, at Blouberg, Tolwe and in the Palapye area in eastern Botswana. The Soutpansberg Group is a 1.85 Ga. volcano-sedimentary sequence (Cheney et al., 1990; Barton and Pretorius, 1997).

The Soutpansberg Group consists of the basal Tshifhefhe Formation, which is only locally developed at the eastern end of the Soutpansberg basin, and is only a few metres thick. It is comprised of strongly epidotised clastic sediments, including shale, greywacke and locally-derived conglomerate (Barker et al., 2006). This is overlain by the generally volcanic Sibasa Formation. The siliciclastic Fundudzi Formation is only developed at the eastern end of the basin. It is mainly comprised of arenaceous and argillaceous sedimentary rocks, though there are rare pyroclastic horizons, and basaltic lavas are intercalated with the sedimentary lithologies close to the top of the formation (Bumby, 2000). Overlying the Fundiudzi Formation is the Wyllie's Poort Formation, composed of northward-dipping red-pink quartzite with minor pebble washes. The base

is marked by a prominent agate pebble conglomerate, and in the east minor basaltic and pyroclastic intercalations are present (Barker, 1979). Wyllie's Poort Formation reaches thicknesses of 4000m. Lastly, the uppermost unit of the Soutpansberg Group is the Nzhelele Formation, which is volcanic at the base (400m), followed by argillaceous sedimentary rocks in the middle, and arenaceous rocks at the top (Barker et al., 2006).

2.1.15. Proposed Models for the formation of the Soutpansberg Group:

A few models pertaining to the deposition of the Soutpansberg Group have been suggested, but the two main models discussed in this report are those of Jansen (1975), Bumby et al. (2001) and that of Cheney et al (1990). Jansen (1975) proposed an aulocogen or failed rift model. Bumby et al. (2002) supplement Jansen's (1975) model by proposing that the Soutpansberg sediments were deposited in an E-W stretching half-graben, which is fault-bounded to the south. Therefore, this first model proposes a syn- to post tectonic depositional environment. On the other hand the second model, proposed by Cheney et al. (1990), suggests a large cover sequence of Soutpansberg strata that were deposited pre-tectonically. According to Cheney et al. (1990), a graben, similar to that proposed by Jansen (1975) formed after the deposition of the Soutpansberg strata, thus preserving the Soutpansberg strata within a graben, rather than being deposited within a graben. Since no Soutpansberg lithologies have been found south of the Palala Shear Zone, the model by Jansen (1975) or Bumby et al. (2001) is most favoured.

2.1.16. Drakensberg Group:

The eastern margin of the study area is marked by the eastern edge of the Kaapvaal craton. This area is underlain by rocks of the Drakensberg Group (Karoo Supergroup), which comprises flood basalts and pyroclastic deposits. According to Smith et al. (1990), these basalts are Early Jurassic in age and are linked with the onset of rifting between East and West Gondwana.

2.2. Fault and joint analysis:

In order to understand the dynamics of faulting one must first grasp the basic properties of the principal stress directions in conjunction with Coulomb's Law of Failure, which states that:

$$\sigma_c = \sigma_0 + \tan\phi(\sigma_N)$$ Coulomb (1773) and Mohr (1990)

where

σ_c = critical shear stress required for faulting

σ_0 = cohesive strength of the rock

$\tan\phi$ = coefficient of internal friction

σ_N = normal stress

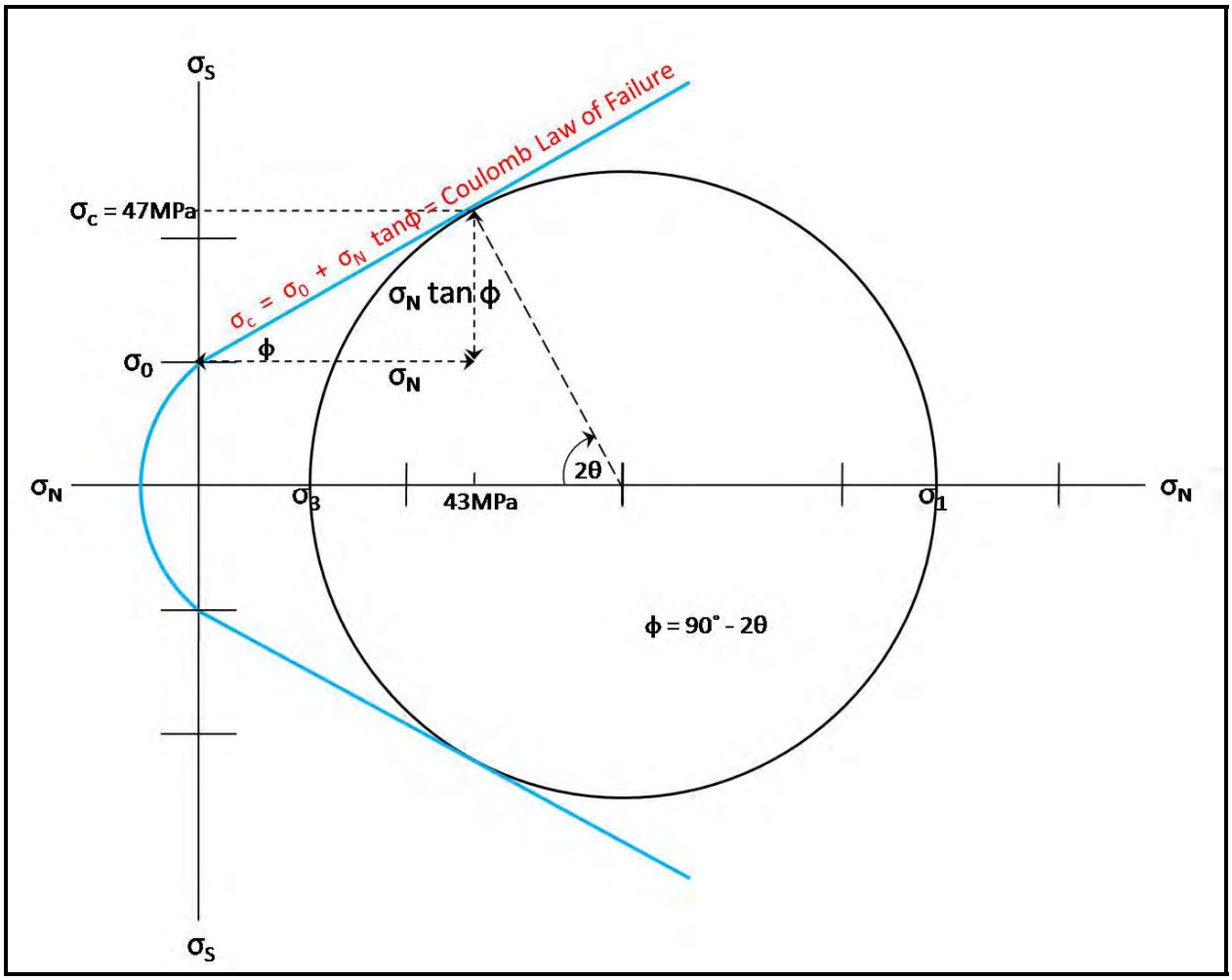

Figure 8: A Mohr diagram illustrating the principles of the Coulomb Law of Failure. Modified after Davis and Reynolds, 1996.

A rock's angle of internal friction (ϕ) determines (θ), which is the angle between the fracture surface and the direction of greatest principal stress (σ_1) (Davis and Reynolds, 1996). From the geometry of the Mohr diagram in Figure 8, one can see that

$\phi = 90^\circ - 2\theta$, therefore

$2\theta = 90^\circ - \phi$

$$\theta = \frac{90^\circ - \phi}{2}$$

Through countless laboratory tests it has been shown that most rocks possess an angle of internal friction equal to about 30˚ (Davis and Reynolds, 1996). Therefore, the value of θ is also 30˚ for most shear fractures.

Anderson (1951) realized that if one considers the Earth to be a perfect sphere, the contact between air and ground at any point on the Earth's surface forms a tangent plane along which shear stress is zero. In that case, since principal stress directions are considered as directions of zero shear stress, the surface of the Earth must be a principal plane containing two of the three principal stress directions. The third principal stress direction lies perpendicular to this principal plane so that it is vertical at any point on the surface of an ideally spherical Earth (Davis and Reynolds, 1996). Using the internal angle of friction ~30˚ as a base, together with the concept of the Earth's surface being a principal stress plane, Anderson (1951) concluded that only normal-slip, strike-slip and thrust-slip faults should be able to form at or near the Earth's surface. Normal-slip faults form when σ_1 is vertical; strike-slip faults form when σ_2 is vertical; and thrust-slip faults form when σ_3 is vertical (Davis and Reynolds, 1996). Furthermore, conjugate pairs of fault planes can form in which case the conjugate angle between such planes is bisected by σ_1. In addition to the faults already mentioned, mode I tension fractures can form parallel to the direction of principal stress (σ_1) and perpendicular to the direction of least principal stress (σ_3). Slickenside lineations are often found on fault surfaces and their orientation is defined as the intersection of the fault plane with the σ_1/σ_3 plane (Davis and Reynolds, 1996).

Strike-slip fault:

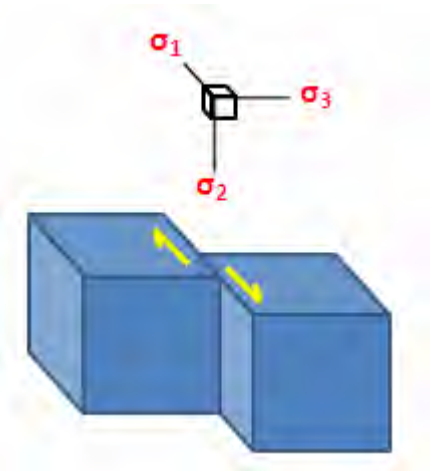

Thrust fault:

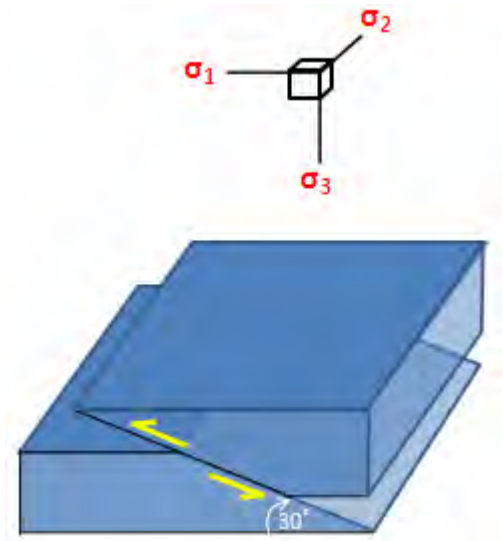

Normal- and reverse faults:

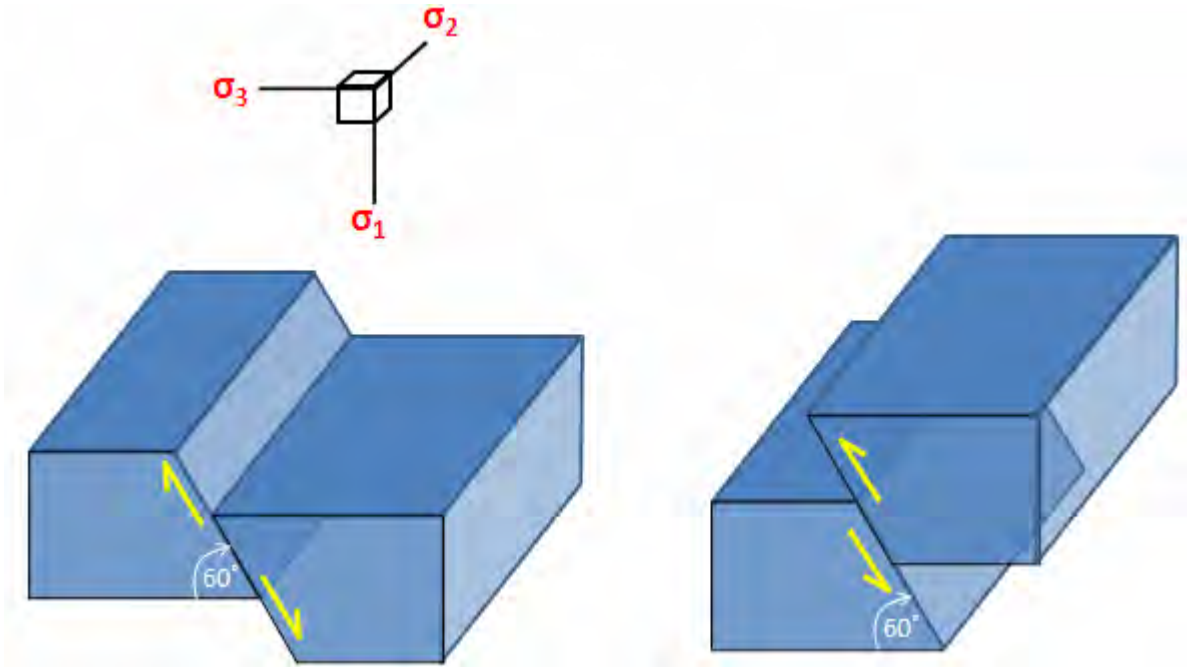

Figure 9: Illustrations of the three fault types described in Anderson's Theory, as well as a reverse fault.

PORE FLUIDS:

Since there are many more variables in nature than just the internal angle of friction and an idealistic principal stress plane, there exist a few exceptions to Anderson's Theory of Faulting and Coulombs Law of Failure. The first variable that has not been discussed yet is the existence of pore fluids at the time of faulting. Hubert and Rubey (1959) showed that high pore fluid pressure (P_f) in rocks decreases the normal stress acting on the fault/fracture plane. This lead to the modification of the Coulomb Law of Failure through the introduction of effective stress (σ^*) which is equal to the normal stress minus the pore fluid pressure. Hence, the critical stress needed to fracture a rock is also affected in the following manner:

$$\sigma_c = \sigma_0 + \tan\phi(\sigma_N - P_f)$$

At depths shallower than 3km, the fluid pressure in the Earth's crust is unconfined and equal to the hydrostatic pressure (P_h) (Twiss and Moores, 1992). Hydrostatic pressure is a function of the density of the fluid (ρ_f), the height of the fluid column (h) and the pull of gravity (g) (Davis and Reynolds, 1996).

$$P_h = \rho_f g h$$

Once below 3km, fluid pressure plays a more complex role. Due to compaction, fluid pressures are forced to occupy less and less space and therefore exceed hydrostatic pressure. To complicate matters even further, the influence of the geothermal gradient causes what is known as aquathermal pressuring. Aquathermal pressuring occurs because water has a higher coefficient of thermal expansion than rocks (Davis and Reynolds, 1996) and this phenomenon can even cause pore fluid pressure to rise to levels exceeding the lithostatic pressure (pressure derived from the weight of the overlying rock) of the host rocks (Davis and Reynolds, 1996). The fluid pressure ratio (λ) is used to describe the ratio of pore fluid pressure to lithostatic pressure:

$$\lambda = \frac{P_f}{Pl} = \frac{P_f}{\rho_r g h}$$ (Hubert and Rubey, 1959)

Elevated fluid pressures are called abnormal fluid pressures and have λ values ranging from 0.5 to 0.9, whereas hydrostatic fluid pressures' λ values range from 0.37 to 0.47 (Suppe, 1985). Abnormal fluid pressure can cause a remarkable phenomenon by forming joints at depths exceeding 10km. Formation of joints at such depths can occur in one of the following ways: 1) If the differential stress between σ_1 and σ_3 is small enough and the abnormal fluid pressure is large enough, tensional joints can form perpendicular to σ_3; 2) If

the differential stress between σ_1 and σ_3 is higher, but the pore fluid pressure remains abnormally high, transitional tensional joints can form at low angles to σ_1 (Secor, 1965). This concept is very important to this project when taking into consideration the fact that many of the basement rocks exposed at the current topographical surface of the study area originally formed at great depths.

ANISOTROPIC ROCKS:

A second variable causing deviations from Anderson's Theory is the anisotropy of rocks. If a rock contains any pre-existing weaknesses such as bedding, faults, fractures or foliation it can alter the way in which the rock reacts to stress. It has been proved that the level of critical stress required to reactivate an existing fracture plane is less than that required to fracture an unfractured sample of the same lithology (Handin, 1969). Even fractures with θ angles as great as 65˚ can sometimes be reactivated as faults (Handin, 1969). A large amount of the basement lithologies in this project's study area are foliated and therefore it is important to take note of the following exceptions to the rule: 1) If foliation lies at a small angle to σ_1, the resulting θ angle of the fracture that forms will be very small ~10˚ to 20˚. 2) If the angle between foliation and σ_1 falls between 25˚ and 45˚ the influence of internal friction can be made ineffective and fault surfaces can form right along foliation (Donath, 1961).

PRE-EXISTING FRACTURES:

As a result of its long tectonic history, the rocks in the study area have experienced many stress regimes throughout their existence. With that in mind it is obvious that pre-existing fractures were often present at the onset of a new tectonic episode. Just as in the case of anisotropic rocks, pre-existing fractures also have a deviating effect on Anderson's Theory. Byerlee's Law (1967, 1978) states that the level of critical shear stress needed for the reactivation of a pre-existing fracture is equal to the coefficient of sliding friction of the rock multiplied by the normal stress acting on the fracture plane.

$$\sigma_c = \sigma_0 + \tan\phi_f(\sigma_N)$$

This basically means that the level of stress required for the reactivation of a pre-existing fracture depends on the friction along the fracture plane and the orientation of that plane (Davis and Reynolds, 1996). Through extensive experimenting, Byerlee (1967, 1978) further concluded that except for conditions of very low confining pressure (<200MPa), friction is effectively the same for all rock types.

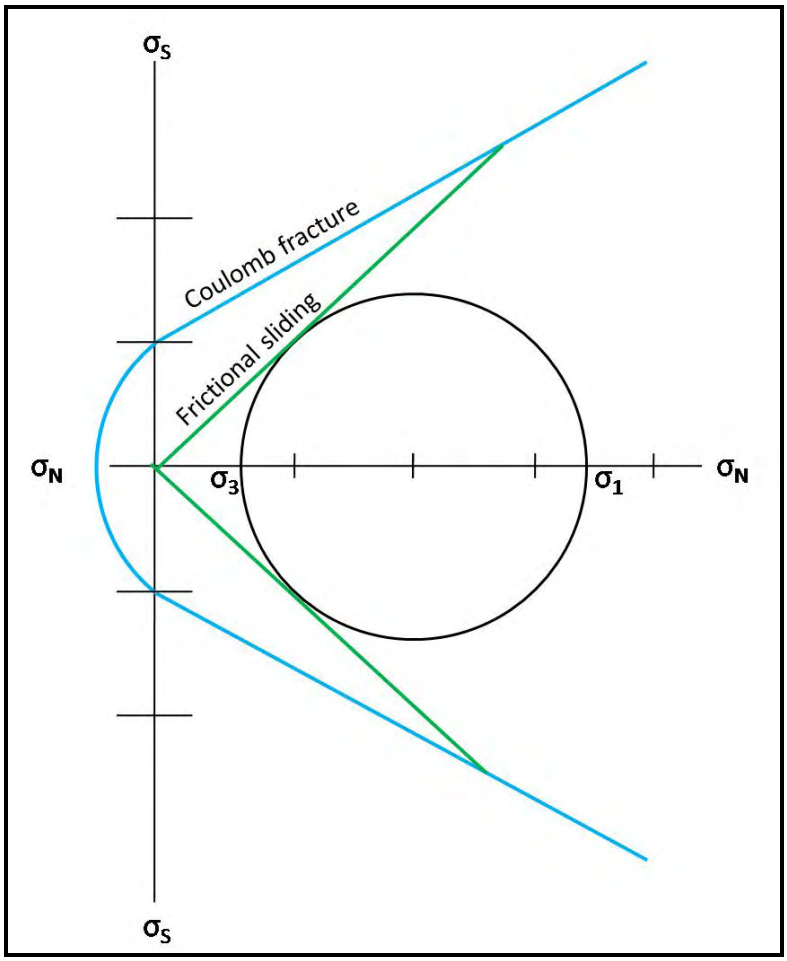

Figure 10: An illustration of the relationship between a Coulomb frictional envelope and a frictional sliding envelope on a Mohr diagram. If the differential stress circle from the stresses in a rock with pre-existing fractures touches the frictional sliding envelope on the diagram, renewed sliding will take place along the existing fractures instead of forming new fractures. Modified after Suppe, 1985.

THREE-DIMENSIONAL STRAIN:

Experiments that test rock deformation properties usually involve conditions of two-dimensional coaxial stress and strain. Under these conditions, Coulomb's Law predicts the formation of one conjugate pair of faults. However, rocks in nature have often been found with two pairs of conjugate faults (four faults). A possible explanation for the two conjugate fault pairs is simply to assume that two separate faulting events took place in the same area (Davis and Reynolds, 1996). However, Reches (1978) proved the presence of more than one fault set (pair) is often due to a single faulting event generated by a three dimensional strain field. For example, three or more fault sets arranged in orthorhombic symmetry is a characteristic fault pattern that occurs when rocks are stretched or shortened by different amounts in three mutually perpendicular directions Reches (1983) (see Figure 11). According Reches' (1983) experiments, the angular relationships among fault sets formed under these conditions depends both on the angle of internal friction (ϕ) and the ratio of strain along the principal finite stretch directions (S_1, S_2 and S_3).

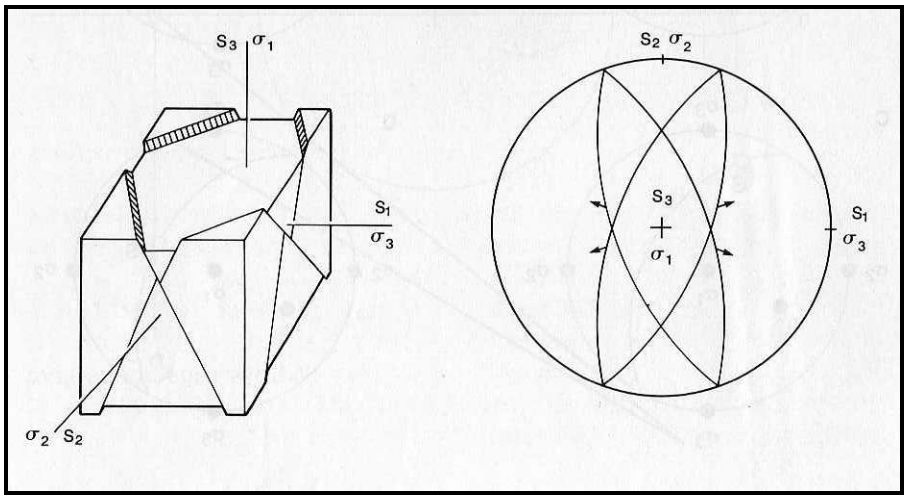

Figure 11: Two pairs of conjugate fault sets produced in a three-dimensional strain field. From Reches, 1983.

REVERSE FAULTS:

Reverse faults are formed by crustal shortening and usually dip ~60˚ or steeper. Although not uncommon, reverse faults don't fit into the typical model of Anderson's Theory. An obvious explanation for the formation of reverse faults is the reactivation of previous normal faults (Davis and Reynolds, 1996). Another explanation for the formation of reverse faults is the fact that stress trajectories become inclined or curved with depth (Davis and Reynolds, 1996). Theoretically, the dissipation of horizontal compressive stress can cause a strain field with curved stress trajectories, causing curved faults which are partly thrust faults which steepen upward into reverse faults (Hafner, 1951). On the other hand, other experiments have shown that shallow thrusts can steepen with depth to become reverse faults (Sandord, 1959).

CHANGES OF ROCK VOLUME DURING FAULTING:

A last variable that causes faults in nature to deviate from the faults described by Anderson's Theory is changes in rock volume during faulting (Aydin, 1978; Aydin and Johnson, 1978). This phenomenon usually occurs in poorly cemented, porous sandstones that can decrease in volume as a result of the collapsing of pores under stress (Davis and Reynolds, 1996) and therefore shouldn't play a role in the basement rocks of the study area. Faults that occur in unison with volume reduction are called deformation bands or band faults and often form together in zones (Davis and Reynolds, 1996).

2.3. Geological stress and strain regimes in Southern Africa:

A very interesting study was conducted by Bird et al. in 2006 regarding patterns of stress and strain rate in Southern Africa. Models were produced of deviatory stress fields, primarily caused by the following three sources: 1) lateral variations in the density moment; 2) resistance of unbroken lithosphere to the relative rotation of the Somalia Plate relative to

the African Plate; 3) stress concentration near the tips of frictionless cracks. Unfortunately, it was impossible to isolate any of these sources in a model. Given that some ancient faults in Southern Africa have been reactivated, including faults from the Limpopo Belt (Brandl, 1995; Partridge and Maude, 2000), it may take generations of research in order to encompass a full understanding of the strain rate field in this area.

In Bird et al.'s study (2006), present stress directions in Southern Africa were obtained through overcoring (a type of in situ stress measurement in which small strains are produced after the stress release around a cylinder at the end of a borehole), from seismic focal mechanisms and from field observations of faults which likely formed during the Holocene Epoch. Unfortunately, all three of these sources are subject to a bit of bias. Nonetheless, the information obtained was used to create a general sense of stress and strain directions and regimes in the area. Stress regimes were predicted by looking at the orientation of the principle stress axes: normal and reverse faulting (NF) occurs when the most compressive stress axis (σ_1) is vertical; strike-slip faulting (SS) occurs where σ_2 is vertical and thrust faulting (TF) occurs when σ_3 is vertical (see Anderson's Theory in the previous section). To accommodate for mixed regimes, "NS" is used to denote a NF regime with a SS component and "TS" signifies a TF regime with a SS component.
According to the data compiled into the World Stress Map (WSM) there exists a vast region that extends from southwest Angola to South Africa in which the most compressive horizontal principal stress (σ_{1H}) is orientated NW to NNW, called the Wegener Stress Anomaly (WSA) (Andreoli et al., 1996; Viola et al., 2005). Initially, it was thought that the WSA is caused by ridge push (horizontal compression in old seafloor adjacent to a spreading rise) generated by the South West Indian Ridge (Viola et al., 2005). On the inland parts of Southern Africa, the primary stress field is one of horizontal tension in a NE-SW direction, branching from the offshore oceanic tension belt at the Indian Ocean margin between 15˚ - 25˚ latitude (Bird et al. in 2006). This stress field continues southwest through the Kaapvaal Craton and offshore into the east Atlantic Ocean (here this stress component becomes σ_{2H}, because there is an even stronger NW-SE tensional component).

Through investigation of the three stress sources mentioned earlier, Bird et al. (2006) reached two conclusions, one of which pertains to this study, namely: The quality of the predicted stress field increases by changing the basal drag from passive to active, which in turn increases the rate of relative rotation between the African- and Somalia Plates. Hence, it is suggested that the WSA and other features of Southern Africa's stress field are mainly due the resistance of unbroken lithosphere to relative plate rotation, with only minor contributions from other sources such as ridge push (Bird et al. 2006

Table 2: Most Compressive Horizontal Principal Stress Azimuths and Stress Regimes in Southern Africa*. After Bird et al., 2006

Latitude (deg.)	Longitude (deg.)	σ_{1H} Azimuth	Type	Quality	Regime	Deth (Km)	Location	Source
-34.783	19.633	115	GFS	A	NF	0	Gansbaai-Quoin Point, South Africa	Andreoli et al. [1996]
-35.170	22.150	145	BO	B	NF	0	Bredasdorp Basin, offshore South Africa	Andreoli et al. [1996]
-30.200	18.400	148	GF	A	NF	0	Santab se Vloer normal faults, Bushmanland	Brandt et al. [2005]
-24.700	16.000	172	GF	A	NS	0	Hebron dextral-normal fault, Namibia	Viola et al. [2005]
-19.900	21.900	40	GF	A	NF	0	Gumare fault, Okawango Delta, Botswana	McCarthy et al. [2002]
-19.640	23.600	39	GF	A	NF	0	Kunyere Fault, Okawango Delta, Botswana	McCarthy et al. [2002]
-19.680	23.800	42	GF	A	NF	0	Thamalakane Fault, Okawango Delta, Botswana	McCarthy et al. [2002]
-17.417	14.250	173	OC	A	TF	0.134	Ruacana Power Sta. RSM 7 and 8, Namibia	Stacey and Wesseloo [1998]
-24.000	34.500	0	GF	B	NF	0	Funhalouro-Mazenga Graben, Mozambique	Ferro and Bouman [1987]
-30.350	15.100	145	GF	A	SS	0	Offshore sinistral(?) ‘‘mud volcano’’ fault	Viola et al. [2005]
-26.500	17.600	167	GF	A	NF	0	Dreylingen-Pfalz oblique-slip fault, Namibia	Viola et al. [2005]
-29.667	22.750	160	OC	A	SS	0.8	Prieska mine, Namaqualand	Andreoli et al. [1996]
-27.800	17.260	167	GF	B	NF	0	Skorpion mine, Namibia	Viola et al. [2005]
-25.667	27.250	135	OC	C	NF	0	Rustenburg and Northam mines, Witwatersrand	Andreoli et al. [1996]
-29.700	17.900	145	OC	A	SS	1.57	Carolusberg mine, Springbok, Namaqualand	Viola et al. [2005]
-29.300	18.800	92	OC	A	SS	0.416	Black Mountain mine, Aggeneys, Namaqualand	Viola et al. [2005]
-21.383	15.367	152	GF	B	TF	0	Otombawe-Elim-Vrede reverse faults, Namibia	Klein [1980]

*** Not already in World Stress Map. Conventions used from the World Stress Map: Azimuth is measured in degrees clockwise from north. Type includes OC overcoring, GFS geologic fault slip orientation, and BO borehole breakout orientation. Quality standards were defined by Zoback and Zoback [1989]. Abbreviations used for regimes are explained in the text.**

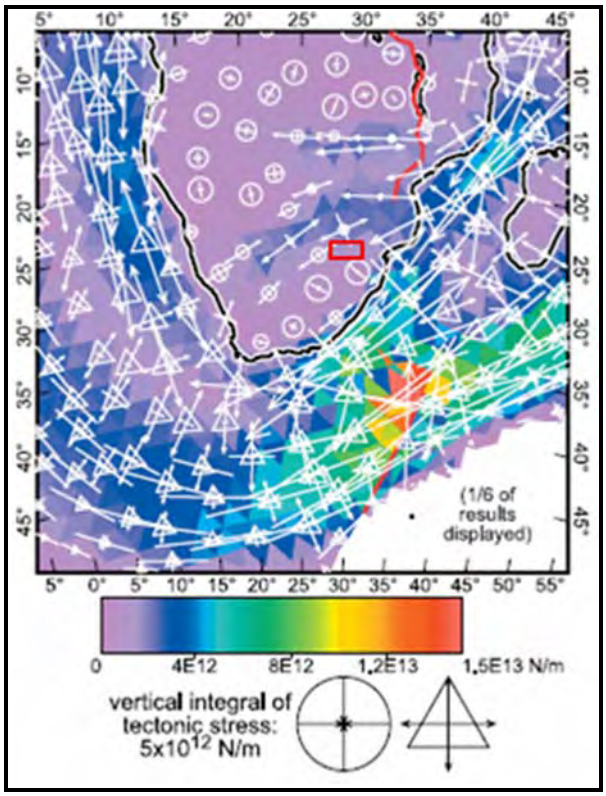

Figure 12: Vertical integrals, through the model lithosphere, of the tectonic stress tensor (symbols) and of the greatest shear stress (colours), for the preferred model AFSO- 013 by Bird et al., 2006. Circles show negative vertical components of the vertical integrals of tectonic stress (on land and in shallow water), and triangles show positive vertical components of the vertical integral of tectonic stress (in ocean basins deeper than the reference spreading ridge). Tensor symbols for vertical integrals of tectonic stress are scaled by radius (not area), and the reference symbols in the margin portray isotropic compression and tension, respectively. After Bird et al. 2006. Red rectangle indicates the study area for this thesis.

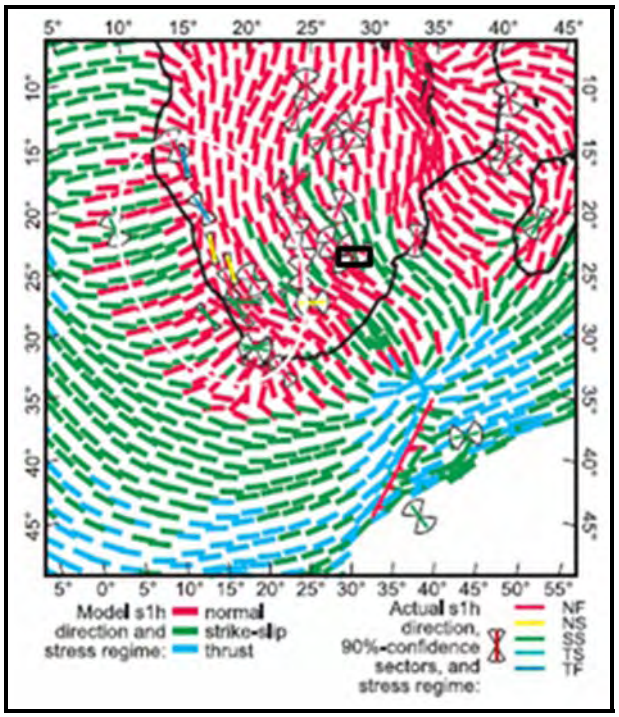

Figure 13: A map showing the most compressive horizontal principal stress directions (σ_{1H}) from AF-SO-013, the preferred model from Bird et al., 2006. Interplate indicators of stress regime are indicated in colour in the legend and the orientations of the coloured lines on the map indicate the azimuth of σ_{1H} at each location. The approximate region of the Wegener stress anomaly (Wegener stress direction province) is suggested by the white ellipse and the black rectangle indicates the study area for this thesis. After Bird et al. 2006.

Overall, the model preferred by Bird et al. (2006) (Model AF-SO-013) shows a belt of highly extensional strain rates running southward along the East African Rift. This belt branches at 12˚ south to avoid the strong region around the Kaapvaal Craton (called the Transgariep

Plate by Hartnady, 2002). The western branch connects to a western arch through Angola, Namibia and South Africa, whereas the eastern branch becomes a less active south-eastern fan which passes offshore through northern Mozambique. A prominent belt of NE-SW instrumental seismicity in South Africa is also a feature of the model predictions, where NE-SW extension is predicted to occur at about 1 x 10^{-16} s^{-1} (Bird et al. 2006). This implies that the earthquakes associated (temporally and spatially) with deep mining in South Africa may be fundamentally natural tectonic earthquakes that have been triggered or accelerated by human intervention.

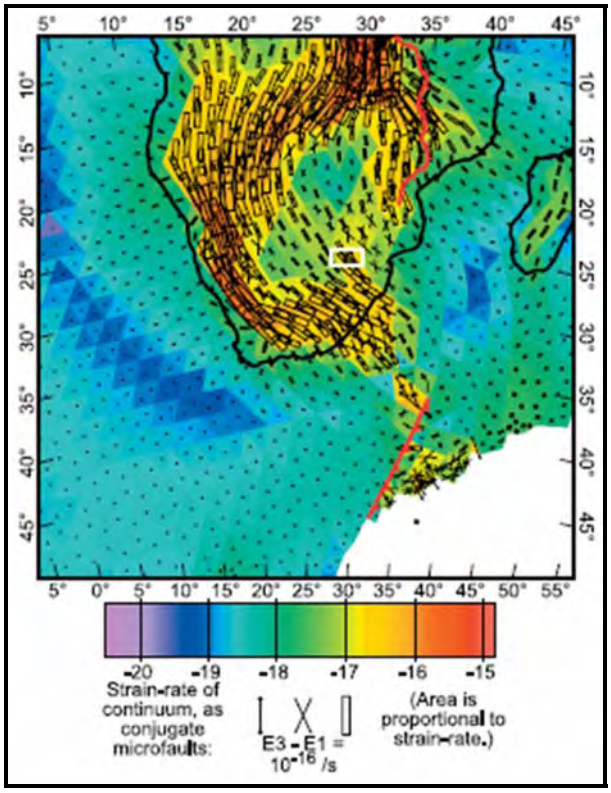

Figure 14: Long-term average (anelastic) strain rates predicted by Bird's (2006) preferred model, AF-SO-013. Color indicates the common logarithm of the magnitude of the principal strain rate with greatest absolute value (in units of s_1). Symbols show orientation of the strain rate tensor in terms of the strikes of conjugate microfaults predicted. Rectangles represent grabens; dumbbells with diamond-shaped terminations represent thrust faults and crosses indicate conjugate strike-slip faults. After Bird et al., 2006. The white rectangle indicates the study area for this thesis.

As in various other studies, artificial models cannot always sufficiently explain natural phenomena and even the preferred model created by Bird et al. (2006) has some discrepancies which have been pointed out. Firstly, in an area adjacent to this paper's focus, one finds the ENE-WSW Tshipise-Bosbokpoort Fault System, striking almost perpendicular to the computed σ_{1H}, even though the predicted regimes in the area are NF and SS. This fault system is >170km long with a well developed and preserved 2m – 10m high scarp (Brandl, 1995). Furthermore, reactivations of the Tshipise-Bosbokpoort Fault have been dated at 101 ka (estimated magnitude ~8), 101–37.5 ka (~6.6), 37.5 ka (~7.6) and 29.3 ka (~6.6) by the U-Th disequilibrium method (T. Partridge, unpublished data). Other inconsistencies regarding Bird's (2006) model includes the historical seismicity, late Pleistocene-Holocene thrust faulting (striking ENE-WSW) and soil liquefaction features in

the southern Kaapvaal Craton (Andreoli et al., 1996). Consequently, much remains to be learned about the complex faulting in certain parts of South Africa.

To sum up Bird et al.'s (2006) study one can say that although Southern Africa is surrounded by spreading ridges, most of it is not in a state of horizontal compression. On the contrary, Southern Africa is generally in a state of horizontal extension due to its high elevations which causes the density moment to be higher than those of the spreading ridges. While the NW-SE band of NW-SE directed most compressive horizontal principal stress (the Wegener stress anomaly) does exist, in many places it is actually caused by NE-SW extensional tectonics (Bird et al. in 2006). As mentioned before, this tension results from the unbroken lithosphere's resistance to relative rotation between the Somalia- and African Plates.

2.4. Previous work pertaining to structural geology's influence on groundwater in the Limpopo Belt:

A study similar to the one discussed by this report was conducted at two locations in the Central Zone (CZ) of the Limpopo Belt by Sami et al. (2002) from the Water Research Commission of South Africa. The first location falls within the Bochum- and Soutpansberg Districts and the second location forms a block between Messina, Tshipise, Gaandrik and Esmefour. Although this paper's study was conducted in the Southern Marginal Zone of the Limpopo Belt, the structural information from the adjacent Central Zone is very useful as the stress regimes causing the structures were not necessarily confined to either of these zones.

STRUCTURES IN PRE-KAROO LITHOLOGIES

First of all, Sami et al. (2002) investigated the structures in pre-Karoo lithologies. It was found that joints are best developed in more siliceous, homogenous lithologies such as granitic orthogneisses and quartz veins, as compared to poor jointing in heterogenous banded supracrustals. The ages of fractures vary from the earliest deformation recorded in the Soutpansberg Group to the young structures that formed during the breakup of Gondwana during Karoo times, as well as structures (if any) developed during post Karoo uplift (Sami et al., 2002). Joints found in pre-Karoo lithologies at location I are dominated by steep dips (>70˚) suggesting a sub-horizontal, extensional environment during formation. Strikes of these joints are predominantly orientated ~N, NW and WNW, where the latter two directions are similar to those found at location II. Most of the joints found in pre-Karoo lithologies at location II also dip steeply (>60˚), but numerous joints with dips <60˚ are also present. The joints dipping <60˚ are likely from the sinistral transpressional faulting observed by Jansen (1975) and Barker (1983). Joints found in pre-Karoo lithologies at location II strike mainly NW to N, with fewer groups striking NE and ENE (Sami et al., 2002).

STRUCTURES IN KAROO-AGED LITHOLOGIES

Karoo-aged lithologies that were investigated by Sami et al. (2002) include sandstones mudrocks and siltstones from the Clarens Formation, Karoo basalts and dolerite dykes. The best developed joints are found in the basalts and dolerites, with lesser joints in the sandstones and mudstones respectively. Karoo-aged joints found at location I once again dip steeply (>70˚) and strike in two main directions, WNW and NE. In location II, Karoo-aged joints dip >60˚, almost without exception and strike ENE to E with minor NNE orientations (Sami et al., 2002). ENE to E-striking joint and dyke orientations are consistent with the extensional regime that existed during Gondwana fragmentation. An inferior NNW direction which suggests ENE extension also exists and correlates with the two-stage Gondwana fragmentation described by Cox (1992) and Grantham (1996).

HYPOTHESIS IN TERMS OF TARGETS FOR GROUNDWATER

When exploring for groundwater, brittle structures that have been subjected to tension for a relatively long time are usually good targets. For this reason Sami et al. (2002) believe that structures striking almost perpendicular to the N-S extension since Waterberg times (such as the Bosbokpoort-Tshipise faults discussed in the previous section) are promising targets for groundwater. Furthermore, it is believed that NW and NE striking structures that have been reactivated by shear might also be good groundwater targets depending on the lithology in which such structures are found (Sami et al., 2002). This belief probably holds some truth, as Anderson and Ainslie (1994) conducted a study in the same area as location I of Sami et al. (2002) and found that NNE and NNW structures were most successful in terms of groundwater exploration.

GROUNDWATER DRILLING RESULTS

Through exploration drilling, Sami et al. (2002) discovered that regional scale normal faults are the most important water bearing targets in their study area, especially rejuvenated shear systems. Small-scale faults and local-scale structures can contain groundwater, but have lower groundwater potentials. Alluvial deposits and deeply weathered overburden (deep weathering on NW or NE striking faults) are additional aquifers. Regions where streams dog-leg in an easterly direction are especially favourable for groundwater. Interestingly, lithological contacts and dyke/sill structures were found to be dry or low yielding, but some ENE tectonic contacts were water-bearing (Sami et al., 2002).

3. RESULTS:

3.1. General:

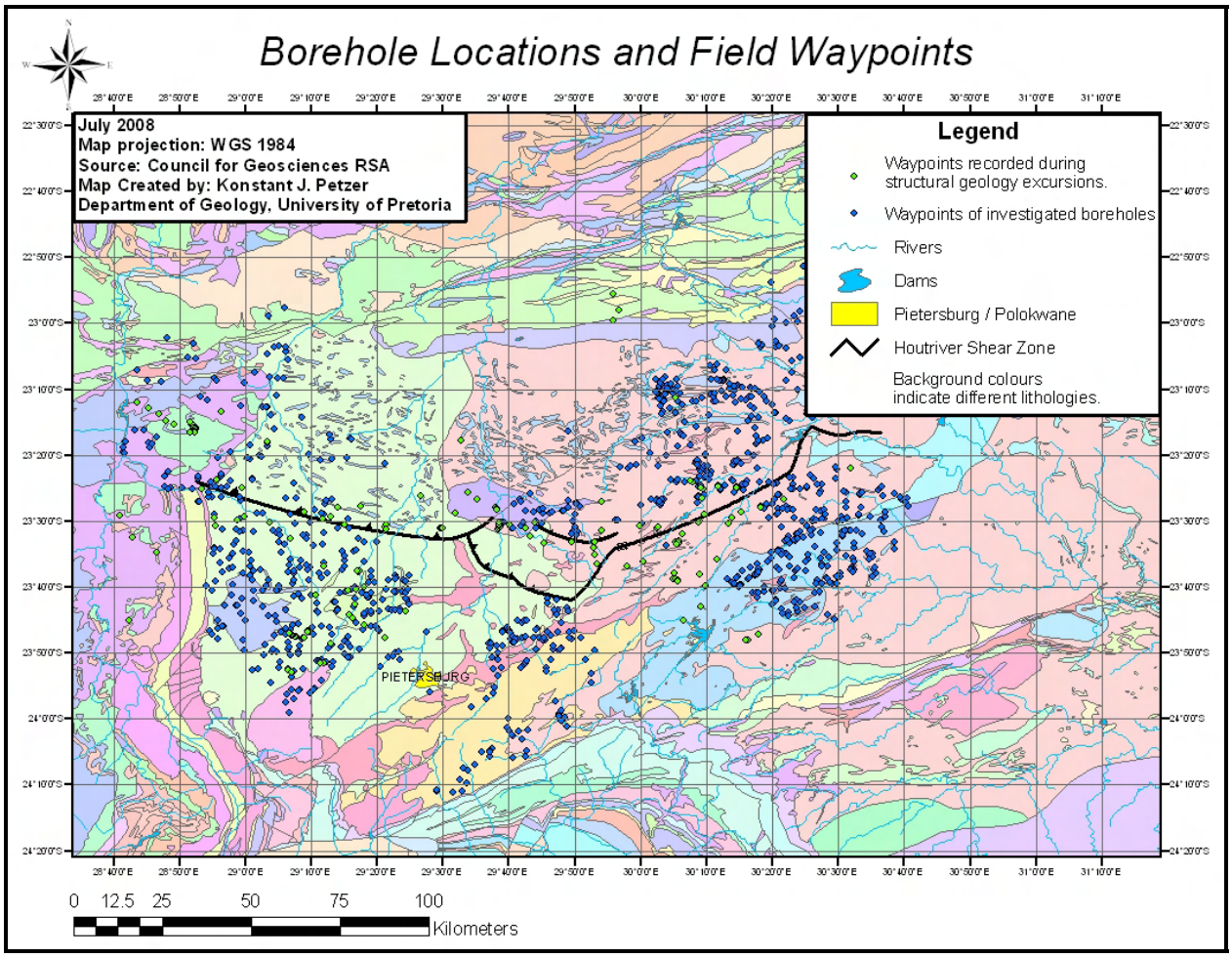

Figure 15: A map showing the location of the boreholes that were analyzed in this study and the waypoints recorded in the field while gathering structural geological data.

3.2. Joints:

JOINTS OVERALL:

Joints play a cardinal role in this project as they are the most common of all the brittle geological structures in the study area. Though joints often form together with faults, the structures described in this section as "joints" refer to the fractures in rocks on which shear displacement (if any) is too small to notice with the unaided eye. Firstly, a combination of dip and strike values were used to construct stereographic projections of the poles of all the measured joint planes (Appendix). Unfortunately, this proved to be less indicative of preferred orientation patterns in three-dimensional space than expected.

Although the overall distribution of joint orientations in the study area is fairly random, some sensible conclusions can still be made from Figure 16, Figure 17 and Figure 18. Firstly, a slight majority of joint strikes are orientated NW-SE and NE-SW. Hypothetically speaking,

NW-SE-striking joints should be favourable for groundwater flow, seeing as the neotectonic tension is NE-SW and should open these joints up (Bird et al. in 2006). Secondly, the NE-SW-striking joints could have been reactivated through strike-slip by the neotectonic stress, causing such joints to also have a water bearing capability. Furthermore, the majority of the joints have steep dips which often indicate formation in a tensional environment (see Anderson's theory in the literature review).

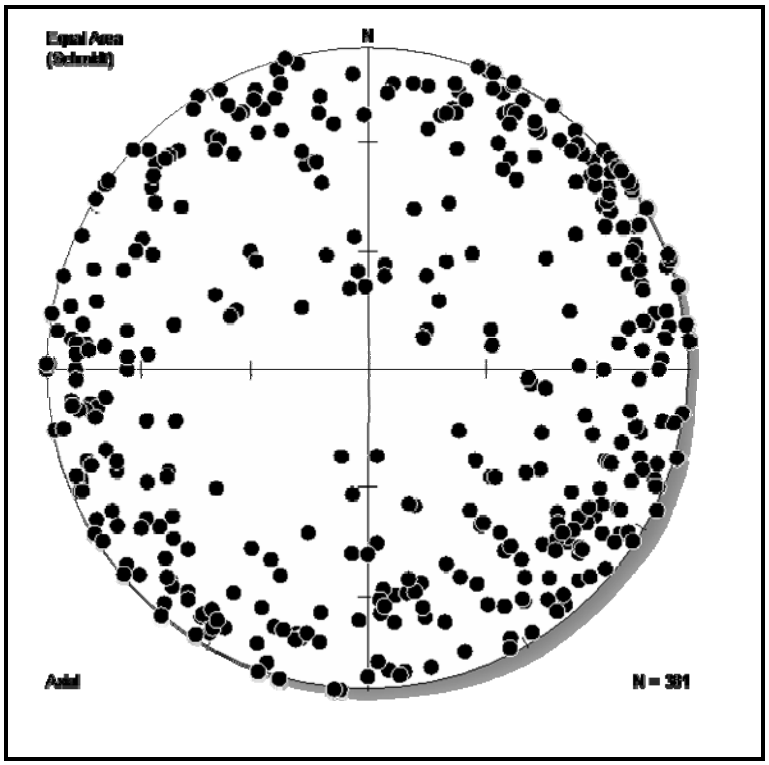

Figure 16: Poles to all joint planes.

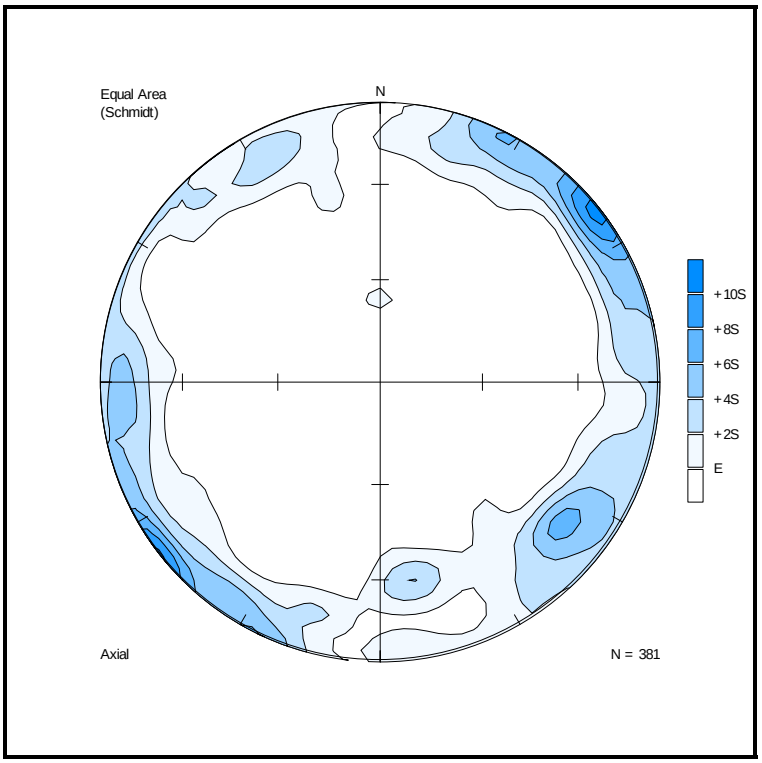

Figure 17: Density distribution of all poles to joint planes.

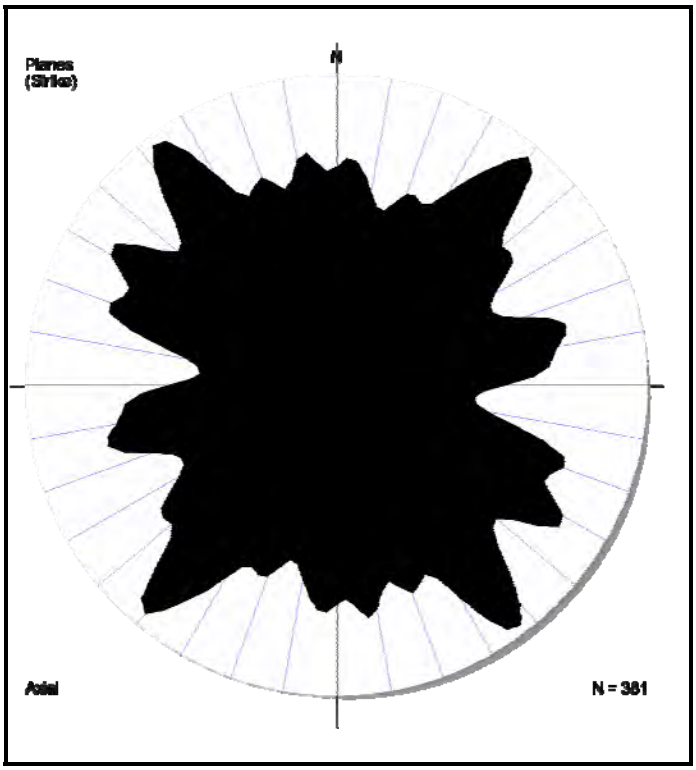

Counting Parameters

Number of Data Points in Set	381
Number of Data Points Included	381
Type of Data	Planes (Strike)
Range of Dip Angles	0° - 90°
Class interval	10°
Class Alignment	Centered at 0°N
Kurtosis, k, of Smoothing Function	206
Half-width of Smoothing Function	±4.7°
Unweighted Calculation	

Frequency Statistics

Mode (Peak)	7.9%
Azimuth Range of Mode	35° - 45°
Smooth Peak	7.6%
Azimuth of Smooth Peak	142.5°
Expected Value, E	5.6%
Standard Deviation	1.7%
95% Confidence Levels	<2.1% & >9.0%

The distribution is statistically uniform.

Figure 18: Rose diagram derived from the strikes of all joint planes.

JOINT INTERSECTION LINEATIONS:

Since no strongly preferred orientation of joints was found locally (i.e. between two or three closely spaced waypoints), the possible existence of another preferred linear orientation was investigated. Lineations along which groundwater flow might be concentrated were calculated from the intersections of joint planes. Theoretically, such intersections can receive water from the two or more joints creating it. The orientation of these linear intersections were plotted stereographically and analyzed for their density distribution on contoured stereographic projections (see Figure 115 to Figure 139 in the appendix). Unfortunately, this exercise also proved inconclusive, since no dominant preferred three dimensional orientation was found regionally from the intersection lineations. Nevertheless one can draw the conclusion that most of the intersection lineations are steeply inclined (making them difficult targets for drilling, but important for the infiltration of surface water) and it appears that a small majority of intersection lineations plunge towards the northwest. Unfortunately, the total amount of intersections was too large for Spheristat2.2 to plot on a single stereographic projection and therefore the intersections were once again plotted on individual 10' x 10' blocks of latitude and longitude (Figure 115 to Figure 139 in appendix). On a more local scale, the following stereographic projections did show some clustering of sub-horizontal intersection lineations: S23˚ 20' E28˚ 50' (SSE); S23˚ 30' E29˚ 20' (NE-SW); S23˚ 40' E30˚ 00' (NW); S23˚

40’ E30˚ 10’ (NW-SE and SW); S23˚ 50’ E29˚ 10’ (NE- SW). Due to their sub-horizontal nature the trends of these clusters are closely related to the major strike directions of the joints that formed them (true for most of the blocks mentioned). It is also worthy to note that the rivers that occur in the blocks mentioned flow parallel to the trend of the sub-horizontal clusters of joint intersects.

JOINT STRIKES:

It was decided to simplify the joint orientation investigation to two dimensions by constructing rose diagrams of the joints’ strikes. Even at a local scale, very few joint sets showed a definite preferred orientation in their strike, and/or matched the preferred orientation of joints at an adjacent waypoint. In Figure 19, the strikes of the joints were grouped together in 10’x10’ blocks on the geology map and plotted onto rose diagrams to determine the major strike directions for each block. The individual rose diagrams can be seen in the appendix. From Figure 19, it quickly becomes apparent that most joints are not confined to lithological boundaries and that the events that caused the joints usually had similar structural effects throughout a certain area, regardless of the lithologies encountered during that event. Consequently, it was decided not to describe the distribution of joints in terms of their lithological location, but rather to relate their spatial distribution to a known regional feature such as the Hout River Shear Zone.

In Figure 19 the rose diagrams indicating the strikes of joints have been spatially represented on a geology map. Each of these rose diagrams were colour coded according to the major strike directions in that specific 10’x10’ block. Due to the lack of outcrops and accessibility, the whole map could not be covered in 10’x10’ rose diagrams, but nonetheless the data available is fairly well spread over the study area. Although this is not the most statistically correct method for orientation interpretations, it does help to quickly identify and group major strike directions of joints in the study area. In this way, if any patterns are observed at a quick glance, it is easy to compare the patterns to the spatial representation of transmissivity and sustainable yield values at a later stage in the investigation.

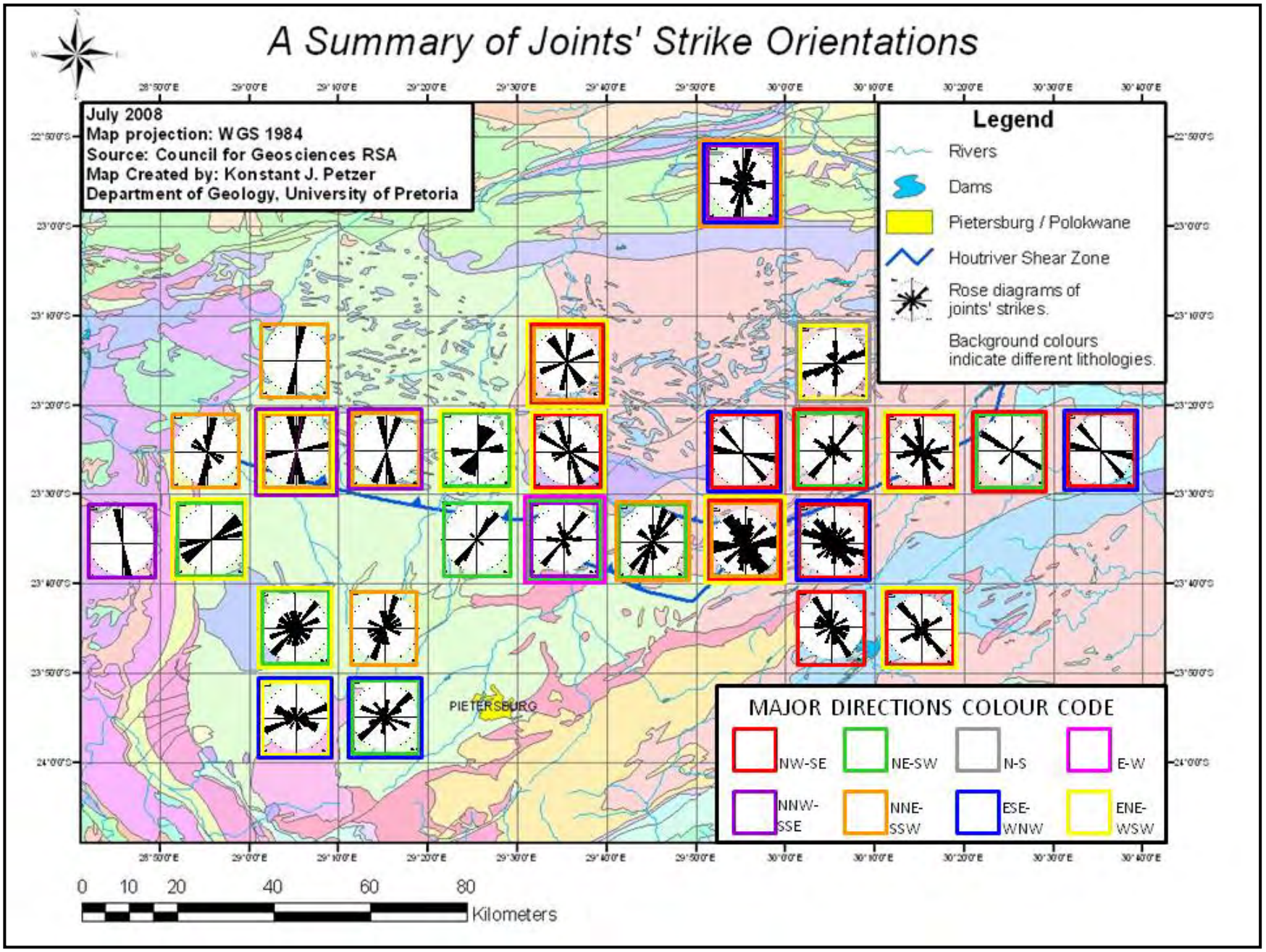

Figure 19: A map summarizing the major strike directions of joints in each 10' x 10' block that yielded field measurements.

Figure 19 shows that the NE-SW striking joints are predominantly found in areas south of or on the Hout River Shear Zone (HRSZ). Apart from the fact that NE-SW joints could have been reactivated as strike-slip faults, they also run parallel to the major dyke swarms of the area which might add an additional advantage in terms of groundwater storage or flow due to compartmentalisation of the aquifers. Unlike the NE-striking joints, areas with major joint strikes orientated approximately N-S were mostly found to the north of the HRSZ. NW-SE striking joints are reasonably continuous throughout the centre of the map in a NW-SE line and also towards the east of the study area. This might mean that the NW-SE striking joints are the most penetrative (i.e. have the longest extent) and that some of the same joints were recorded at more than one locality. If this assumption holds true, the NW-SE trending joints are once again likely to be favourable conduits for groundwater. However, with a lack of outcrop and generally limited exposure, it is difficult to establish the lateral extent of joints. Despite being the most penetrative, NW-striking joint sets run perpendicular to most of the other structures observed in the area (such as dolerite dykes; Figure 7). Since the NE-trending structures cross-cut the NW-trending joints, the theory that these joints are favourable pathways for groundwater might be invalid. Perhaps the intersections of the NW-trending joints and the perpendicular structures blocking these joints are worthy targets for groundwater, but this has yet to be demonstrated through more precise drilling in the future. If the dykes that intersect the NW-striking joints are themselves conduits for groundwater, as they often are, the intersections of these features would especially be worth investigating. Lastly, East-northeast (a direction demonstrated by many of the geological structures in the area, including the LB) is one of the other strike directions of joint planes fairly commonly recorded throughout the study area.

It is important to note that just because certain joint orientations are dominant doesn't necessarily mean that these joints are better groundwater conduits than others. The considerable number of variables controlling groundwater flow/occurrence does not require a direct relationship between dominant joint orientation and flow direction to exist. Minor joint sets or other secondary structures may also be important conduits.

JOINT GROUPS BASED ON DIP ANGLES:

After investigating all joints jointly, it was decided to divide the joints up into groups based on their respective dip angles. The reason for this subdivision is the fact that different dips in joints and shear joints are mostly the result of different stress/strain regimes during times of formation (Anderson's Theory). Figure 20 shows a rose diagram of joints with shallow dip angles, ranging from 0˚ to 45˚. According to Anderson (1951), shallow dips (~30˚ from horizontal) are the result of thrusting, where σ_3 is vertical. If one disregards the formation of permeable mylonite during thrusting and only consider the stress/strain conditions at

work, compressional thrust faults and their associated joints are less favourable for groundwater exploration than their tensional counterparts.

Table 3: Measured joint quantities. (* Sum not exactly equal to 100% due to rounded averages)

Dip angle of joints	Comment	Amount of joints	Percentage
Shallow (0˚ - 45˚)	Usually thrust (compression) induced or decompressional	36	9.45%
Moderate (46˚ - 79˚)	Usually tensionally induced	188	49.34%
Steep (80˚ - 90˚)	Strike-slip, or Mode I tensional joints	157	41.21%
All joints (0˚ - 90˚)		381	100% *

Of all the measured joints, the shallow dipping ones were by far the least common. Even though the statistical distribution on the rose diagram (Figure 20) was once again uniform, a majority of shallow angle joints striking NE-SW does exist. Thrusts striking NE-SW are possibly from Neoarchaean times, as many of the tectonic features from this time have north-eastern trends. Moreover, older thrusts with NE strikes also exist from when the Pietersburg- and Giyani Greenstone Belts formed (De Wit et al., 1992). There is also a minor NNE-SSW strike present among the shallow joints, possibly from the $\mathbf{D_1}$ event mentioned by Passeraub et al. (1999) prior to formation of the HRSZ, or from the Limpopo Orogeny. Sub-horizontal joints can also form by dilatation (pressure release i.e. by means of erosion) or as cooling joints of plutons. The distribution of shallow-dipping joints is fairly well spread over the study area, implying that the whole area was likely subjected to compression at one time or another, with σ_1 orientated horizontally (see Figure 21).

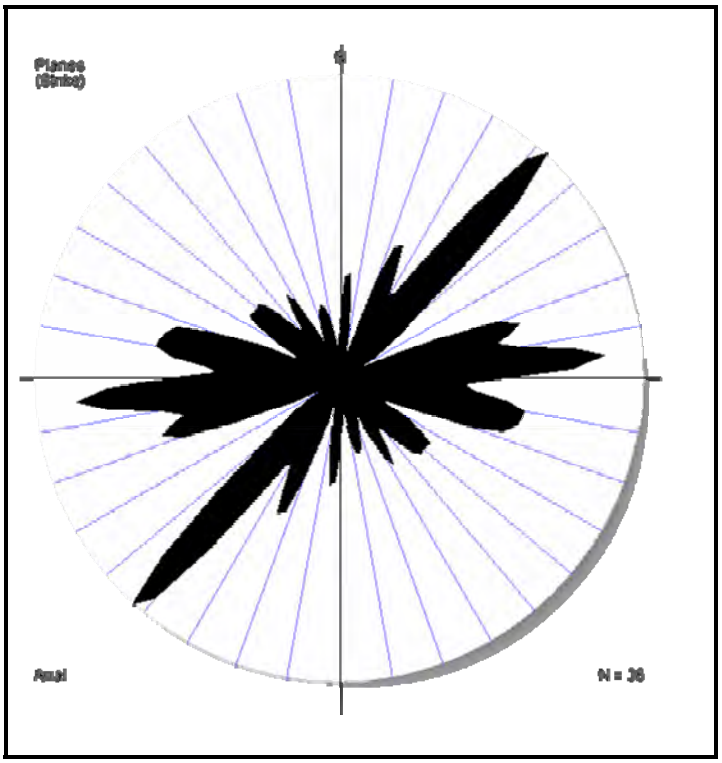

Counting Parameters	
Number of Data Points in Set	36
Number of Data Points Included	36
Type of Data	Planes (Strike)
Range of Dip Angles	0° - 45°
Class interval	10°
Class Alignment	Centered at 0°N
Kurtosis, k, of Smoothing Function	206
Half-width of Smoothing Function	±4.7°
Unweighted Calculation	

Frequency Statistics	
Mode (Peak)	13.9%
Azimuth Range of Mode	35° - 45°
Smooth Peak	15.1%
Azimuth of Smooth Peak	42.5°
Expected Value, E	5.6%
Standard Deviation	5.6%
95% Confidence Level	>16.8%

The distribution is statistically uniform.

Figure 20: Rose diagram derived from the strikes of shallow-dipping (0˚ - 45˚) joints.

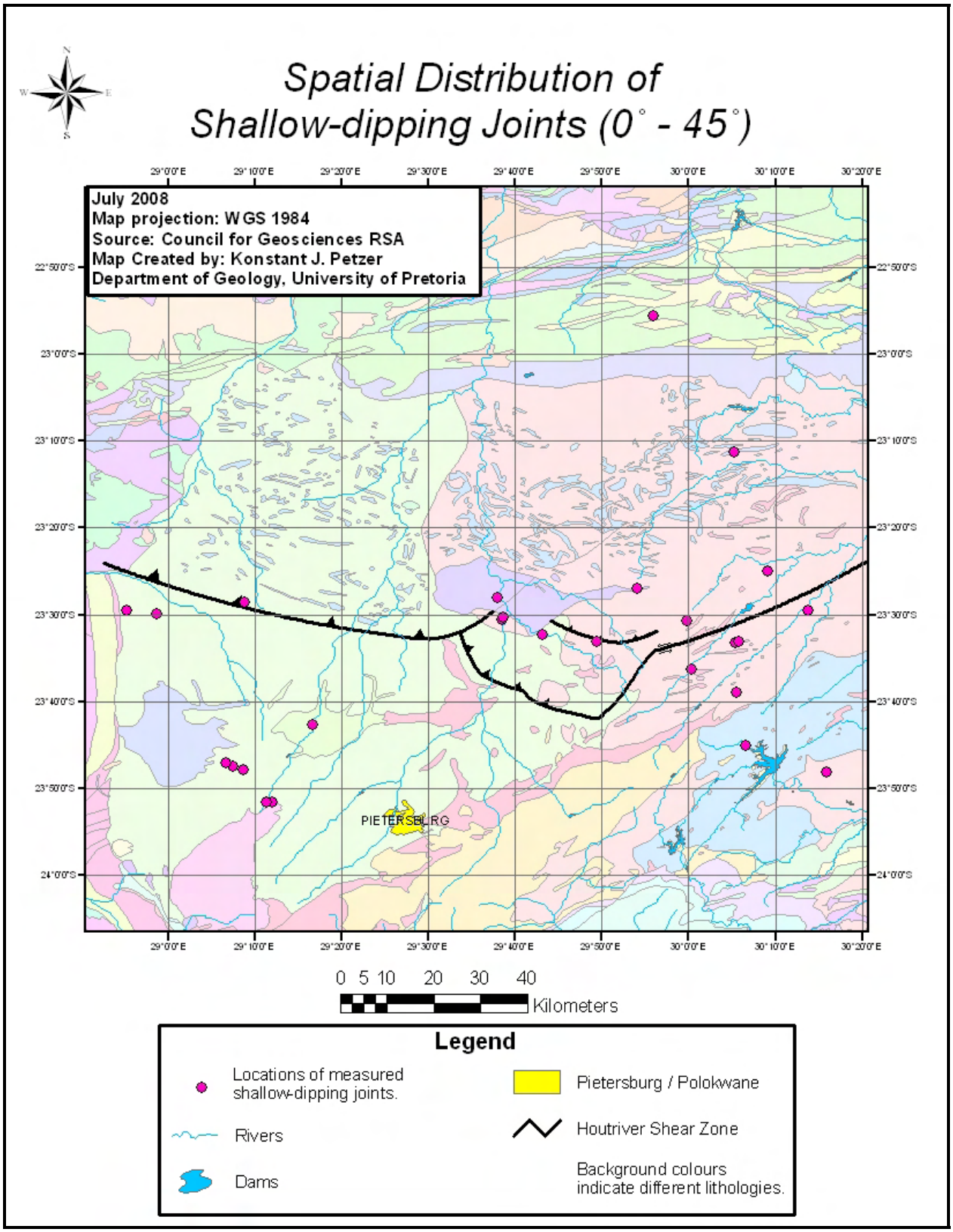

Figure 21: A map showing the spatial distribution of shallow-dipping joints that were measured. Note that the distribution of shallow dipping joints is not confined to one specific measured area on the map.

Moderately dipping joints (46˚ – 79˚) were investigated in Figure 22. This range of dips includes the dips formed during normal (or reverse) faulting (~60˚ dip). Normal faults and their associated joints form in a tensional regime in which σ_1 is vertical and S_1 is perpendicular to strike (Anderson, 1951). Theoretically, joints that formed under these conditions are the most suitable joints in the search for groundwater due to their dilation property. When looking at Figure 23 one can see that the distribution of azimuths for moderately dipping joints is statistically uniform. Only a slight majority of moderately dipping joints (9.6%) are striking NE-SW. Since no clear preferred orientation was found in the strikes of the moderately dipping joints it was decided to investigate the ones that are orientated sub-parallel to the more recent tectonic regimes (Karoo and Neotectonic regimes). Moderately dipping joints that strike approximately E-W (perpendicular to the N-S extension that occurred during the breakup of Gondwana), as well as those that strike approximately NW-SE (perpendicular to neotectonic extension) are both spread out quite uniformly over the study area, but are mainly found south of the HRSZ (See Figure 19 and Figure 23). However, it might only be the lack of outcrop north of the HRSZ that lead to this observation.

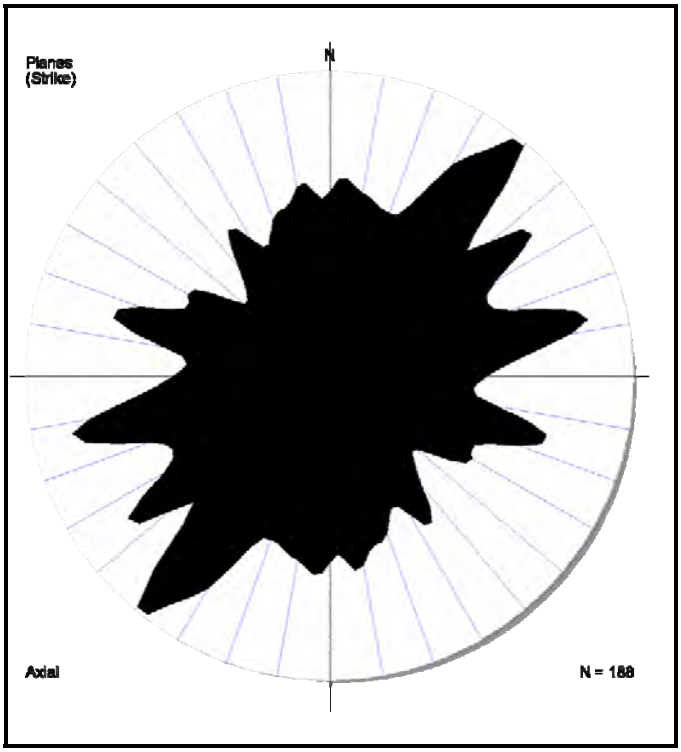

Figure 22: Rose diagram derived from the strikes of moderately dipping (46˚ - 79˚) joints.

Counting Parameters

Number of Data Points in Set	188
Number of Data Points Included	188
Type of Data	Planes (Strike)
Range of Dip Angles	46˚ - 79˚
Class interval	10˚
Class Alignment	Centered at 0˚N
Kurtosis, k, of Smoothing Function	206
Half-width of Smoothing Function	±4.7˚
Unweighted Calculation	

Frequency Statistics

Mode (Peak)	9.6%
Azimuth Range of Mode	35˚ - 45˚
Smooth Peak	8.9%
Azimuth of Smooth Peak	40.0˚
Expected Value, E	5.6%
Standard Deviation	2.5%
95% Confidence Levels	<0.6% & >10.5%

The distribution is statistically uniform.

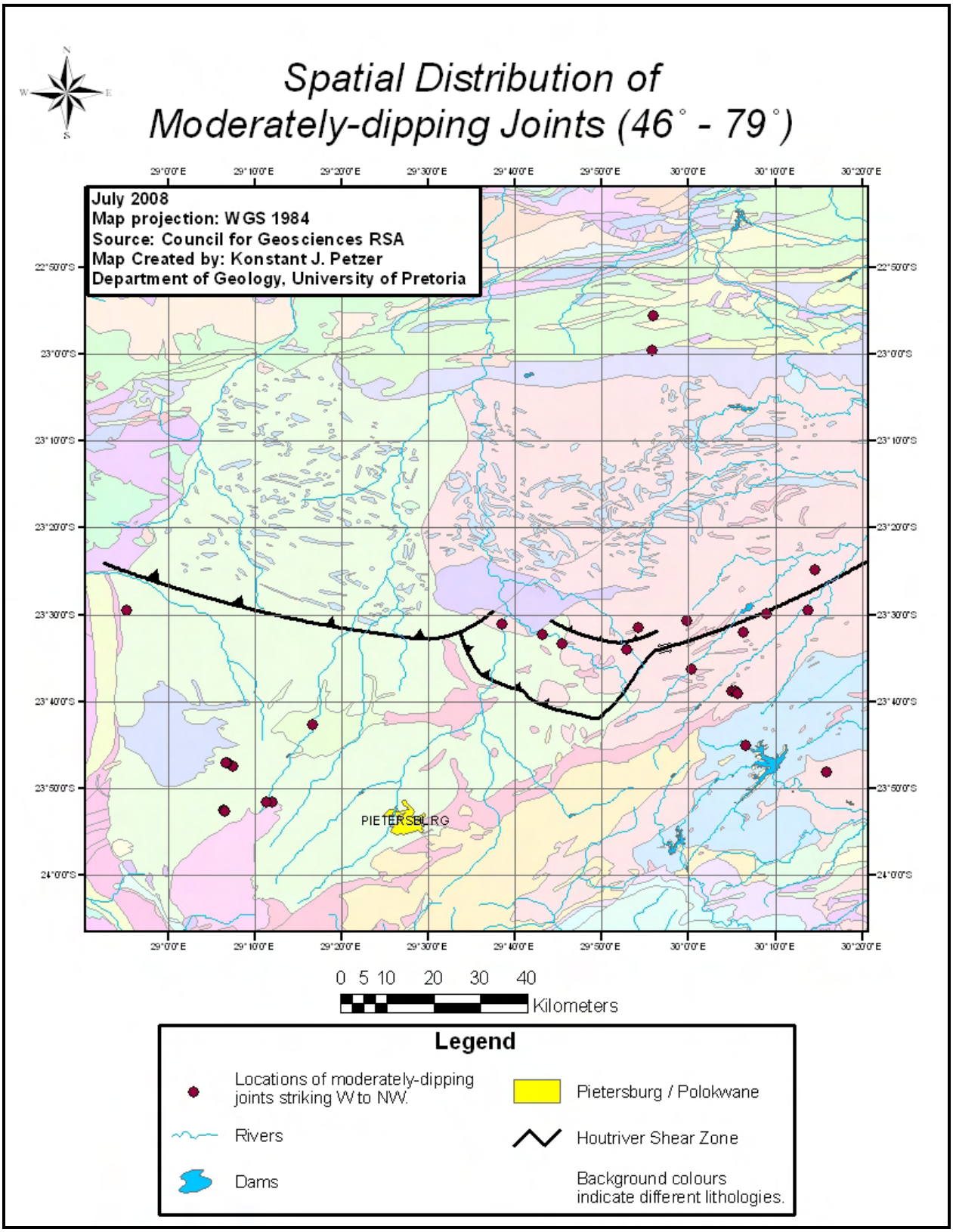

Figure 23: A map showing the spatial distribution of measured joints with moderate dip angles and strikes between W and NW. The distribution of moderately-dipping joints is slightly concentrated on the eastern side of the study area, but still fairly dispersed over all the measured areas.

The last group of joints are sub-vertical to vertically dipping (80˚ - 90˚) which are either strike-slip shear joints or mode I tensional joints. Strike-slip faults and their associated joints form when σ_2 is vertical (Anderson, 1951). However, since no shear displacement was noticed in these joints, the majority of the steep joints measured are classified as mode I tensional joints. Once again, the "opening up" property of these joints is what makes them sought after as possible conduits for the flow of groundwater. Unlike the other groups of joints, the steep joints did show a statistical preferred orientation striking NW-SE, as seen on the rose diagram in Figure 24. Then again, just as the joint groups discussed previously, the steep joints also show a uniform spatial distribution over the study area and are not concentrated in a specific area (see Figure 25). Due to their strike, the steep joints in the area likely formed under neotectonic stress conditions and show potential for groundwater.

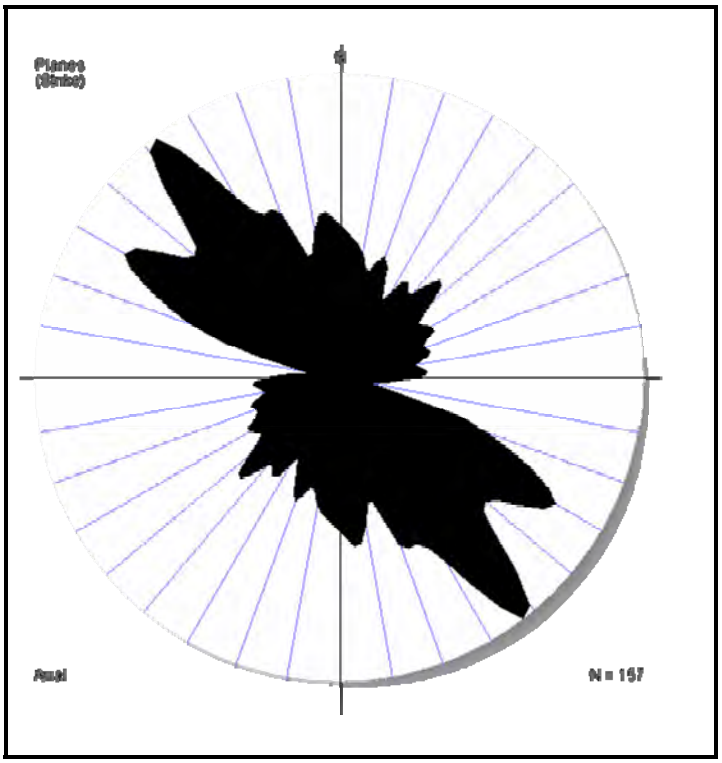

Counting Parameters

Number of Data Points in Set	157
Number of Data Points Included	157
Type of Data	Planes (Strike)
Range of Dip Angles	80° - 90°
Class interval	10°
Class Alignment	Centered at 0°N
Kurtosis, k, of Smoothing Function	206
Half-width of Smoothing Function	±4.7°
Unweighted Calculation	

Frequency Statistics

Mode (Peak)	12.1%
Azimuth Range of Mode	135° - 145°
Smooth Peak	12.0%
Azimuth of Smooth Peak	142.5°
Expected Value, E	5.6%
Standard Deviation	2.7%
95% Confidence Levels	<0.2% & >10.9%

The distribution has a preferred trend.

Figure 24: Rose diagram derived from the strikes of steeply dipping (80˚ - 90˚) joints.

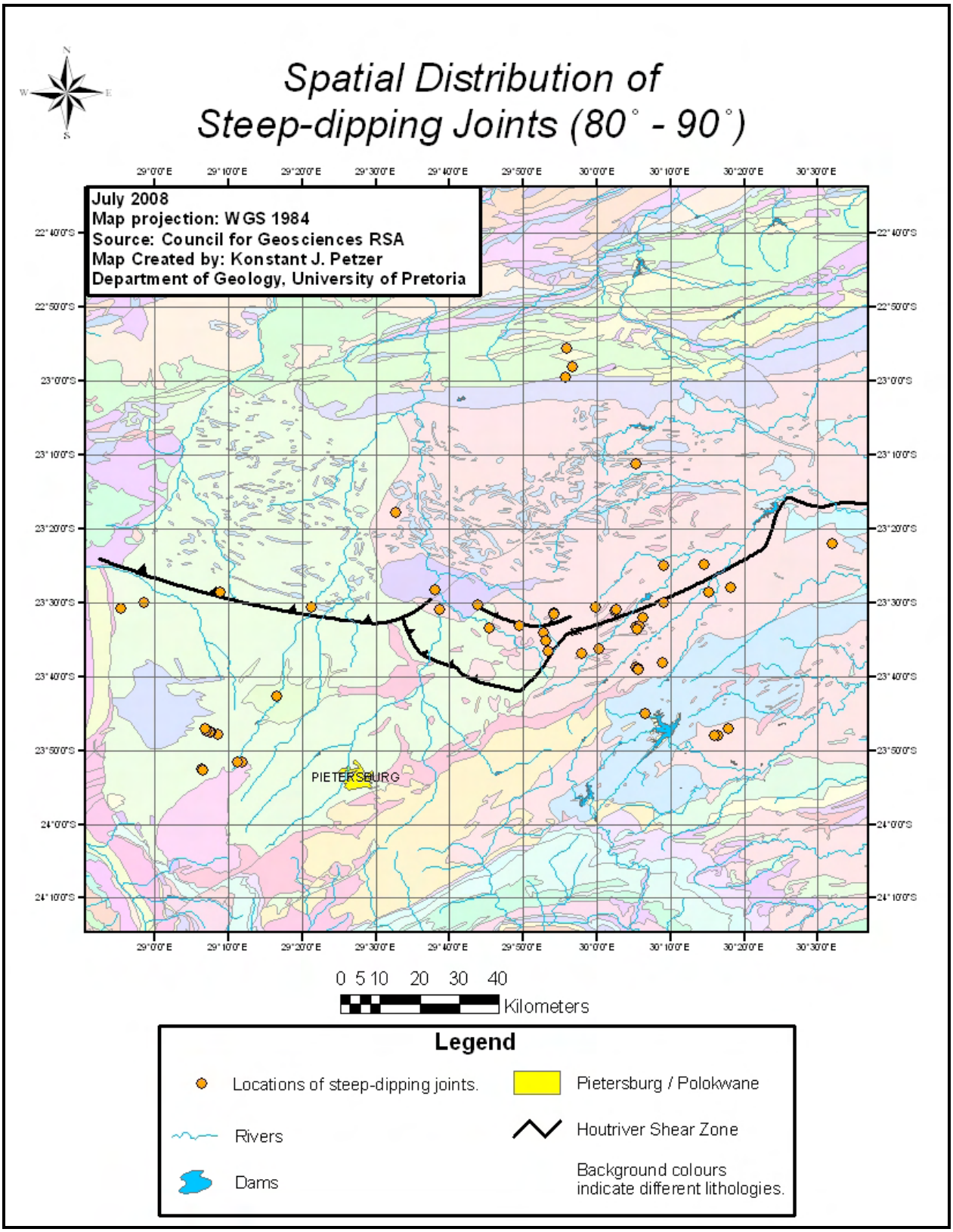

Figure 25: A map showing the spatial distribution of measured joints with steep dip angles. Steep-dipping joints are the most uniformly distributed spatially throughout the study area.

It is essential to note that not all joints will exactly meet the description of the joints described above and that combinations of joints may also occur. Often, joints are formed due to simultaneous lateral and vertical forces acting on a rock in which case a combined name such as “normal dextral fault” is used to describe it. However, as mentioned before, this section only deals with joints in which displacement is too small to notice. Thus the joints were only grouped based on their angle of dip and not on their sense of movement, as this will be discussed under the section for faults.

Figure 26: A Google Earth satellite image of the eastern margin of the Waterberg Group (the western boundary of the study area). Note how clearly visible the NE, E and SSE-striking joints are in the supracrustal rocks of the Waterberg and how these joints dissipate in the basement lothologies on the east.

Figure 27: Slightly weathered gneiss with well-preserved joint sets.

3.3. Faults and shears:

FAULTS AND SHEARS GENERAL INFORMATION:

Although not quite as common as joints, faults are invaluable to the study of structural geology and its relevance to the flow of groundwater. The same principles of groundwater flow in joints are also applicable to faults. Larger, brittle faults that contain brecciated material are especially favourable settings for groundwater movement and normal faults might be of great interest to this study, as they represent extension. Of all the faults observed in the field, N-S and WNW-ESE striking faults were most common, followed by NE-SW and ENE-WSW striking faults. However, as mentioned before, there is a lack of outcrops in certain parts of the study area and therefore only a few faults could be identified and measured. Besides the lack of outcrop, the lack of positive topography displayed by pre-tectonic lithologies made the task of identifying the vertical sense of movement of faults extremely difficult. In fact, only a handful of faults could be classified based on their vertical movement (not nearly enough for any statistical conclusions to be drawn) so the faults were compared to one another more on the basis of their lateral sense of movement. This is one of the main reasons why the author decided to divide the joints up into different groups based on their dip angles. In fact, all the information discussed under the section for joints (section 4.1) can be considered under this section for faults, because most of the principles of formation are identical for both these types of structures.

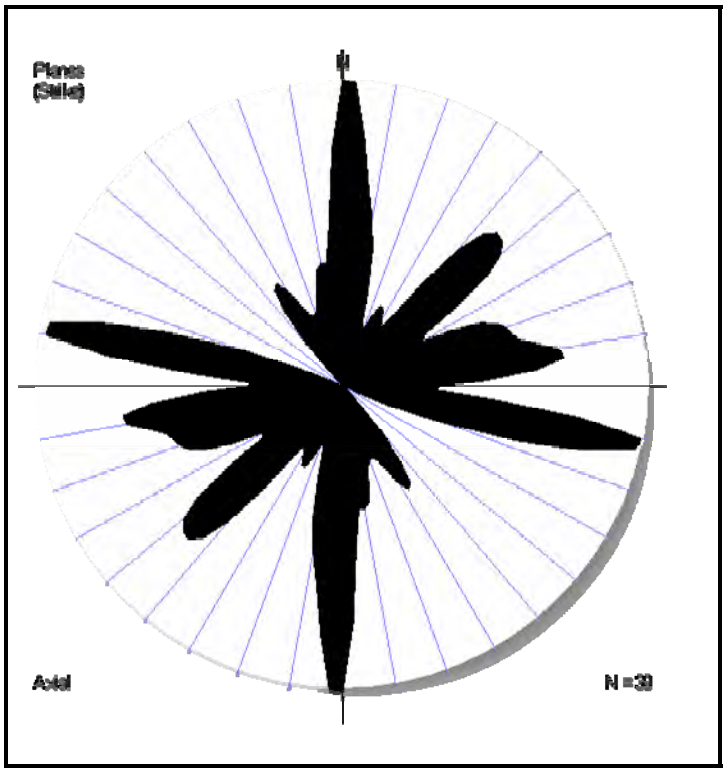

Counting Parameters	
Number of Data Points in Set	39
Number of Data Points Included	39
Type of Data	Planes (Strike)
Range of Dip Angles	0° - 90°
Class interval	10°
Class Alignment	Centered at 0°N
Kurtosis, k, of Smoothing Function	206
Half-width of Smoothing Function	±4.7°
Unweighted Calculation	

Frequency Statistics	
Mode (Peak)	12.8%
Azimuth Range of Mode	-5° - 5°
Smooth Peak	13.2%
Azimuth of Smooth Peak	0.0°
Expected Value, E	5.6%
Standard Deviation	5.4%
95% Confidence Level	>16.4%
The distribution is statistically uniform.	

Figure 28: Rose diagram derived from strikes of faults observed in the field.

In order to better grasp the spatial distribution of faults in the area of interest, geophysical data (aerial magnetic survey) was acquired to look for the displacement of dykes and other features as an indication of faulting. Unfortunately this method also mainly looks at lateral displacement (of dykes in this case) and it is uncertain whether all the normal and reverse faults, as well as faults parallel to the dolerite dykes were properly detected. It was also found that the data supplied by the Council for Geoscience of South Africa only covers patches of the total study area. By using the aerial magnetic data available, it appears as if the regional scale faults found in the basement lithologies mostly strike NW-SE (Figure 29), except in the Giyani Greenstone Belt region, where the regional faults mostly strike NE-SW. One must remember that the majority of dolerite dykes in the area strike NE or NNE, which could have made it more difficult to detect NE-SW striking faults.

Once again, when taking into consideration the neotectonic stress/strain directions (NE extension and NW compression; Bird et al., 2006), the NW- trending faults may be worthy targets for groundwater exploration. Faults that are sub-parallel to the extension direction (NE-SW) could also have been reactivated by strike-slip, which means that such faults can't be excluded as targets for groundwater.

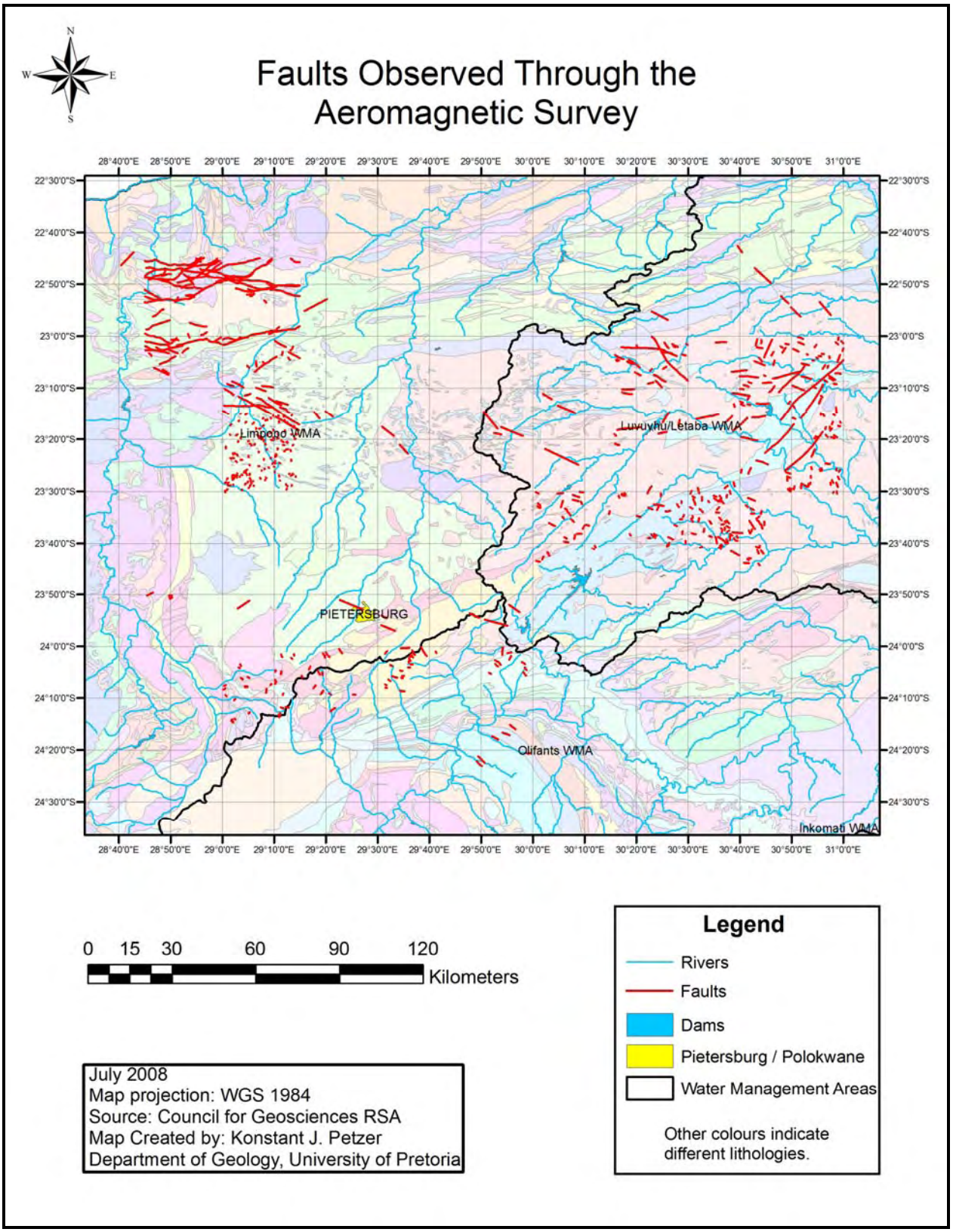

Figure 29: A map indicating some of the faults in the study area that were observed through an aeromagnetic survey by the Council for Geosciences of South Africa.

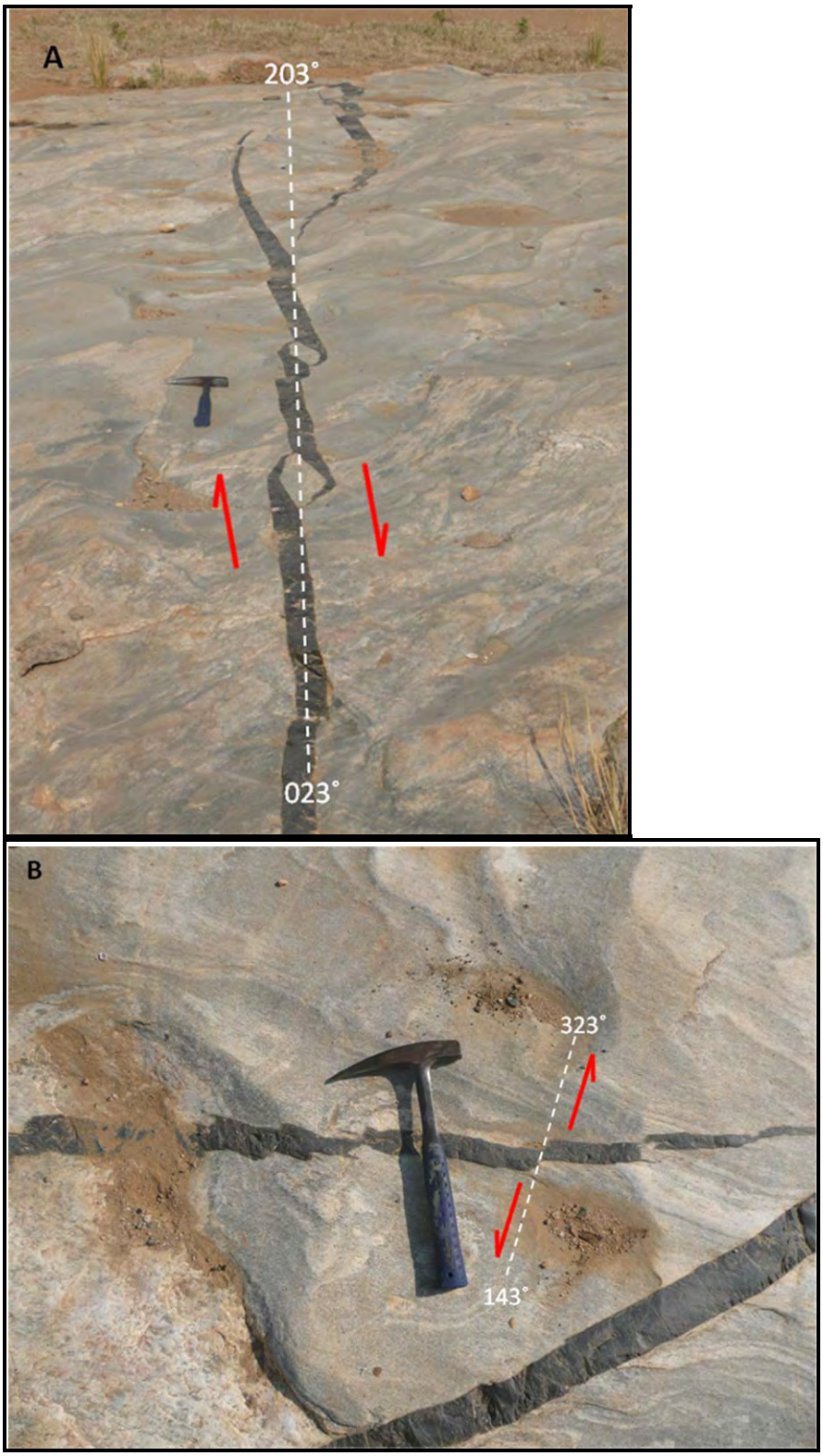

Figure 30: Near the township of Middelwater is an interesting outcrop of migmatite containing some joints, dolerite stringers, and evidence for a few episodes of shearing. (A) In this figure an episode of dextral shear caused the dolerite stringer to form characteristic "pull-apart" formations in the dolerite stringer. The azimuth of this shearing event is slightly offset from the original azimuth of the dolerite stringer, indicated in white. (B) A later event caused step-like sinistral shear in the dolerite stringers along a different orientation.

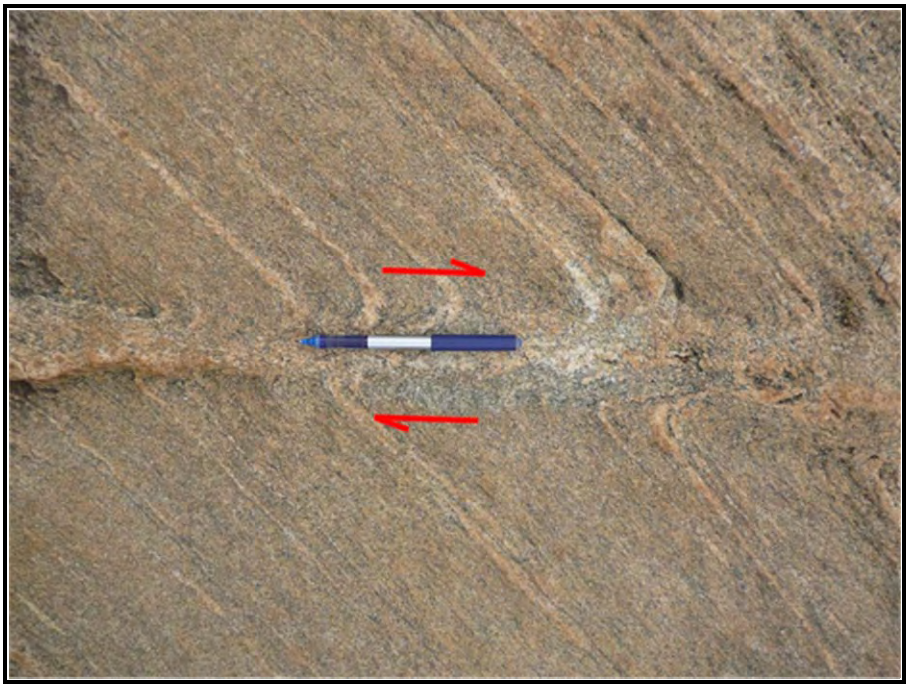

Figure 31: Dextral shear in a banded granitoid.

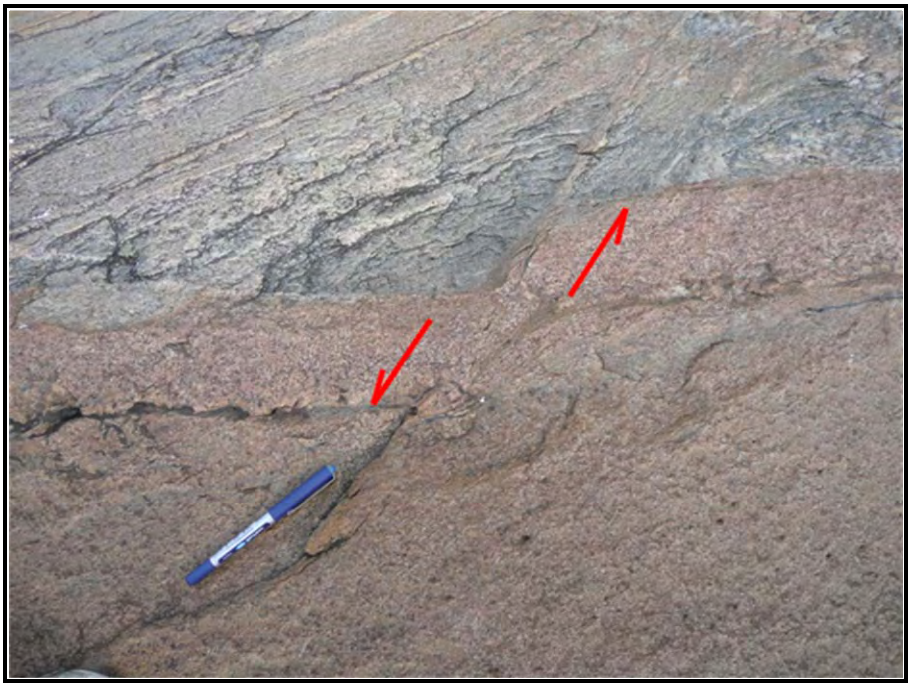

Figure 32: A small sinistral fault shown by the displacement of a pegmatite vein in granitic gneiss.

THE HOUT RIVER SHEAR ZONE:

According to Perchuk (2000) the Hout River Shear Zone can be up to 5km wide in some areas. With that in mind, it was decided to build a 2.5km buffer (a locus of all points on the topographical surface that are 2.5km and closer from the HRSZ) around the approximate location of the HRSZ (on ArcGIS 9.2) so that the total width of the buffer is equal to 5km (Figure 33). Boreholes that fall within the HRSZ buffer demonstrated a higher average transmissivity value than that of the boreholes outside of the buffer, but the average sustainable yield value within the buffer proved to be less favourable than the average value from the rest of the boreholes (refer to Table 4). Considering the tremendous amount of displacement undergone by the HRSZ (vertical displacement of up to 15km; Miyano et al., 1992; Perchuk et al., 1996), it comes as no surprise that the transmissivity in the buffer is above average. The displacement along the shear planes most definitely would have formed more rocks such as mylonite (at greater depths under brittle-ductile conditions) and cataclasite (at shallower depths under brittle conditions). Brittle reactivation along the shear zone could also have converted mylonite into more permeable cataclasite, which could ultimately be responsible for the high transmissivity readings. A lower average of sustainable yield within the HRSZ could be due to a number of factors. The author suspects that the high transmissivity, combined with the geometry of the HRSZ might actually be some of the culprits causing the low Q-values in the following manner: Previous studies have shown that the HRSZ is a relatively steep structure that extends to deep crustal levels (for example Smit et al., 1992). Therefore, surface water and groundwater probably infiltrate and descend quickly (high transmissivity and strong pull by gravity down a steep angle) along the HRSZ to very deep levels that lie beneath the average drilling depth for water exploration. However, very few of the available borehole entries fall within the buffer created and therefore the T and Q relationships found will have to be substantiated by more data.

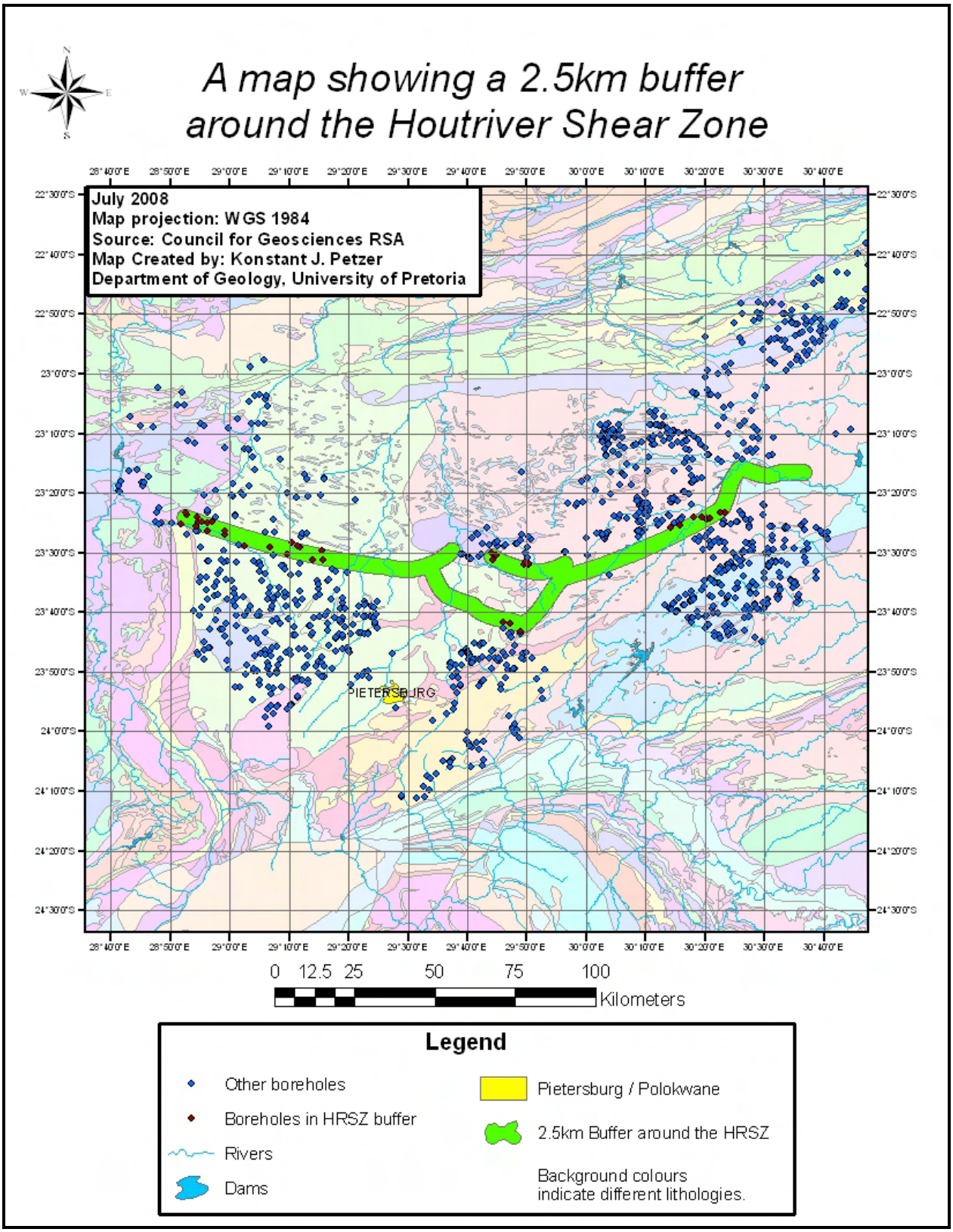

Figure 33: A map showing a 2.5km buffer around the Hout River Shear Zone (i.e. 5km wide) and the boreholes that fall within that buffer. Unfortunately not many of the boreholes that were analyzed fall within the buffer. Nonetheless, the mean average T-value of these boreholes did prove to be slightly higher than the average T-value of those outside of the buffer but that same relationship was not shown in the average Q-values.

Table 4: The mean average T and Q values from inside and outside of the 2.5km buffer around the Hout River Shear Zone.

	Mean Average Logan Transmissivity (T) $m^2/24hr$	Mean Average Yield (Q) L/sec./24hr
Inside HRSZ Buffer	47.33	1.08
Outside HRSZ Buffer	42.83	1.17

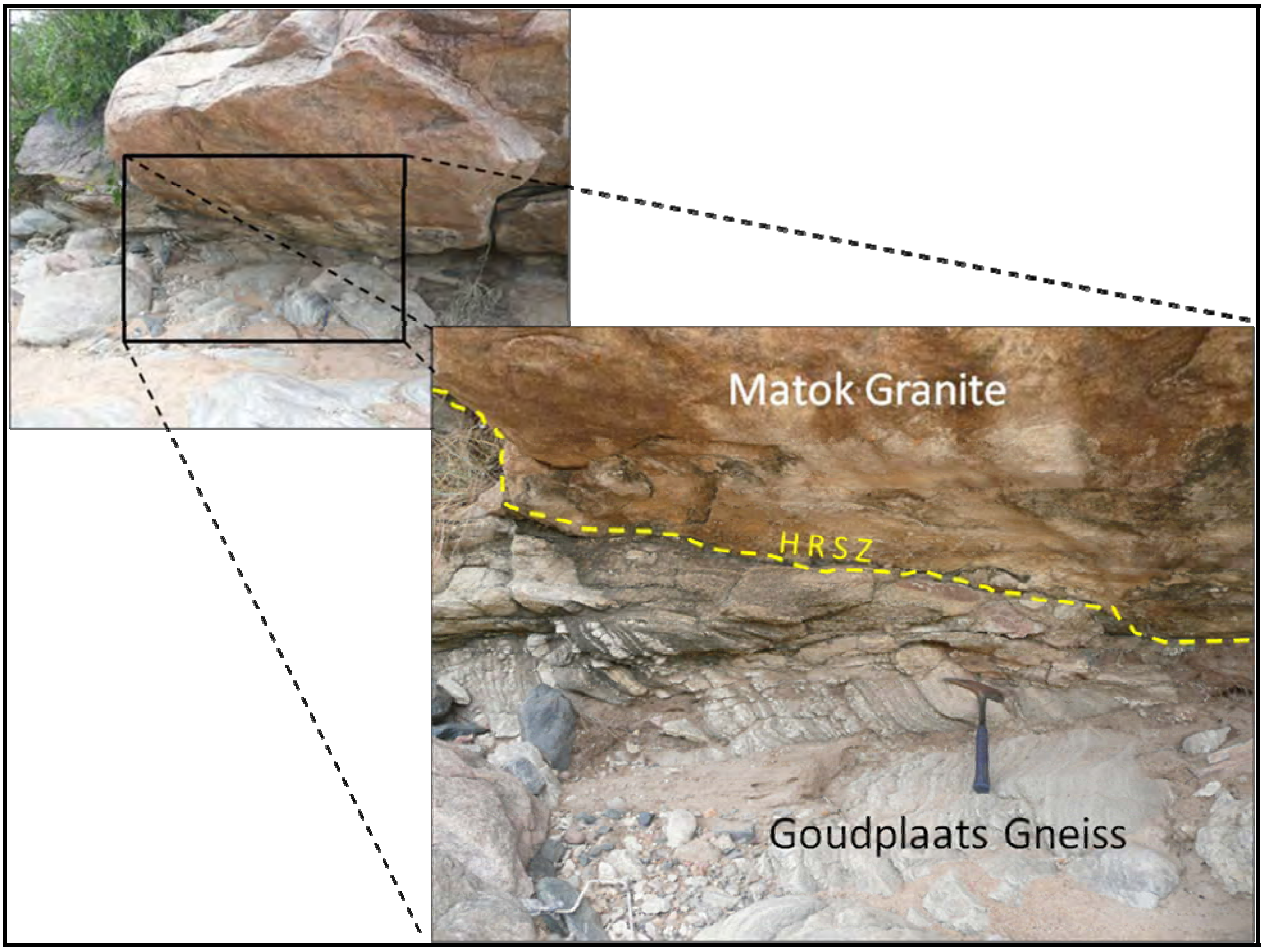

Figure 34: An outcrop showing a small part of the HRSZ between the Matok Granite and the Goudplaats Gneiss.

3.4. Folds:

When rocks are folded, dilational openings and longitudinal joints sometimes form along the hinge lines of the folds due to flexural slip and strain compensation. Since water usually flows following the path of least resistance (but under the influence of gravity) these hinge lines could act as conduits for groundwater flow. However, not many of the hinge lines observed in the field showed signs of longitudinal joints and therefore other brittle structures are still favoured over hinge lines for groundwater exploration. Hinge lines measured in the field are dominantly trending E-W to ESE-WNW. It is likely that the majority of the folds were formed through the D_1 and D_2 events recorded in the HRSZ by Smit et al. (1992) or by the 2.0 Ga. southward-verging reactivation event of the Palala Shear Zone mentioned by Bumby et al. (2004). Furthermore, there are also a number of folds with hinge lines trending approximately NE-SW, possibly as a result of the NW-vergent thrusting between the Pietersburg- and Giyani greenstone belts or the NW-SE compression related to the Wegener Stress Anomaly described by Bird et al. (2006), depending on the age of the folds.

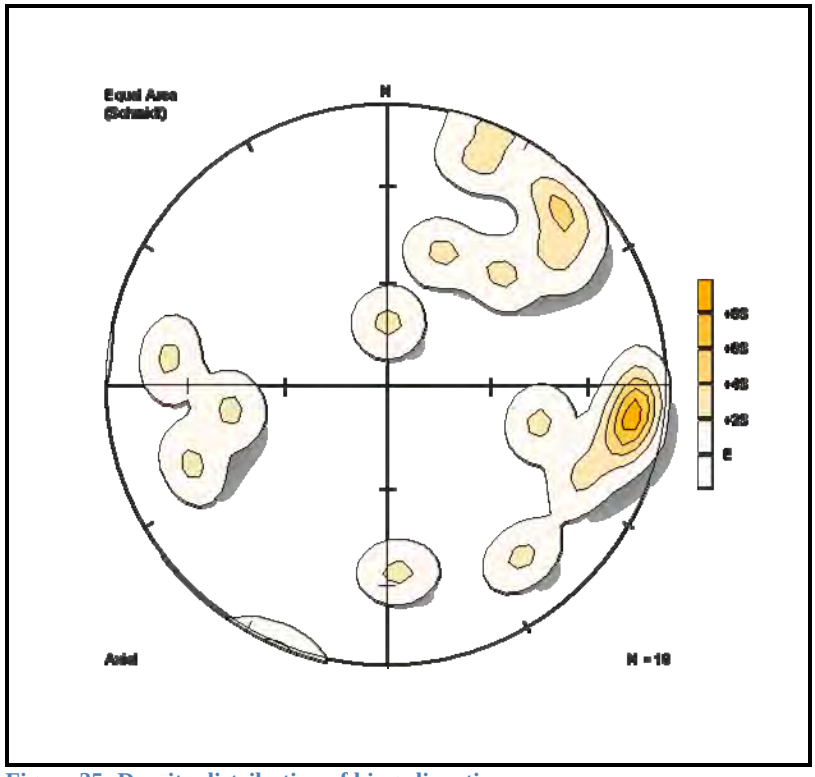

Figure 35: Density distribution of hinge lineations.

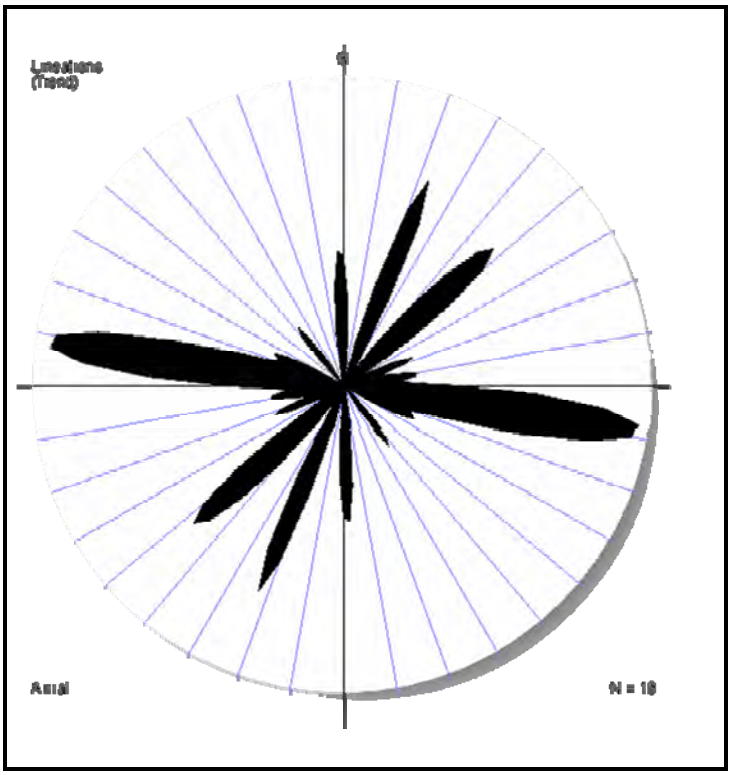

Counting Parameters

Number of Data Points in Set	19
Number of Data Points Included	19
Type of Data	Lines (Trend)
Range of Plunge Angles	0° - 90°
Class interval	10°
Class Alignment	Centered at 0°N
Kurtosis, k, of Smoothing Function	206
Half-width of Smoothing Function	±4.7°
Unweighted Calculation	

Frequency Statistics

Mode (Peak)	26.3%
Azimuth Range of Mode	95° - 105°
Smooth Peak	20.8%
Azimuth of Smooth Peak	97.5°
Expected Value, E	5.6%
Standard Deviation	7.7%
95% Confidence Level	>21.0%

The distribution has a preferred trend.

Figure 36: Rose diagram derived from trends of fold hinges found throughout the study area.

Figure 37: An example of some small, open, symmetric folds in the Goudplaats Gneiss.

Figure 38: An example of small folds which formed adjacent to the Matok Granite in the Goudplaats Gneiss as a result of the compression along the HRSZ.

3.5. Foliation:

Although foliation doesn't fall under brittle deformational structures, it was also measured. A stereographic projection (Figure 39) and a rose diagram of the foliation planes' orientations (Figure 40), show that NE and ENE-striking foliation is the most common, with a fairly large variation in dip angles. East-northeast is an azimuthal value analogous to the Limpopo Orogeny, an event that arguably had the largest structural influence on vast parts of the study area. The major strike directions of the foliation planes are almost identical to the major trends of the dolerite dykes in the area. For this reason it is likely that the dykes had exploited foliation by intruding parallel to the strikes of foliation planes in areas where NE and ENE-striking joints were uncommon at the time of emplacement. Hence, if dolerite dykes have an influence on the flow/occurrence of groundwater; foliation may be viewed as an indirect control in this regard.

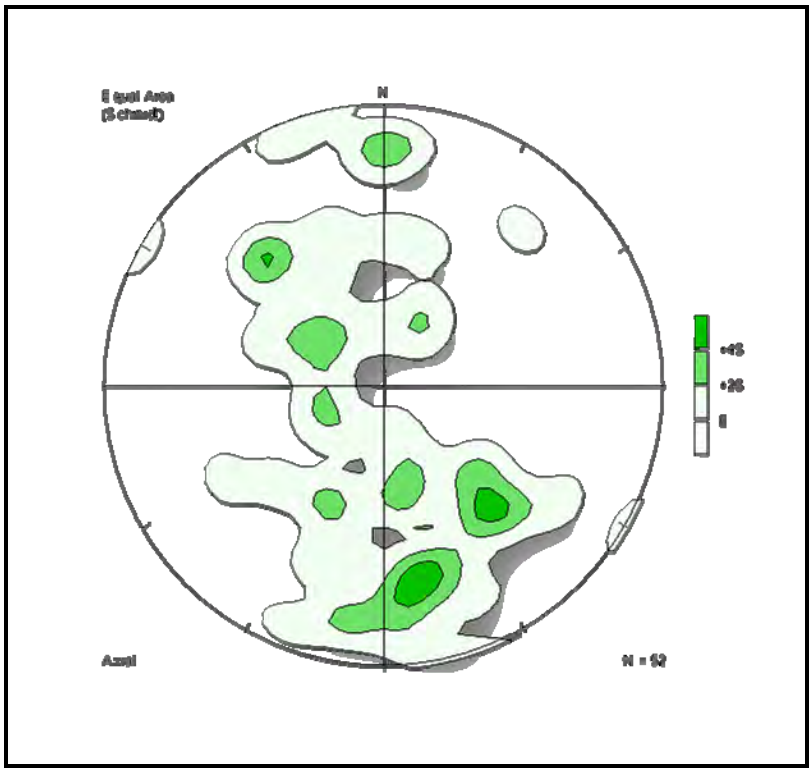

Figure 39: Density distribution of the poles to foliation planes.

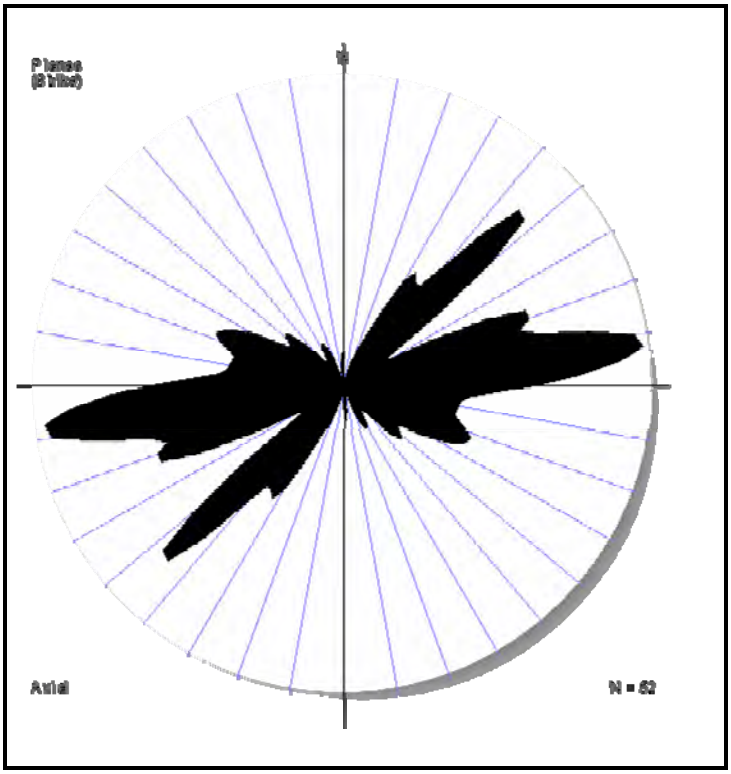

Figure 40: Rose diagram derived from the trends of foliation.

Counting Parameters	
Number of Data Points in Set	52
Number of Data Points Included	52
Type of Data	Planes (Strike)
Range of Dip Angles	0° - 90°
Class interval	10°
Class Alignment	Start at 0°N
Kurtosis, k, of Smoothing Function	206
Half-width of Smoothing Function	±4.7°
Unweighted Calculation	

Frequency Statistics	
Mode (Peak)	17.3%
Azimuth Range of Mode	80° - 90°
Smooth Peak	16.8%
Azimuth of Smooth Peak	82.5°
Expected Value, E	5.6%
Standard Deviation	4.7%
95% Confidence Level	>15.0%

The distribution has a preferred trend.

Figure 41: A picture showing strong foliation in gneisses near the township called Middelwater.

3.6. Dykes:

As with so many of the other geological structures in this study area, the trends of dolerite dykes observed are dominated by two directions, namely NE-SW and NNE-SSW (Figure 42). Such orientations measured from the field compare agreeably with interpretations based on regional aeromagnetic surveys and previous measurements of dykes seen in the literature review (refer to Figure 43 and section 3.6). Dolerite dykes may play a major controlling role on groundwater flow in this study area. Unjointed dolerite dykes can behave as aquicludes in some instances (Cook, 2003), but having the properties of an aquiclude doesn't restrict a dyke from having an influence on the orientation of groundwater flow. It might simply act as a type of barrier, which redirects water to flow or accumulate groundwater along its surface. Highly jointed dolerite dykes (e.g. those containing penetrating cooling joints) also make for good groundwater channels (Cook, 2003). The majority of the dykes observed in the field are less than 10m wide and therefore, according to Bromley et al. (1994) can be considered as good permeable conduits for groundwater. On the other hand, according to the current neotectonic stress-strain regime (NE-SW tension and NW-SE compression), the dykes are likely to be closed.

One of the complicating factors with regards to dolerite dykes in this study is the high spatial density within the dyke swarms. At a regional scale (on a small scale map) it is especially difficult to tell whether or not a borehole did actually strike a dolerite dyke or not. The only way to surely know whether dolerite dykes have a major influence on the flow or occurrence of groundwater in this specific study area is to analyze the borehole logs, which were not available at the time of printing this document. Presently available results are rendered inconclusive with regard to the influence of dolerites on groundwater at a regional scale. In the event of attaining borehole logs in the future, it is important to note the following attributes with regard to dolerites' influence on groundwater: 1.) To confirm whether a dolerite was struck or not (and at what depth); 2) the properties of the dolerite (weathering and jointing); 3) whether the borehole yielded water and if it did, at what depth, what transmissivity and what yield? A more in depth analysis could also consider the geometry, grain size and degree of weathering, as these also influence a dolerite's hydrogeological properties, but are regarded as being outside of this study.

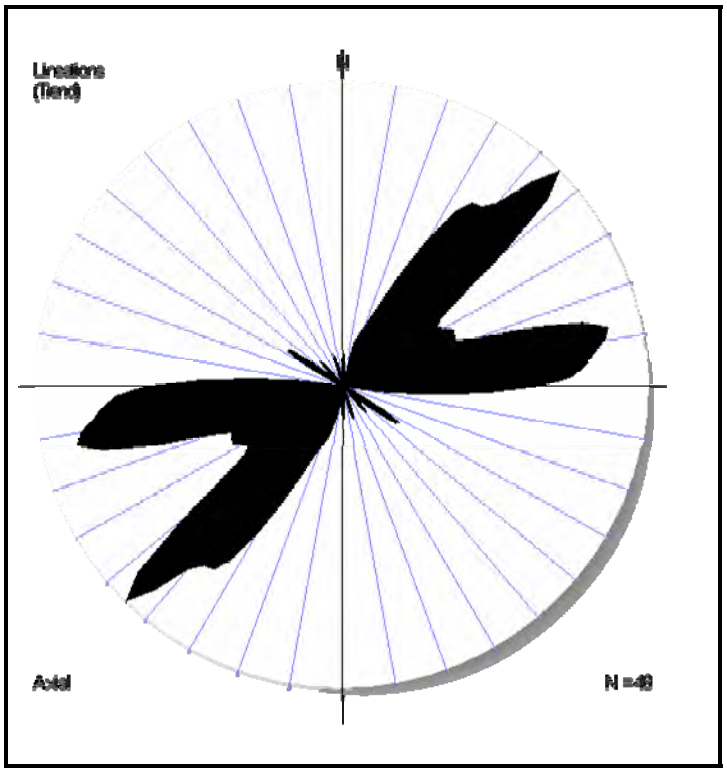

Counting Parameters	
Number of Data Points in Set	48
Number of Data Points Included	48
Type of Data	Lines (Trend)
Range of Plunge Angles	0° - 0°
Class interval	10°
Class Alignment	Centered at 0°N
Kurtosis, k, of Smoothing Function	206
Half-width of Smoothing Function	±4.7°
Unweighted Calculation	

Frequency Statistics	
Mode (Peak)	18.8%
Azimuth Range of Mode	45° - 55°
Smooth Peak	18.6%
Azimuth of Smooth Peak	45.0°
Expected Value, E	5.6%
Standard Deviation	4.9%
95% Confidence Level	>15.3%

The distribution has a preferred trend.

Figure 42: Rose diagram derived from strikes of dolerite dykes in the study area.

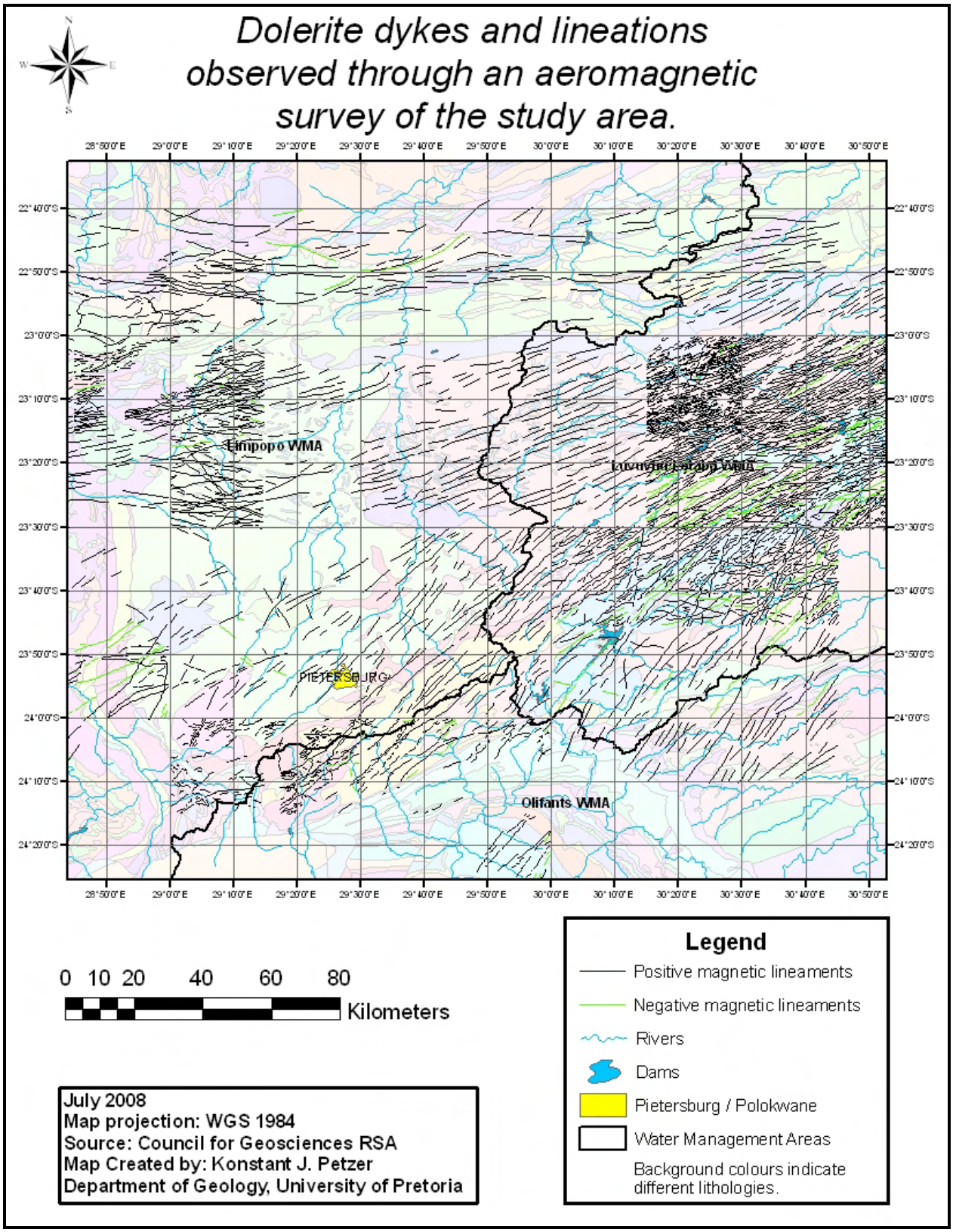

Figure 43: A map indicating the dolerite dykes and other lineaments that were observed through an aeromagnetic survey of the study area done by the Council for Geosciences. Not all areas of the map were covered at the same resolution. Note the dominant NE and NNE trends.

Figure 44: A 60cm wide, dolerite dyke with sharp edges (256˚, 84˚ NW), implying that it intruded into one of the pre-existing joints with the same orientation found in the area.

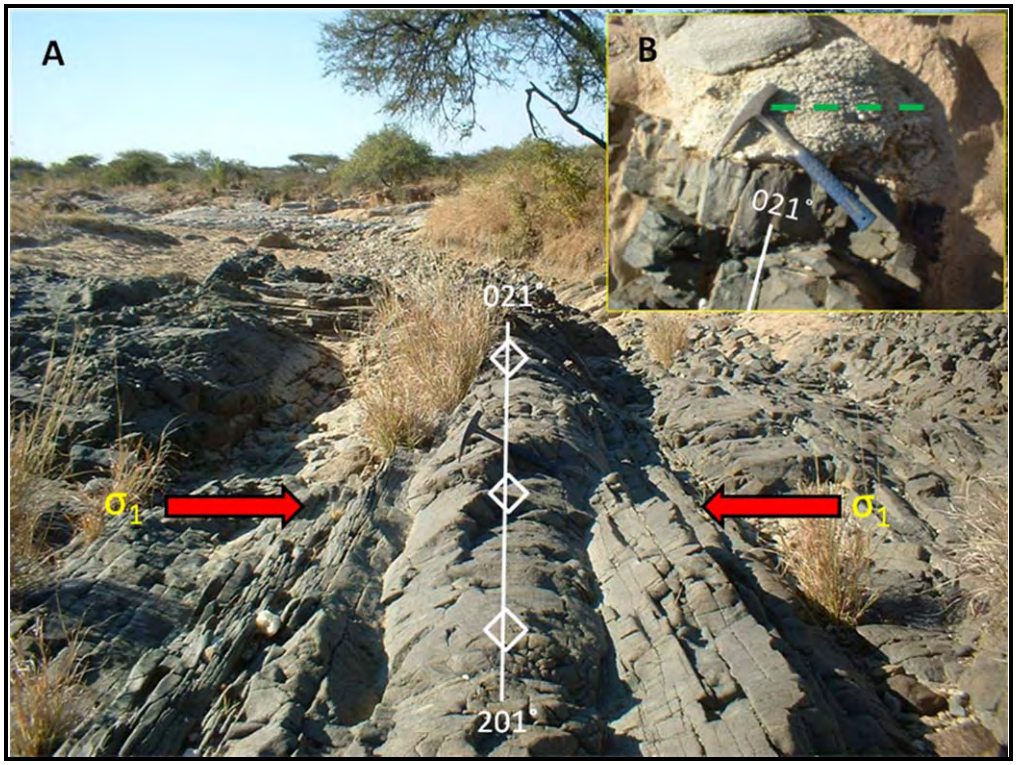

Figure 45: (A) A dolerite sill with outcrop dimensions of about 60m x 40m (long axis trending 152˚). This photo was taken along an anticline in the dolerite (hinge: trend 021˚, plunge 02˚, λ = 8m) which probably formed as a result of primary folding (when the dolerite was still molten), because the pre-existing gneiss surrounding the area seems to be unaffected by the σ_1 compression which caused the folds. (B) In fact the surrounding gneiss shows foliation (indicated by green stipple line) which strikes approximately perpendicular to the trend of the folds in the dolerite.

3.7. Summary of strikes/trends:

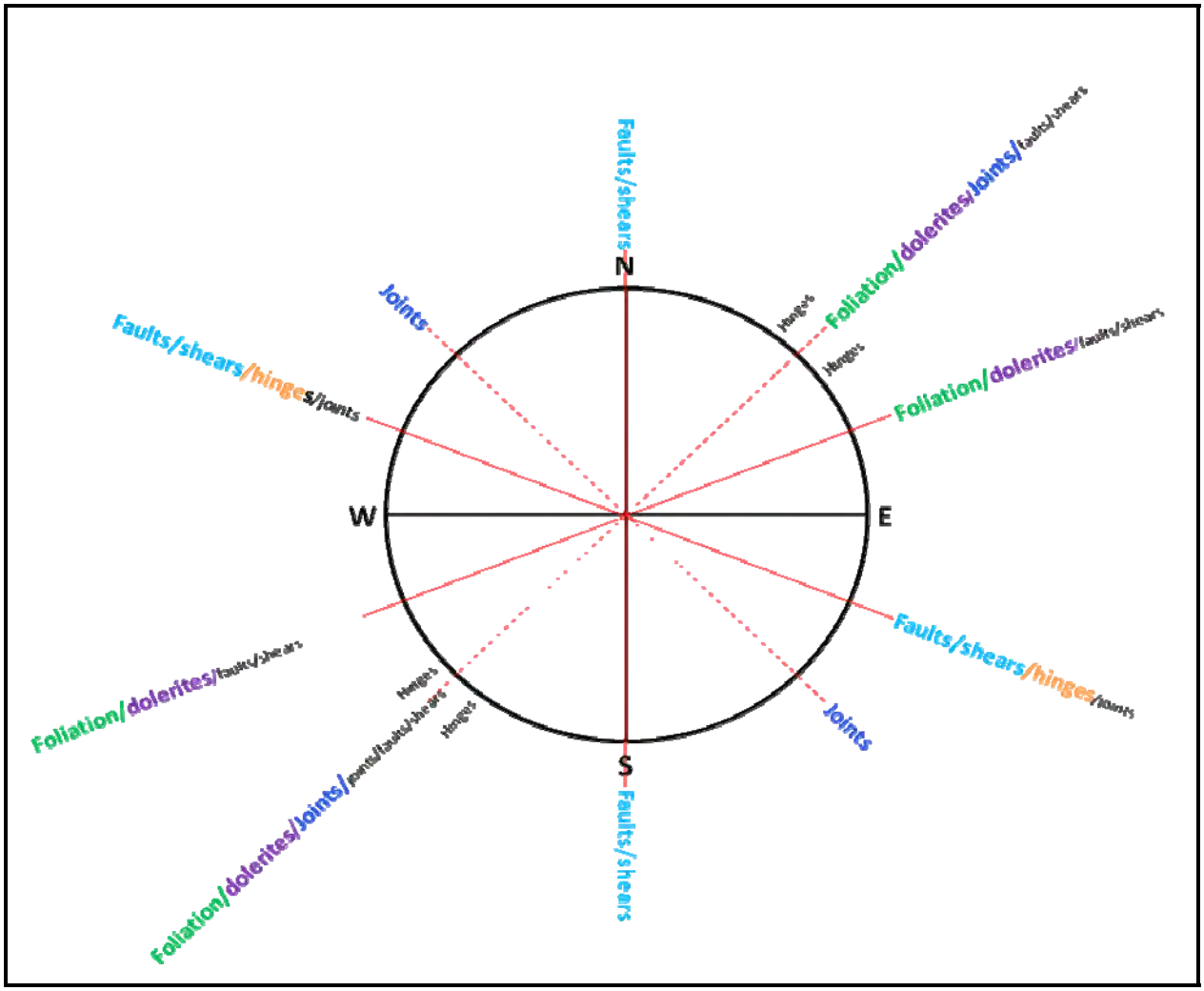

Figure 46: A summary of the strikes/trends of structures observed in the field.

3.8. Lithological Contacts:

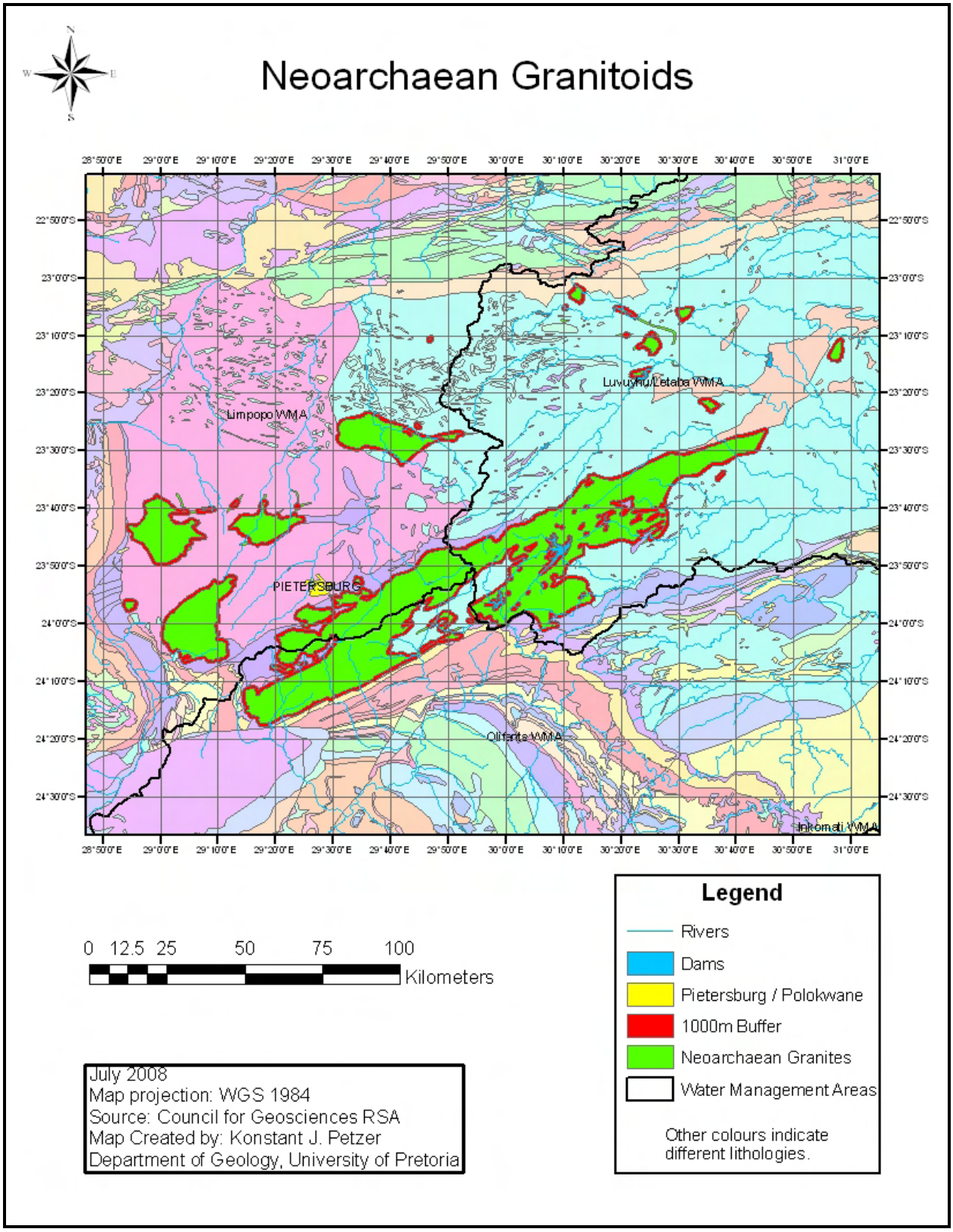

Figure 47: A map indicating the location of the Neoarchaean granitoids in the study area and a 1000m buffer (500m inside & 500m outside) around their contacts.

Table 5: A table showing the average T and Q values for different groups of boreholes in relation to their spatial distribution relative to Neoarchaean Granitoids.

Property of borehole	Boreholes in Neoarchaean Granitoids	Boreholes in the 1000m buffer at Neoarchaean granitoid contacts	Boreholes outside of the Neoarchaean Granitoids
Mean Average Transmissivity (T-logan) (M^2/d)	25.37	55.52	42.53
Mean Average Sustainable yield (Q) (L/sec./24hr)	0.77	1.57	1.19

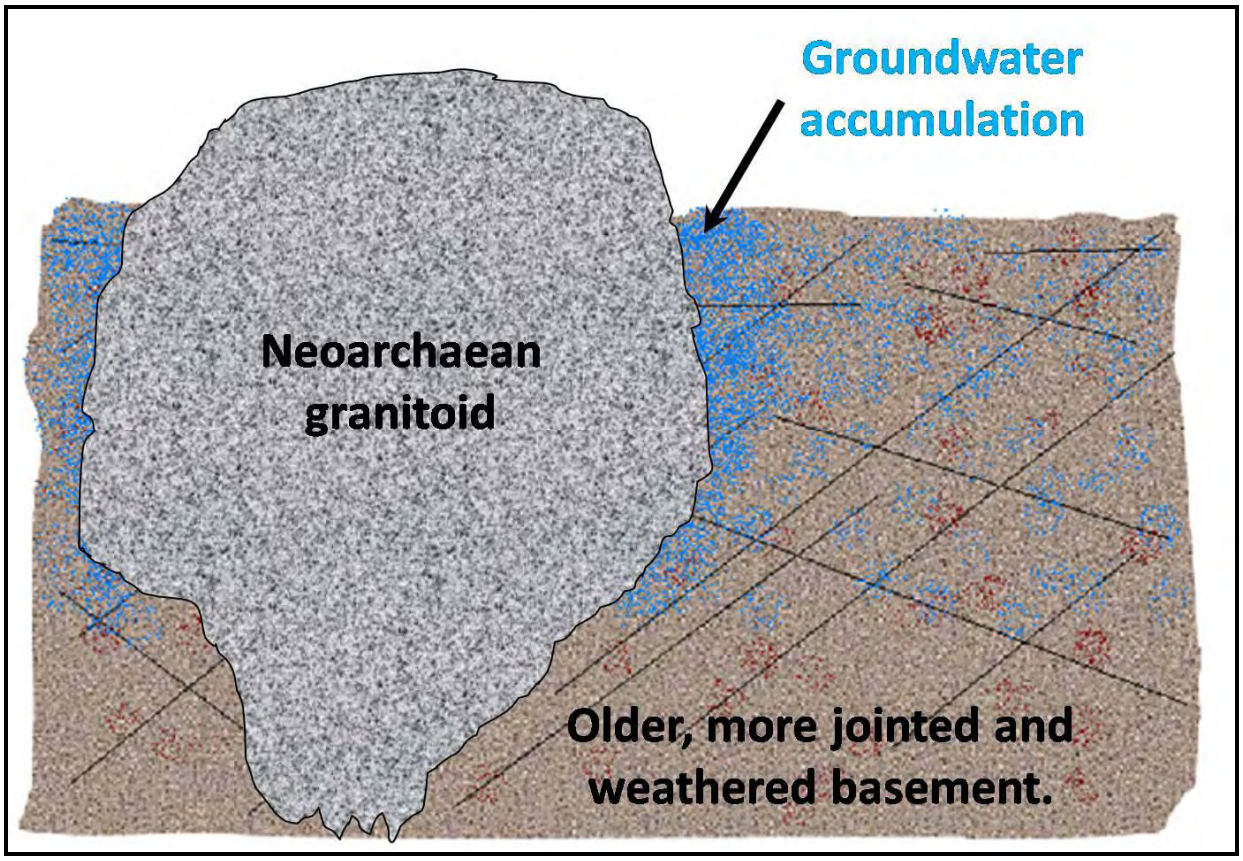

Figure 48: Groundwater accumulation related to the lithological contacts between Neoarchaean granitoids and older basement rocks in the study area.

As hypothesized, the averages of both the transmissivity- (T) and yield (Q) values are ranked in the following manner based on their lithological location: Firstly, the highest average T and Q values were obtained at the contacts between the Neoarchaean granitoids and the surrounding basement rocks. This is because groundwater can move relatively freely through the weathered and jointed old basement lithologies, but dams up against the post-tectonic, unweathered Neoarchaean granitoids which are less penetrable. The second highest average T and Q values were obtained from the surrounding old basement lithologies and the lowest averages came from within the Neoarchaean granitoids.

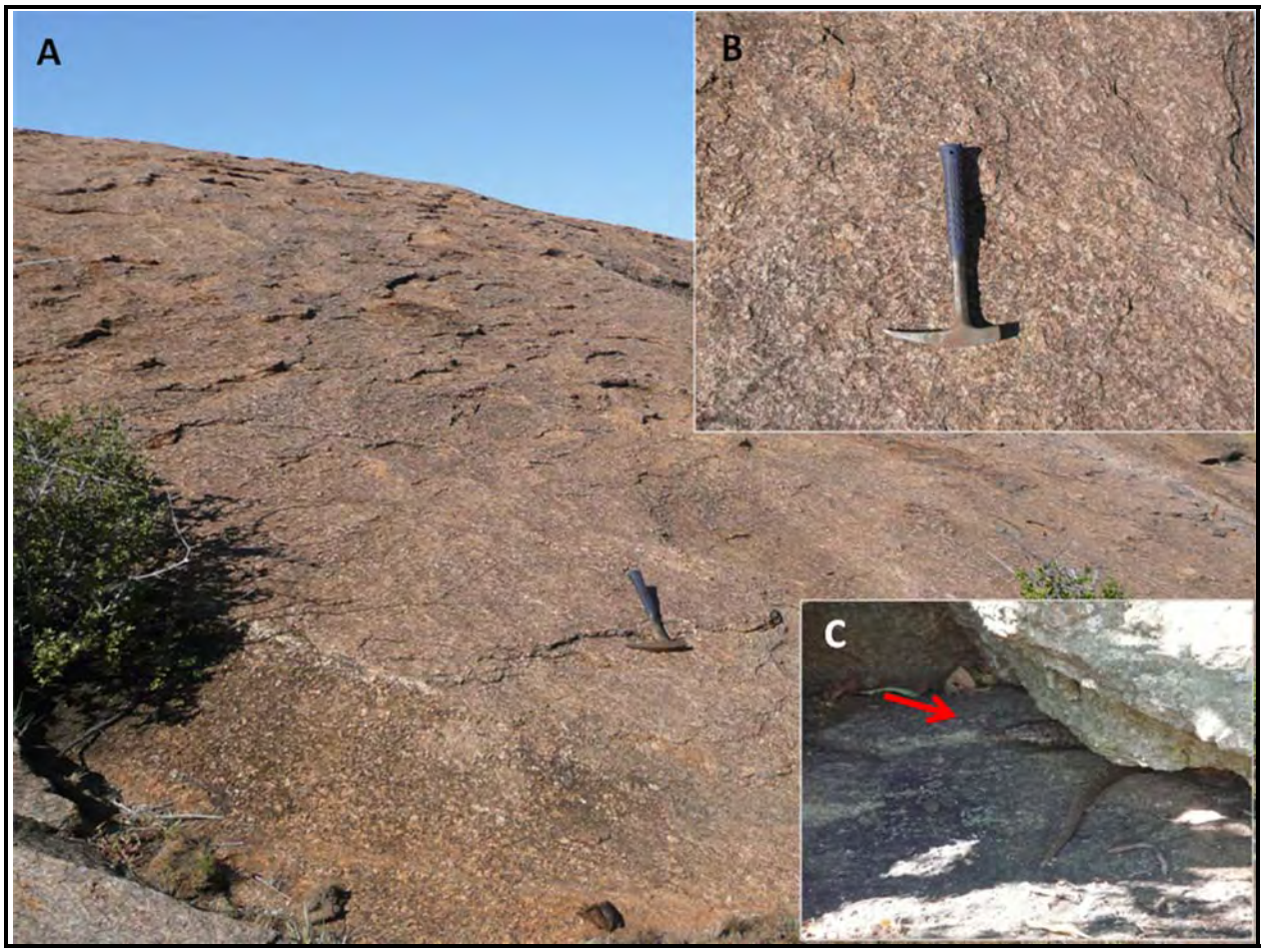

Figure 49: (A) An example of a Neoarchaean Granite, which only shows a dilatational pressure-release surface, but not any tectonically induced joints. (B) A close-up look at the same granite still doesn't indicate any joints. (C) Some animals use the dilatational cracks in the granite as a shelter.

3.9. Groundwater flow/occurrence:

From Figure 50 to Figure 55, the spatial interpolation of the inverse distance weighted yield and transmissivity values were plotted for different portions of the study area. When comparing these interpolations with the brittle geological structures that have been observed in the field, there doesn't seem to be a strong spatial correlation, at least not on a regional scale. The following observations can be made from slight local scale trends in the interpolated plots: Firstly, in Figure 50 there seems to be a slight NE-trend in the interpolated transmissivity values near the centre of the map. Although this trend is not bound to a specific lithology, it does match the trend of the rivers, the major strike direction of joints (Figure 19) and the trend of the sub-horizontal cluster of joint intersections (mentioned in section 4.1). A similar relationship can be seen on the same area of the map in Figure 51 in which the interpolated sustainable yield values form one very slight trend orientated approximately NNE-SSW. Another observation is the fact that the Pietersburg Greenstone Belt (seen only as an outline in Figure 52; verify location with Figure 5) definitely has low transmissivity compared to the lithologies north of it (Figure 15 contains many boreholes located in the PGSB to confirm this statement). Another approach was taken in Figure 56 by plotting a three-dimensional model of the transmissivities of a part of the study area with a good spatial distribution of boreholes over a corresponding geological map. Although a slight trend in higher transmissivity could be argued around a portion of the HRSZ, the three-dimensional model created does not correlate well with the area's structural geology at a regional scale.

After the disappointment of not finding a strong structural control of groundwater at a regional scale, it was decided to take a closer look at the specific boreholes that did possess high Q-values. A query was run on the borehole database to find the following boreholes with Q > 6L/sec/24h: H04-0848, H04-0905, H04-0962, H04-0988, H04-1022A, H07-1061, H10-0548, H10-0657, H16-0358, H16-0426, H16-0471, H16-0485, H16-0551, H16-0580. The properties of these boreholes, in terms of their localities, were investigated to look for a reoccurring similarity. Lithologically, many of these boreholes are located on or near to NE-SW trending dolerite dykes (must be confirmed with borehole logs in the future). NNE-SSW and NE-SW striking faults were also observed at a few of these boreholes. Other than the structural controls on groundwater, two possible other controls were also observed. Firstly many of the high-yielding boreholes are located in the alluvium of rivers. It is no surprise that this type of weathered environment can act as a good aquifer.

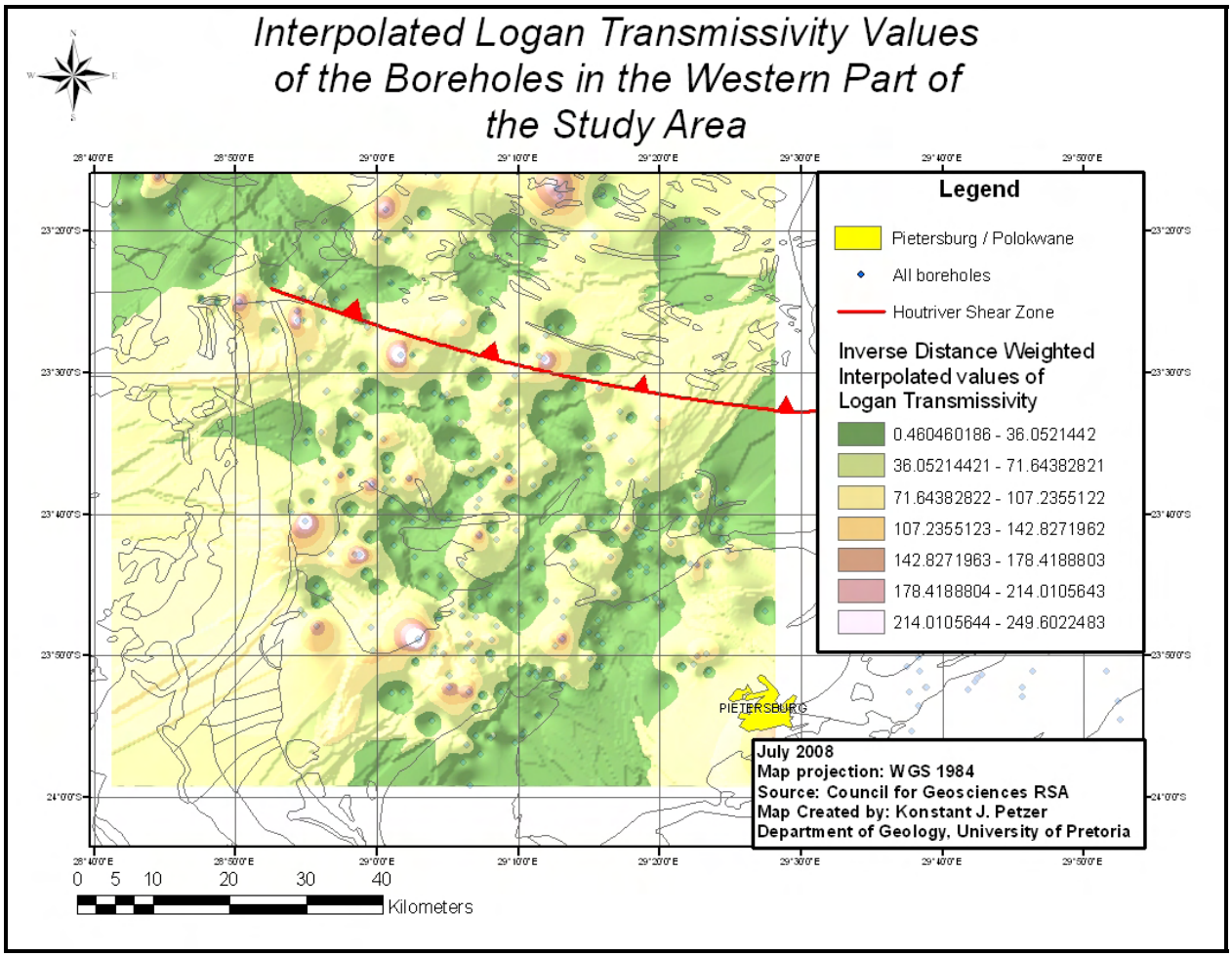

Figure 50: A map of the interpolated (inverse distance weighted) Logan transmissivity values of the western part of the study area.

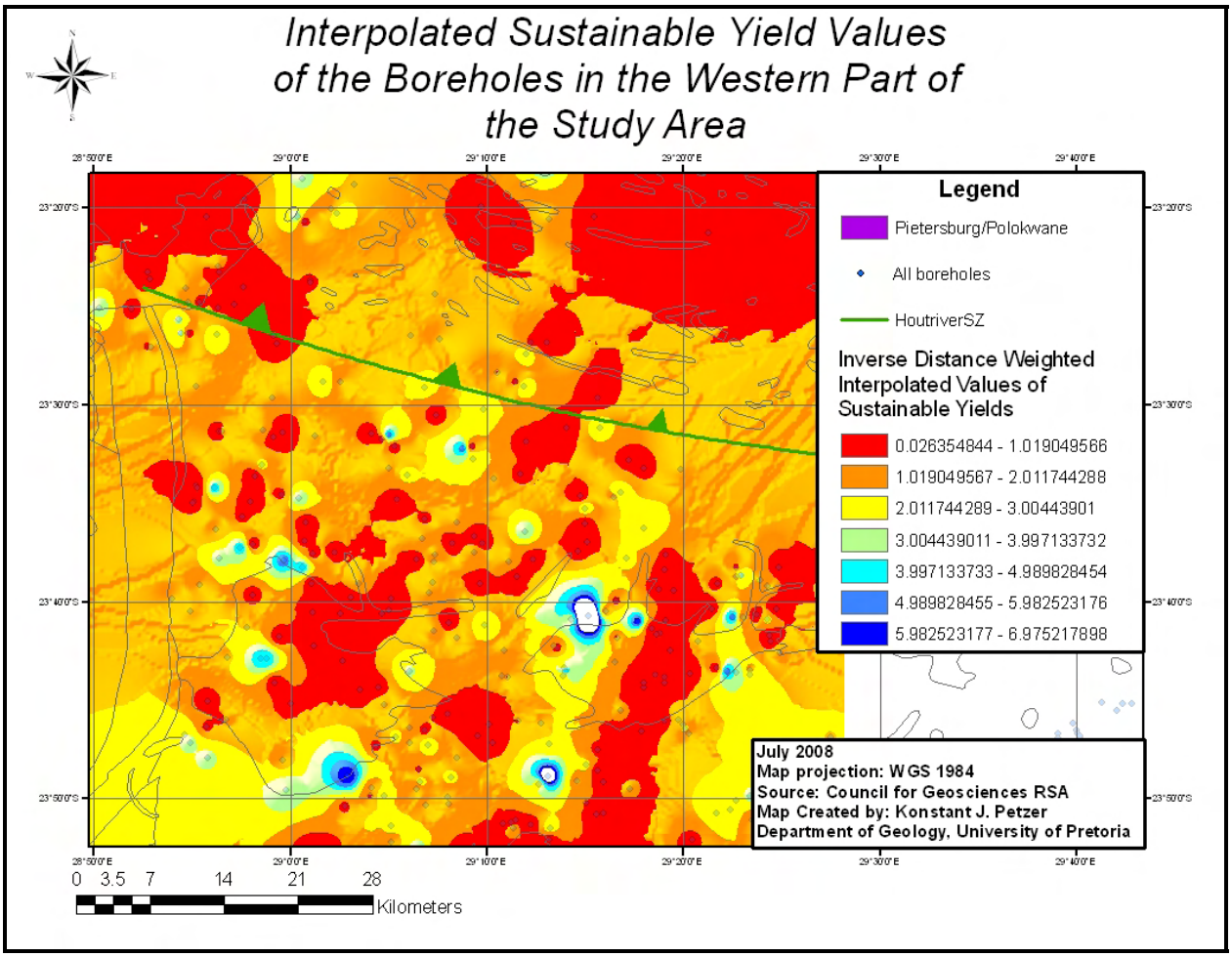

Figure 51: A map of the interpolated (inverse distance weighted) sustainable yield values of the western part of the study area.

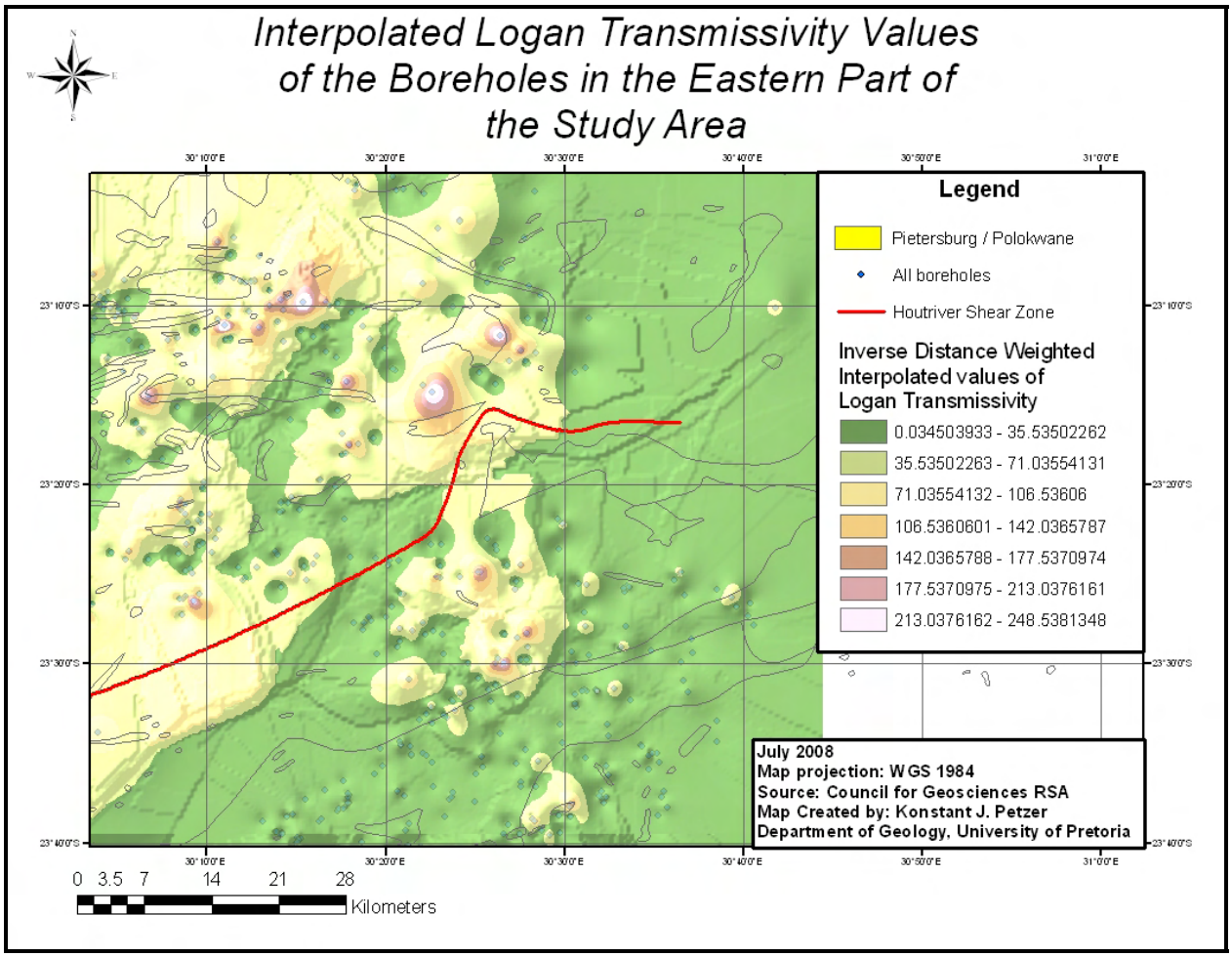

Figure 52: A map of the interpolated (inverse distance weighted) Logan transmissivity values of the eastern part of the study area.

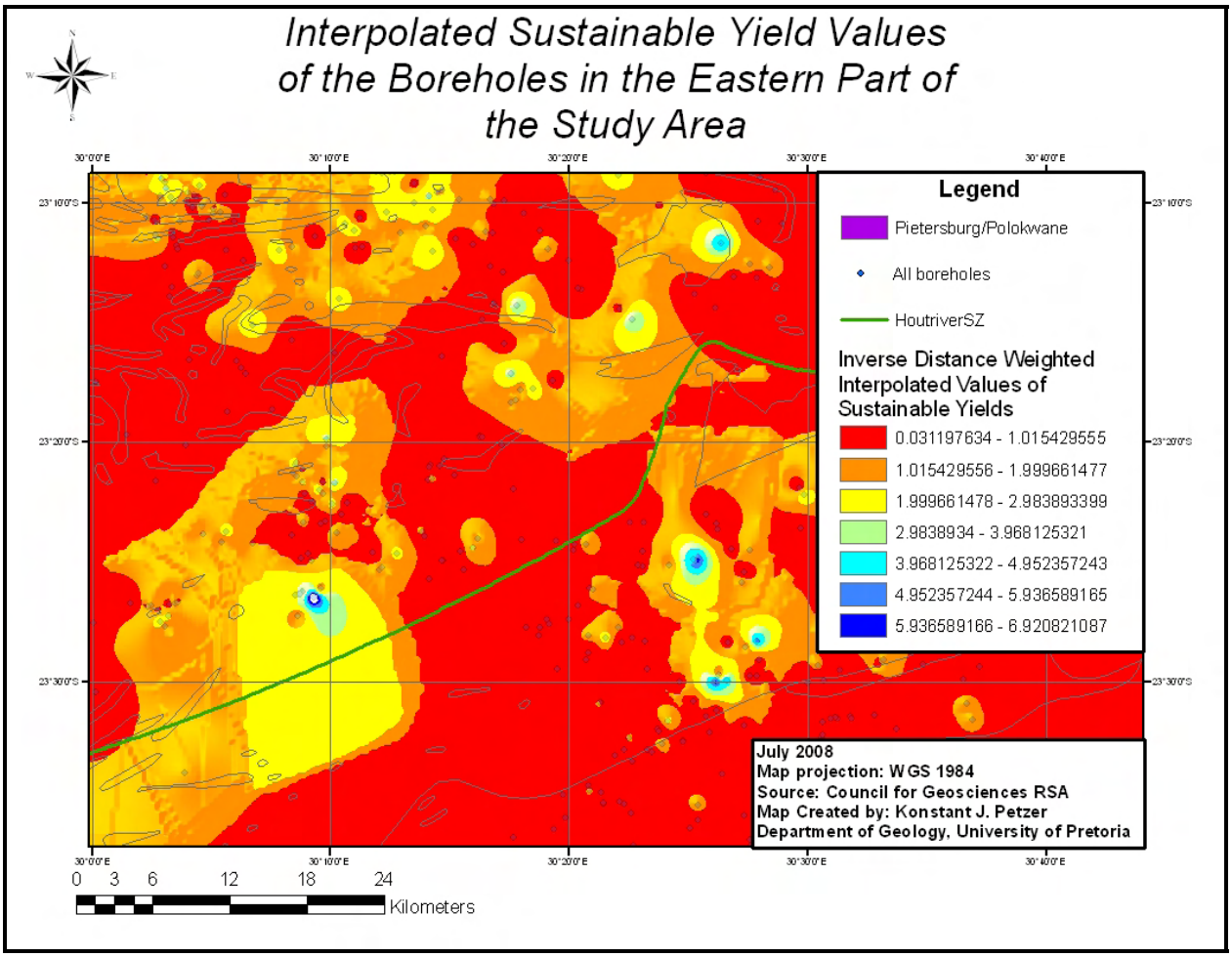

Figure 53: A map of the interpolated (inverse distance weighted) sustainable yield values of the eastern part of the study area.

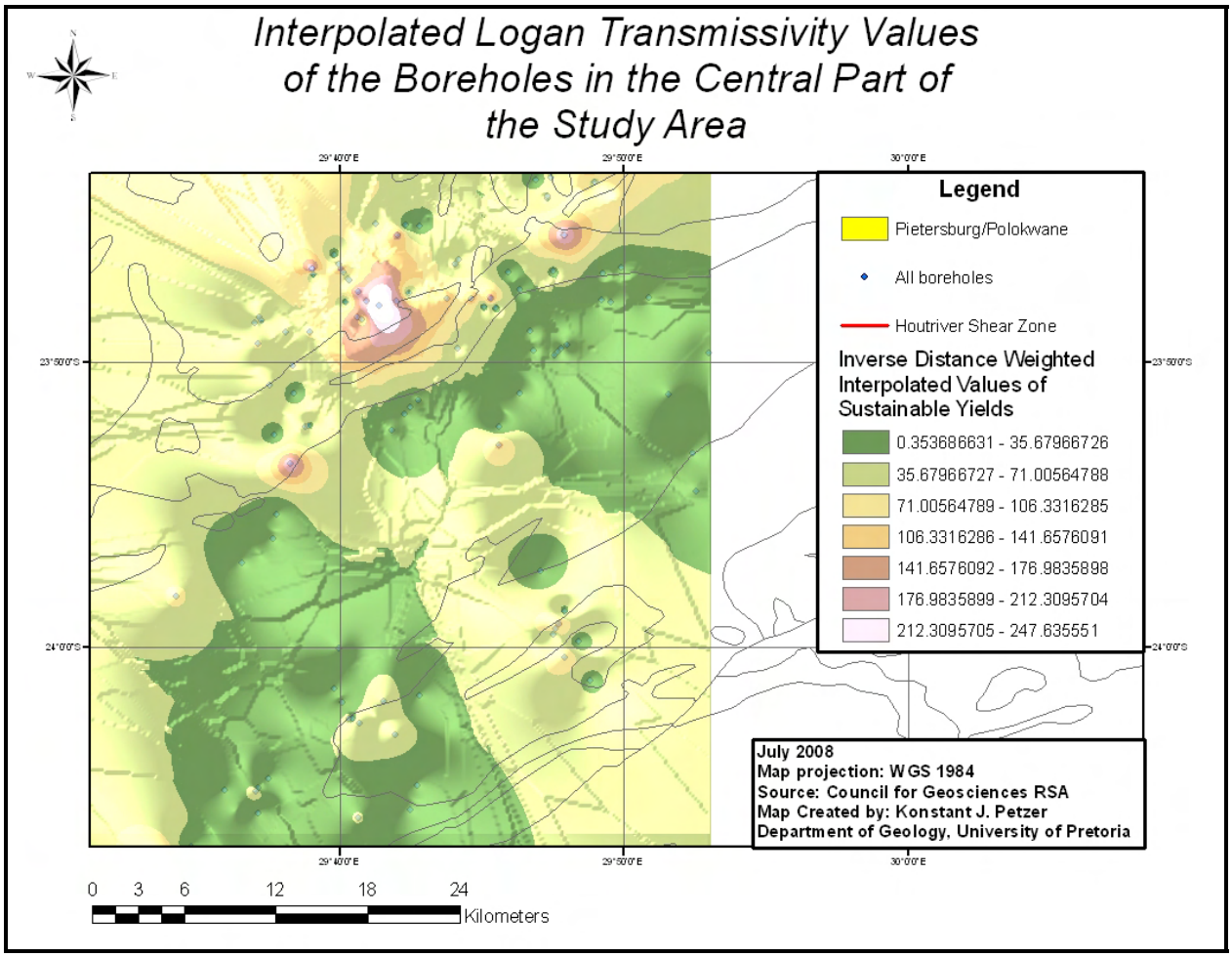

Figure 54: A map of the interpolated (inverse distance weighted) Logan transmissivity values of the central part of the study area.

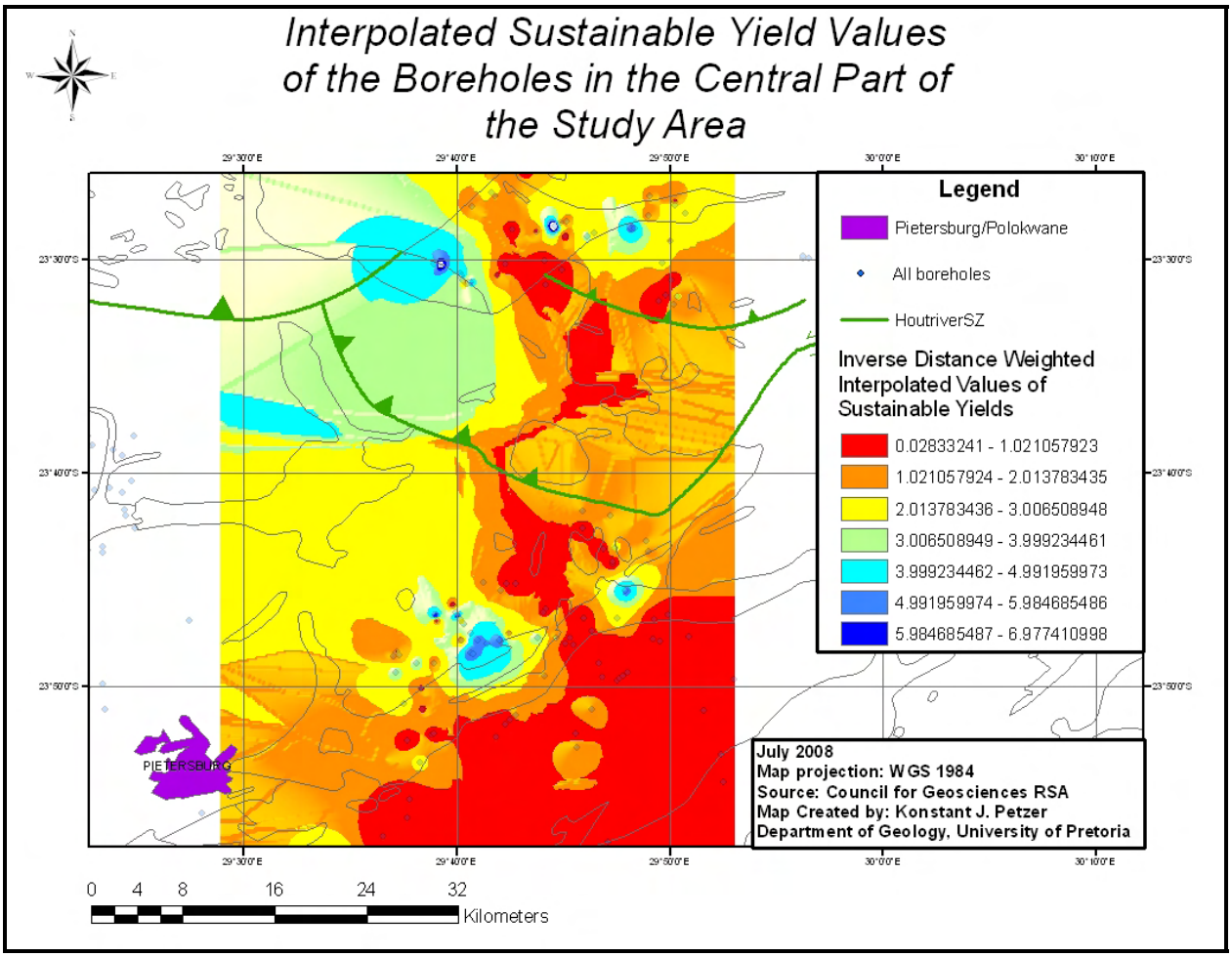

Figure 55: A map of the interpolated (inverse distance weighted) sustainable yield values of the central part of the study area.

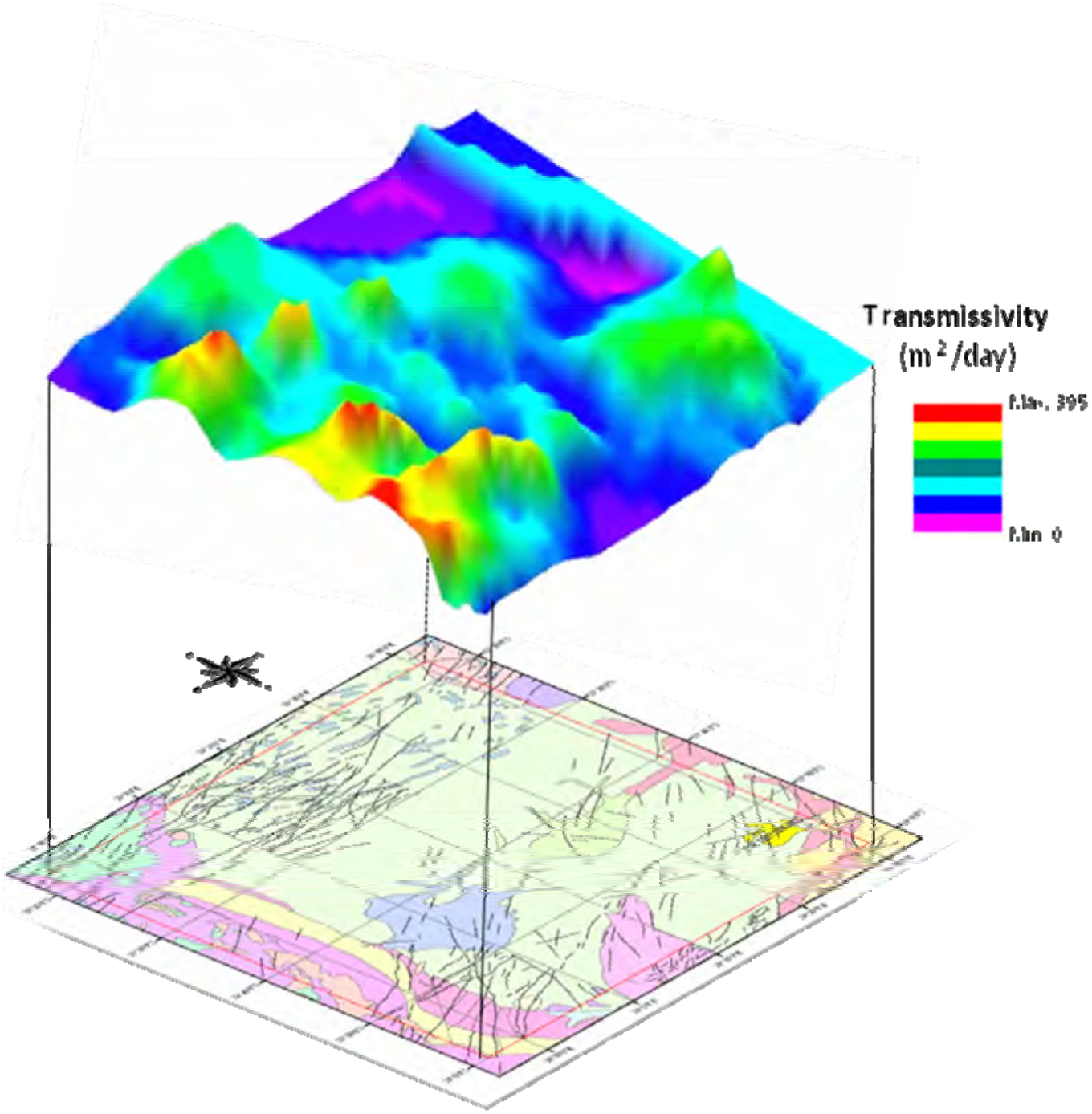

Figure 56: A Three-dimensional model of the Logan Transmissivities from a part of the study area with a good spatial distribution of boreholes, superimposed onto a corresponding geological map of the area. Although the patterns on the three-dimensional model do not seem totally random, they cannot be clearly correlated with structural geology at a regional scale. The three-dimensional model was created using Rockworks 2006 © software.

3.10. Surface Drainage Patterns:

When looking at Figure 57, one can draw a few conclusions based on the surface drainage patterns of the study area. Firstly, the density of rivers in WMA2 is higher than the spread out distribution of rivers in WMA1. There might be more rivers in WMA2 due to the greater annual rainfall in this area. Furthermore, WMA1's drainage pattern is dendritic, whereas drainage patterns of the rivers in WMA2 vary from dendritic to blocky (caused by joints). Rivers in WMA1 mainly trend in the following directions: N-S, NE-SW and NW-SE and rivers flowing parallel to the first two directions mentioned are especially long and continuous. NE-SW is also a major trending direction of rivers in WMA2, along with E-W and NNW-SSE (this direction becomes more common as one move from west to east in WMA2). For the most part, the rivers in the study area flow sub-parallel to the major joint orientations found at that location, especially where the joint intersection lineations form sub-horizontal clusters (refer to "Joint intersection lineations" under section 3.2 and compare Figure 57 with Figure 19).

The trends of the rivers mentioned above also compares well with the rose diagram constructed for faults (Figure 28). In areas where the rivers don't flow sub-parallel to the major joint directions, there are still at least some joints striking in the same direction as the flow of the river albeit a so called "major strike direction" or not. Despite not finding very strong correlations between groundwater flow/occurrence in the previous sections, structural geological controls on a few of the surface drainage patterns are unmistakable even though the influences are mainly seen at a local scale (see Figure 58). Unfortunately, the structural controls seen on the surface are not necessarily exactly an indication as to what is happening underground. For example, the three-dimensional strain mentioned in section 2.2 can cause joints/faults to deviate from the "standard" joints/faults described in Anderson's Theory, which produces a difference in joint patterns between the surface and underground (see Figure 59 and Figure 60). Lastly, other controls such as topography also have an influence on surface drainage patterns. For example, one finds closely-spaced, short rivers on the escarpment next to the Lowveld, as compared to longer, widely-spaced rivers of the flat plains.

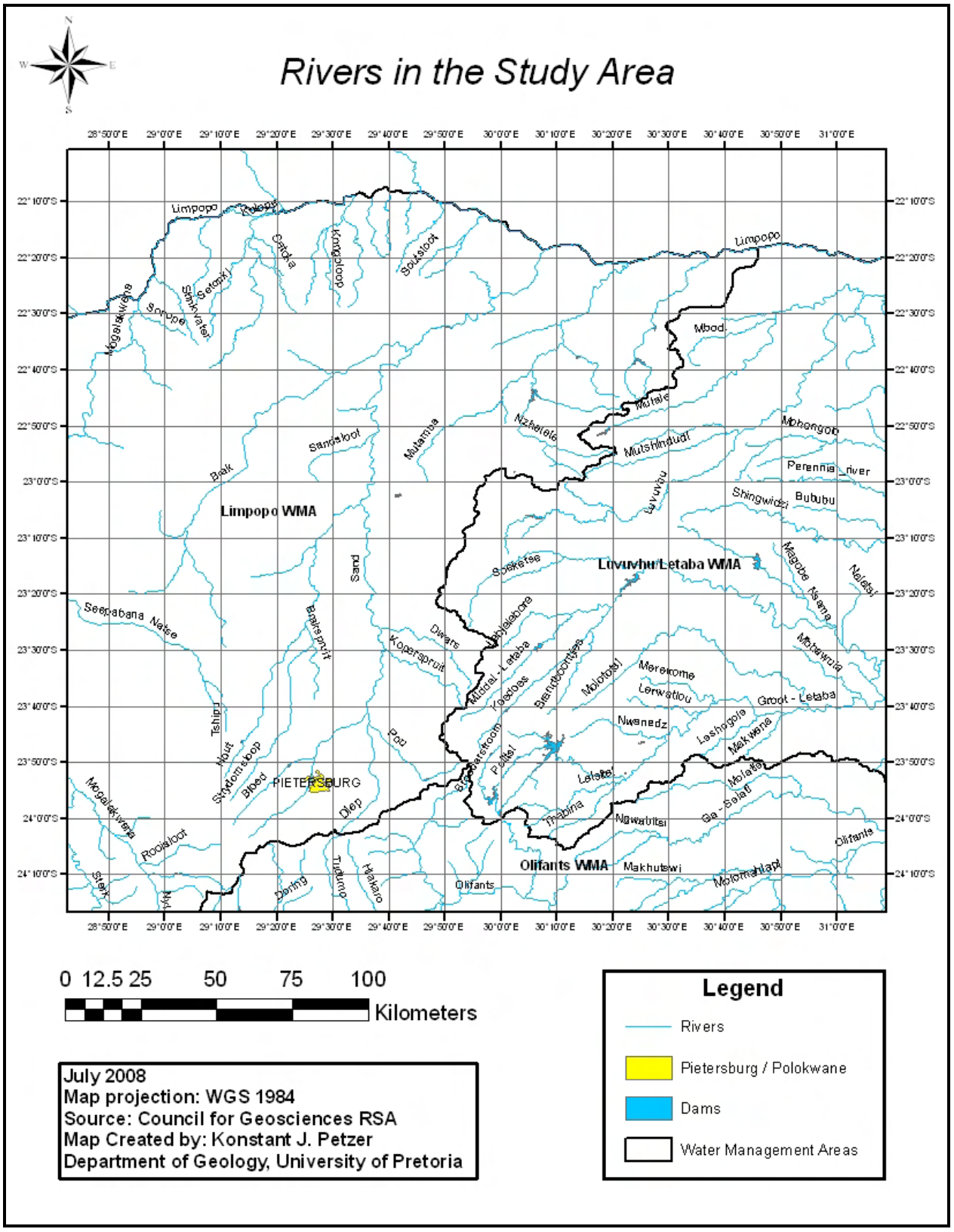

Figure 57: A map indicating the surface drainage patterns of the study area.

Figure 58: A Google Earth satellite image taken near the Giyani Greenstone Belt showing NNE, NE and lesser NW trending joint sets. Note that the flow of the river is guided by the underlying joints in most sections.

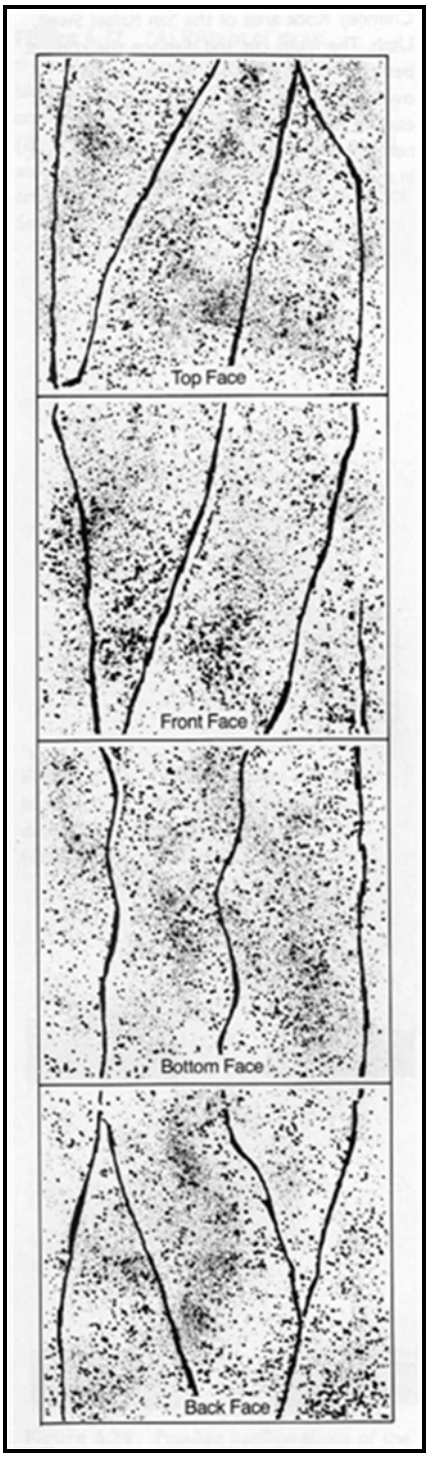

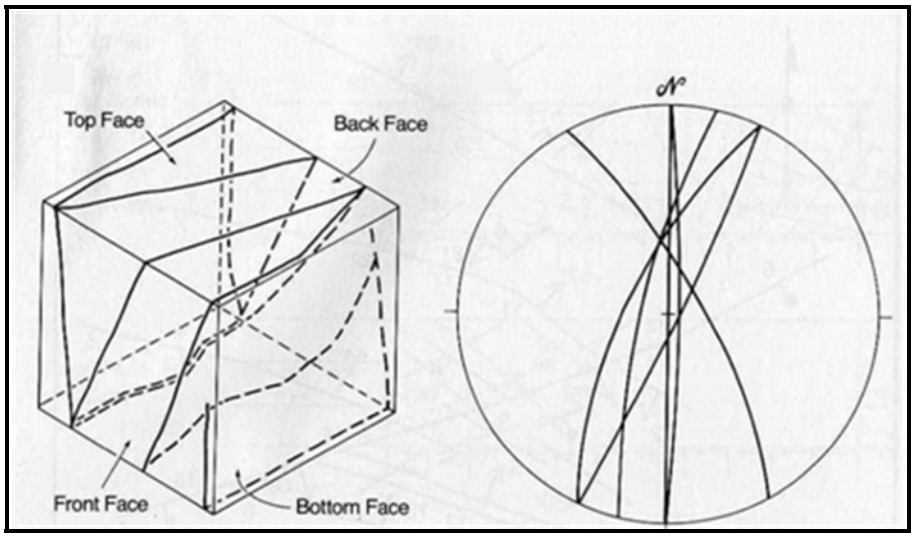

Figure 59: A three-dimensional illustration and an associated stereographic projection of fault patterns produced in rock subjected to three-dimensional strain. From Reches and Dieterich, 1983.

Figure 60: The traces of faults correlating to the fault patterns seen in Figure 59 Note that the fault pattern changes with depth and might mean that surface drainage patterns (which often follow faults and joints) might not give a good indication as to the patterns in groundwater conduits at depth. From Reches and Dieterich, 1983.

4. CONCLUSION:

After investigating all the results from this study, no strong spatial correlation between structural geology and groundwater can be identified at a regional scale. It is believed that the extremely old age (starting from the middle of the Archaean Eon) of the rocks in the area is the major factor which is indirectly responsible for this poor correlation. Numerous tectonic and magmatic events have had an influence on the geology of the study area which have ultimately brought about a structurally complex terrain. The complexity of the basement's structural geology in the Limpopo Province makes it difficult to isolate the effects of a specific set of structures on the flow and occurrence of groundwater. Nevertheless, the following observations regarding the presence of water in the basement rocks of the Limpopo Province have been made.

Firstly, the influence of the neotectonic stress direction on the presence of groundwater appears to be negligible, at least at a regional scale. With a dominant NE-SW extensional regime one would have expected to find more favourable groundwater conduits striking NW-SE, but this hypothesis was rejected. When looking at surface water, it was interesting to find that in areas with preferred clusters of sub-horizontal joint intersections (figures in appendix), the rivers in those areas flow parallel to the trends of such clusters (see section 4.1 "Joint intersection lineations").

Unlike the other groups of joints, those inclined at angles ranging from eighty to ninety degrees did show preferred orientation trending NW-SE. Many of these joints might well have formed due to the neotectonic stress regime. However, as mentioned before, the occurrence of groundwater does not seem to be influenced by neotectonic stess to the extent that an associated preferred orientation of proven conduits are found in the area.

When examining the shallow-dipping joints (those inclined from zero to forty-five degrees), it was found that the distribution of these joints is well spread out over the entire study area. Whereas some of the shallow-dipping joints could have formed due to dilatation (i.e. pressure release as a result of erosion or plutonism), it is believed that many of these joints are actually tectonically induced, suggesting that the whole study area was likely subjected to compression at one stage or another. This being said, many of the brittle structures that might have been favourable groundwater conduits long ago could subsequently have been closed up.

Despite the fact that NW-SE trending joints were initially believed to be the most promising targets for groundwater (due to their orientation relative to the neotectonic stress direction), the importance of the other major direction observed, NE-SW, cannot be overlooked. Joints striking NE-SW were likely reactivated during successive tectonic events

(for example the N-S extension during later Karoo times) and lie parallel to one of two strong preferred orientations (NE-SW and NNE-SSW) displayed by dolerite dykes in the area. Unfortunately, not even those properties resulted in groundwater conduits showing dominant NE-SW strike directions.

From the results it is clear that the tectonic structures (including large structures like the Hout River Shear Zone) and dolerite dykes from the study area produced hardly any positive conclusions in terms of groundwater exploration on a regional scale. Thus, conclusions regarding the influence of weathering and lithology on groundwater occurrence are also recorded below.

One part of the investigation which yielded positive proven results involves the relationship between groundwater occurrence and the lithological location relative to Neoarchaean granitoids. By investigating the following three lithological locations: 1) Inside Neoarchaean granitoids; 2) the contacts between Neoarchaean granitoids and the surrounding older basement rocks; 3) inside the surrounding basement rocks, it was shown that the highest averages of both the transmissivity- (T) and yield (Q) values were obtained at the contacts between the Neoarchaean granitoids and the surrounding basement rocks (See Table 5.) This phenomenon occurs because groundwater can move comparatively freely through the weathered and jointed old basement lithologies, but dams up against the post-tectonic, unweathered Neoarchaean granitoids which are less penetrable (Figure 48). The second highest average T and Q values were obtained from the surrounding old basement lithologies and the lowest averages came from within the Neoarchaean granitoids themselves.

Unsurprisingly, boreholes located in the alluvium of rivers produced relatively higher yields and transmissivities of groundwater. Where the law does not restrict it, boreholes close to rivers are often promising targets when drilling for water.

In conclusion, the structural geology in the basement lithologies of the Limpopo Province of South-Africa does not have a clearly identifiable influence in terms of spatial patterns in groundwater flow and occurrence at a regional scale. Groundwater targets created through weathering rather than tectonics are evidently more easily recognized. Structural controls on groundwater in the granitic aquifers from this specific area are not totally negligible, although it is believed that such influences will be better identified through intensive local scale investigations.

5. SUGGESTIONS FOR FURTHER STUDY:

In order to better identify the structural controls on groundwater in the area it is suggested that more intensive studies be conducted in much smaller areas. In this way, the local scale influences of structures on groundwater could be easily isolated and identified. If the budget allows it, it is also recommended to change the order of investigation. In other words, to map geological structures first and then drill at a specific location/structure to prove or disprove its hypothesized influence on groundwater instead of relying on interpolated groundwater data between existing boreholes. Furthermore, more emphasis should be placed on joint density (spacing between joints), aperture width and interconnectivity instead of only relying on the three-dimensional orientation and locations of joints.

Unfortunately not enough borehole logs were available at the time of submission of this thesis. To better understand the influence of dolerite dykes on groundwater the borehole logs can be investigated to see whether dolerite was struck at specific boreholes and whether water was encountered above, below or within a dyke and what types of yields were acquired. Such data can then be statistically analysed. As mentioned before, the degree of weathering, geometry and grain size of dolerites can also be recorded and analysed.

According to the information gathered through this study, the most suitable groundwater targets for further investigation are recommended to meet the following criteria. Where sub-horizontal clusters of joint intersects correlate with the strike direction of rivers in that area: Drill in highly weathered features (preferably ones that formed under tensional conditions) striking parallel to these clusters/rivers and if possible at the contacts between different lithologies.

6. REFERENCES:

Andersen, N. J. B. and Ainslie, L. C, 1994. Neotectonic reactivation – an aid to the location of groundwater. African Geoscience Review 1 (no.1): 1-10.

Anderson, E. M. 1951. *The dynamics of faulting and dyke formation with applications to Britain*. Edinburgh: Oliver & Boyd. 206 p.

Andreoli, M. A. G., M. Doucoure, J. Van Bever Donker, D. Brandt, and N. J. B. Andersen 1996. Neotectonics of southern Africa: A review. Africa Geosc. Rev. 3 (no.1): 1-16.

Anhaeusser, C.R. 1992. Structures in granitoid gneisses and associated migmatites close to the boundary of the Limpopo Belt, South Africa. Precambrian Res., 55: 81-92.

Aydin, A. 1978. Small faults formed as deformation bands in sandstone. Pure and Applied Geophysics. 116: 913-930.

Aydin, A. and Johnson, A. M., 1978. Development of faults as zones of deformation bands and as slip surfaces in sandstone. Pure and Applied Geophysics. 116: 931-942.

Barker, O.B. 1979. "A contribution to the geology of the Soutpansberg Group, Waterberg Supergroup, northern Transvaal." Unpublished M.Sc. thesis, University of the Witwatersrand, Johannesburg.

Barker, O. B., 1983. A proposed geotectonic model for the Soutpansberg Group within the Limpopo Mobile Belt, South Africa. Special Publication of the Geological Society of South Africa. 8: 181-190.

Barker, O. B., Brandl, G., Callaghan, C. C., Eriksson P. G. and Van der Neut, M. 2006. The Soutpansberg and Waterberg Groups and the Blouberg Formation. *In:* Johnson, M. R. (Ed.), *The geology of South Africa.* Pretoria: The Geological Society of South Africa and the Council for Geoscience.

Barton, J.M., Robb, L.J., Anhaeusser, C.R. and van Nierop, D.A. 1983. Geochronologic and Sr-isotopic studies of certain units in the Barberton granite-greenstone terrane, South Africa. *In*: Anhaeusser, C.R. (Ed.), *Contributions to the geology of the Barberton Mountainland*. Spec. Publ. Geol. Soc. S. Afr. 9: 6-72.

Barton Jr., J. M., Van Reenen, D.D., Roering, C.A. 1990. The significance of 3000 Ma granulite facies mafic dykes in the central zone of the Limpopo belt, southern Africa. Precamb. Res., 48: 299-308.

Barton, J.M., Doig, R., Smith, C.B., Bohelnder, F. and van Reenen, D.D. 1992. Isotopic and REE characteristics of the intrusive charnoenderbite and enderbite geographically associated with the Matok Pluton, Limpopo Belt, southern Africa. Precambrian Res., 55: 451-467.

Barton Jr., J.M., Pretorius, W. 1997. Soutpansberg age (1.85 Ga.) magmatism and metallogenesis in southern Africa: a result of regional rifting. Abstract: International Symposium on Plumes, Plates and Mineralization. University of Pretoria, South Africa.

Bird, P., Ben-Avraham, Z., Schubert, G., Andreoli, M., and Viola, G. 2006. Patterns of stress and strain rate in southern Africa. Journal of Geophysical Research 111, B08402.

Bohlender, F. 1992. "Igneous and metamorphic charnockitic rocks in the Southern Marginal Zone of the Limpopo Belt with special emphasis on the Matok enderbitic-granitic suite." Unpublished Ph.D. thesis, Rand Afrikaans University, Johannesburg, 261pp.

Bosch, P.J.A. (1992). "Die Geologie van die Wolkberg Groep tussen die Abel Erasmuspas en Graskop, Oos Transvaal." Unpublished M.Sc. thesis, University of Pretoria, South Africa, 290pp.

Brandl, G. (1985). Sheet 2328 Pietersburg (1:250000 Geological series). Geol Surv. S. Afr.

Brandl, G. (1986). The geology of the Pietersburg area. Explanation of sheet 2328 (1:250000 Geological series) Geol Surv. S. Afr., 43pp.

Brandl, G., 1987. The geology of the Tzaneen area. Explanation of sheet 2330. Geol. Surv. S. Afr., Pretoria 43 pp.

Brandl, G. (1987). The geology of the Tzaneen area. Explanation of Sheet 2330 (1:250000 Geological series) Geol Surv. S. Afr., 55pp.

Brandl, G. and Kröner, A. 1993. Preliminary results from single zircon studies from various Archaean rocks of the north-eastern Transvaal. Abstr. 16th Coll. African geology, Mbabane, Swaziland. 1: 54-56.

Brandl, G. 1995. Reactivation of certain faults in the Limpopo Belt during the Quaternary. *In* Extended Abstracts of the Centennial Geocongress, vol. 1, J. M. Barton and Y. E. Copperthwaite, pp. 442– 444, Geol. Soc. of S. Africa, Johannesburg.

Brandl, G., Jaeckel, P. and Kröner, A. (1996). Single zircon age for the felsic Rubbervale Formation, Murchison greenstone belt, South Africa. S. Afr. J. Geol., 99, 229-234.

Brandl, G. (in press). Mashashane Suite, including the Lunsklip, Uitloop and Uitvlught granite. In: Johnson, M.R. (Ed.), Catalogue of South African Lithostratigraphic Units. S. Afr. Comm. Strat.
Bromley, J. Mannström, B., Nisca, D. and Jamtlid, A. (1994). Airborne geophysics: application to ground-water study in Botswana. Ground Water, 32. 79-90.

Bumby, A.J., 2000. "The geology of the Blouberg Formation. Waterberg and Soutpansberg Groups in the area of Blouberg mountain, Northern Province, South Africa." Unpublished Ph.D. thesis, University of Pretoria, South Africa.

Bumby, A.J., Eriksson, P.G., van der Merwe, R., Maier, W.D., 2001. The stratigraphic relationship between the Waterberg Group and the Soutpansberg Group (Northern Province, South Africa): Evidence from the Blouberg area. S. Afr. J. Geol. 104 (3).

Bumby, A.J., et al. 2002. A half-graben setting for the Proterozoic Soutpansberg Group (South Africa): evidence from the Blouberg area. Sedimentary Geology 147: 37-56.

Bumby, A.J., et al. 2004. The early Proterozoic sedimentary record in the Blouberg area, Limpopo Province, South Africa; implications for the timing of the Limpopo orogenic event. Journal of African Earth Sciences 39: 123-131.

Burke, K. & Dewey, J.F. 1973. Plume-generated triple junctions: key indicators in applying plate tectonics to old rocks. J. Geol., 81: 406-433.

Button, A. 1973. A study of the stratigraphy and development of the Transvaal basin in the eastern and northeastern Transvaal. Unpublished Ph. D. thesis, University of the Witwatersrand, Johannesburg, 133pp.

Byerlee, J. D. 1967. Frictional characteristics of granite under high confining pressure. Journal of Geophysical Research 72: 3639-3648.

Byerlee, J. D. 1978. Friction of Rocks. Pure and Applied Geophysics 116: 615-626.

Cheney, E.S., Barton Jr., J.M., Brandl, G. 1990. Extent and age of the Soutpansberg sequences of southern Africa. S. Afr. J. Geol. 93: 644– 675.

Cook, P.G. 2003. A guide to regional groundwater flow in rock aquifers. CSIRO, Australia. 108 pp.

Coulomb, C. A. 1773. Sur une application des regles de maximus et minimis a quelques ploblemes de statique relatives a l'architecture: Academie Royale des Sciences, Memoires de Mathematique de Physique par divers Savants. 7: 343-382.

Cox, K. G. 1992. Karoo igneous activity and the early stages of break-up of Gondwanaland. *In: Magmatism and the causes of continental breakup*. Sotey, B. C., Alabaster, A. And Pankhurst, R. J. (eds.). Geological Society of London Special Publication.

Davis, G. H. and Reynolds, S. J. 1996. Structural geology of rocks and regions. Second edition: Wiley & Sons, New York.

The Municipal Demarcation Board of South Africa (cited Nov. 10, 2008).
Available at: www.demarcation.org.za

De Villiers, S.B. and Brandl, G. 1977. Die Mashashane granietplutoon noordoos van Potgietersrus. Ann. Geol, Surv. S. Afr., 11: 7-13.

De Wit, M. J., et al. 1992. Formation of an Archaean continent. Nature 357: 553-562.

De Wit, M. J., et al., 1993. Gold-bearing sediments in the Pietersburg greenstone belt: age equivalents of the Witwatersrand Supergroup sediments, South Africa. Econ. Geol. 88: 1242-1252.

Donath, F. A., 1961. Experimental study of shear failure in anisotropic rocks: Geological Society of America Bulletin 72: 985-989.

Government Communication and Information System (GCIS) 2004. South Africa Yearbook 2003/04. Pretoria: GCIS and STE Publishers. ISBN 1-919855-18-1. Available: http://www.gcis.gov.za/docs/ publications/yearbook.htm [2008, 7 November]

Grantham, G. H. 1996. Aspects of Jurassic Magmatism and Faulting in western Dronning Maud Land, Antarctica: Implications for Gondwana breakup. pp. 63-71 in *Weddell Sea Tectonics and Gondwana Break-up*. Sorey, B. C., King, E. C. and Livingstone, R. A. (Eds.). Geological Society Special Publication No. 108.

Groundwater Resources Information Project, 2002. Department of Water Affairs and Forestry of South Africa.

Hafner, W. 1951. Stress distribution and faulting. Geological Society of America Bulletin 62: 373-398.

Hatton, C. J. 1995. Primary magmas in the Ventersdorp and Bushveld Igneous Provinces: Magma extraction from a lower mantle plume. *Ext. Abstr. Centennial Geocongress,* Geol. Soc. S. Afr., Rand Afrikaans Univ. 1, 520-521.

Handin, J. 1969. On the Coulomb-Mohr failure criterion. Journal of Geophysical Research 74: 5343-5348.

Hartnady, C. J. H. 2002. Earthquake hazard in Africa: Perspectives on the Nubia-Somalia boundary, S. Afr. J. Sci. 98: 425– 428.

Henderson, D.R., Long, L.E. and Barton, J.M. 2000. Isotopic ages and chemical and isotopic composition of the Archaean Turfloop batholith, Pietersburg granite-greenstone terrane, Kaapvaal Craton, South Africa. S. Afr. J. Geol. 103: 38-46.

Holzer, L., Frei, R., Barton, Jr., J.M., Kramers, J.D. 1998. Unravelling the record of successive high grade events in the Central Zone of the Limpopo belt using Pb single phase dating of metamorphic minerals. Precambrian Res. 83: 87-115.

Horton, G. A., 1999. *Water Words Dictionary*. Nevada Division of Water Planning, Department of Conservation and Natural Resources, Nevada.

Hubbert, M. K., and Rubey, W. W. 1959. Role of fluid pressure in mechanics of overthrust faulting. Part 1: Geological Society of America Bulletin 70: 115-166.

Jansen, H. 1975. The Soutpansberg Trough – An Aulocagen. Transactions of the Geological Society of South Africa 78: 129-136.

Klein, J. A. 1980. Pleistocene to Recent faulting in the area west of Omaruru (SWA/Namibia). Reg. Geol. Ser. Open File Rep. RG-4, 28 pp., Geol. Surv. of Namibia, Windhoek.

Kröner, A., Jaeckel, P., Brandl, G. 2000. Single zircon ages for felsic to intermediate rocks from the Pietersburg and Giyani greenstone belts and bordering granitoid orogneisses, northern Kaapvaal Craton, South Africa. J. Afr. Earth Sci. 30 (no.4): 773-793.

McCarthy, T. S., N. D. Smith, W. N. Ellery and T. Gumbricht 2002. The Okavango delta: Semiarid alluvial-fan sedimentation related to incipient rifting, in Sedimentation in Continental Rifts, Spec. Publ. SEPM Soc. Sediment. Geol. 73: 179– 193.

McCourt, S., Armstrong, R.A., 1998. SHRIMP U-Pb zircon chronology of granites from the Central Zone, Limpopo Belt, southern Africa: implications for the age of the Limpopo Orogeny. S. Afr. J. Geol. 101: 329-337.

Mohr, O. C., 1990. Welche Umstande bedingen die Elastizitatsgrenze und den Bruch eines Materials: Zeitschrift der Vereines Deutscher Ingenieure 44: 1524-1530 and 1572-1577.

Mulwa, J., Gaciri, S., Barongo, J., Opiyo-Akech, N. and K., 2005. Geological and structural influence on groundwater distribution and flow in Ngong area, Kenya. African Journal of Science and Technology, Science and Engineering Series, V. 6, No. 1: 105-115.

Partridge, T. C. and R. R. Maude 2000. Macro-scale geomorphic evolution of southern Africa, in The Cenozoic of Southern Africa, Oxford Monogr. Geol. Geophys. 40: 3-18. Oxford Univ. Press, New York. (edited by T. C. Partridge and R. R. Maude)

Perchuk, L. L., Gerya, T. V., Van Reenen, D. D., Smit, C. A. and Krotov, A. V., 2000. P-T paths and tectonic evolution of shear zones separating high-grade terrains from cratons: examples from the Kola Peninsula (Russia) and the Limpopo Region (South Africa). Mineralogy and Petrology. 69: 109-142.

Poujol, M., Robb, L.J., Respaut, J.P., Anhaeusser, C.R. 1996. 3.07-2.97 Ga. greenstone belt formation in the northeastern Kaapvaal Craton: Implications for the origin of the Witwatersrand Basin. Econ. Geol. 91 (no.8): 1455-1461.

Poujol, M. and Robb, L.J. 1999. New U-Pb zircon ages on gneisses and pegmatite from south of the Murchison greenstone belt, South Africa. S. Afr. J. Geol. 102: 93-97.

Poujol, M. 2001. U-Pb isotopic evidence for episodic granitoid emplacement in the Murchison greenstone belt, South Africa. J. Afr. Earth Sci. 33: 155-163.

Poujol, M., Robb, L.J., Anhaeusser, C.R. and Gericke, B. 2003. A review of the geochronological constraints on the evolution of the Kaapvaal Craton, South Africa. Precambrian Research 127: 181-213.

Reches, Z. 1978. Analysis of faulting in a three-dimensional strain field: Tectonophysics 47: 109-129.

Reches, Z. 1983. Faulting of rocks in three-dimensional strain fields: 1. Failure of rocks in polyaxial, servo-control experiments: Tectonophysics 95: 111-132.

Robb, L.J. 1978. A general geological description of the Archaean granitic terrane between Nelspruit and Bushbuckridge, eastern Transvaal. Trans. Geol. Soc. S. Afr. 81: 331-338.

Robb, L.J. 1994. Cunning Moor Tonalite. *In*: Johnson, M.R. (Ed.) *Catalogue of South African Lithostratigraphic Units*. S. Afr. Comm. Strat. 5-11, 5-12.

Robb, L.J., Brandl, G., Anhaeusser, C.R. and Poujol, M. 2006. Arachaean Granitoid Intrusions. *In*: Johnson, M.R., Anhaeusser, C.R. and Thomas, R.J. (Eds.) *The Geology of South Africa*. Geological Society of South Africa, Johannesburg/Council for Geoscience, Pretoria 57-94.

Sami, K., Neumann, I., Gqiba, D., De Kock, G. and Grantham, G. 2002. Groundwater exploration in geologically complex and problematic terrain: Limpopo Mobile Belt. Water Research Commission Report, v. 2, chp.3.

Sanford, A. R. 1959. Analytical and experimental study of simple geologic structures: Geological Society of America Bulletin 70: 19-52.

Schaller, M. et al. 1999. Exhumation of Limpopo Central Zone granulites and dextral continent-scale transcurrent movement at 2.0Ga. along the Palala Shear Zone, Northern Province, South Africa. Precambrian Res. 96: 263-288.

Secor, D. T. 1965. Role of fluid pressure in jointing: American Journal of Science 263: 633-646.

Smit, C. A., Roering, C. and Van Reenen, D. D., 1992. The structural framework of the northern margin of the Limpopo Belt, South Africa. Precambrian Research. 55: 51-67.

Statistics South Africa 1998. The people of South Africa, Population Census, 1996: Census in Brief. Report No. 1: 03-01-11 (1996). Pretoria: Statistics South Africa.

SSA (2002a). *Income and Expenditure Survey 2000,* Pretoria: Statistics South Africa.

SSA (2002b). *Labour Force Survey September 2000,* Pretoria: Statistics South Africa.

SSA (2003a). *Census 2001,* Pretoria: Statistics South Africa.

Statistics South Africa. 2003. Census 2001: Census in Brief. Report No. 03-02-03 (2001). Pretoria: Statistics South Africa.

Stacey, T. R., and J. Wesseloo 1998. Final Project Report: Evaluation and upgrading of records of stress measurement data in the mining industry, GAP 511b, 31 pp. + appendices, Safety in Mines Res. Adv. Comm. (SIMRAC), Johannesburg.

Stettler, E.H., de Beer, J.H. and Blom, M.P. 1989. Crustal domains in the northern Kaapvaal as defined by magnetic lineaments. Precambrian Res. 45: 263-276.

Suppe, J., 1985. *Principles of structural geology*. Prentice-Hall: Englewood Cliffs, New Jersey, 537p.

Twiss, R. J., and Moores, E. M. 1992. *Structural geology*. New York: W. H. Freeman & Company, 532p.

Uken, R., Watkeys, M.K. 1997. An interpretation of mafic dyke swarms and their relationship with major mafic magmatic events on the Kaapvaal Craton and Limpopo Belt. S. Afr. J. Geol. 100 (no.4): 341-348.

University of Idaho's Glossary of Hydrogeology Terms.
Available from: http://www.if.uidaho.edu/~johnson/ifiwrri/sr3/gloss.html.

Van Eeden, O.R., Partridge, F.C., Kent, L.E. and Brandt, J.W. 1939. The mineral deposits of the Murchison range east of Leydsdorp. Mem. Geol. Surv. S. Afr. 36: 172pp.

Vearncombe, J.R., Barton, J.M., Cheshire, P.E., de Beer, J.H., Stettler, E.H. and Brandl, G. 1992. Geology, geophysics and mineralization of the Murchison Schist belt, Rooiwater Complex and surrounding granitoids. Mem. Geol. Surv. S. Afr. 81: 139pp.

Viola, G., M. Andreoli, Z. Ben-Avraham, I. Stengel, and M. Reshef 2005. Offshore mud volcanoes and onland faulting in southwestern Africa: Neotectonic implications and constraints on the regional stress field, Earth Planet. Sci. Lett., 231: 147–160.

Vorster, C.J. 1979. Die geologie van die Klein Letabagebied, noordoos Transvaal, met spesiale verwysing na die granietiese gesteentes. Unpublished M.Sc thesis. Rand Afrikaans Univ., Johannesburg 138pp.

Walraven, F. 1989. The geology of the Pilgrim's Rest area. Explanation of Sheet 2430 (1:250000) Geol. Surv. S. Afr., 24pp.

Wikipedia (modified Aug. 28, 2008; cited Dec. 3, 2008). Tm. Wikipedia Foundation Inc., U.S. registered 501(c)(3) tax-deductible nonprofit charity. Inverse distance weighting. Available from: http:/en.wikipedia.org/wiki/Inverse_distance_weighting

Willmitzer, H. (cited Oct. 15, 2008). Available from:
http://www.waterquality.de/hydrobio.hw/XYZTERMS.HTM

Zoback, M. L., and M. D. Zoback 1989. Tectonic stress field of the continental United States. Mem. Geol. Soc. Am. 172: 523– 539.

7. APPENDIX:

i.

Table 6: A table containing the coordinates for all the waypoints recorded in the field in decimal degrees.

Waypoint	Latitude	Longitude	Waypoint	Latitude	Longitude
1	-23.859917	29.199417	36	-23.2586	28.86785
2	-23.859850	29.188900	37	-23.2661	28.86938
3	-23.875550	29.106550	38	-23.2668	28.87483
4	-23.876733	29.107550	39	-23.2652	28.87315
5	-23.878267	29.109117	40	-23.2682	28.87362
6	-23.883800	29.116100	41	-23.2659	28.86957
7	-23.810050	29.215600	42	-23.2671	28.87025
8	-23.779533	29.158550	43	-23.2738	28.8685
9	-23.782517	29.158233	44	-23.2743	28.86915
10	-23.797417	29.145133	45	-23.2751	28.8718
11	-23.795933	29.149917	46	-23.2755	28.87248
12	-23.792533	29.127583	47	-23.2782	28.86103
13	-23.302867	29.054250	48	-23.2236	28.93787
14	-23.301033	29.055183	49	-23.6371	30.14962
15	-23.515233	29.353417	50	-23.6636	30.1652
16	-23.510683	29.355133	51	-23.5987	30.19453
17	-23.510433	29.355283	52	-23.4836	30.16018
18	-23.745950	29.271083	53	-23.4835	30.16018
19	-23.737683	29.262600	54	-23.551	30.09645
20	-23.688817	29.176383	55	-23.5579	30.09725
21	-23.626733	29.288500	56	-23.555	30.08915
22	-23.791833	29.124950	57	-23.5528	30.09513
23	-23.791500	29.118533	58	-23.5604	30.09147
24	-23.791200	29.117517	59	-23.5339	30.10513
25	-23.788833	29.116100	60	-23.5002	30.14985
26	-23.785917	29.114200	61	-23.5031	30.14532
27	-23.784383	29.111550	62	-23.5189	30.04257
28	-23.486617	28.681667	63	-23.5166	30.04402

Waypoint	Latitude	Longitude	Waypoint	Latitude	Longitude
29	-23.20175	28.72478	60	-23.50015	30.14985
30	-23.21578	28.75555	61	-23.50312	30.14532
31	-23.23052	28.77955	62	-23.5189	30.04257
32	-23.249	28.79877	63	-23.51657	30.04402
33	-23.25727	28.81843	64	-23.5123	29.9966
34	-23.25608	28.86162	65	-22.99323	29.92943
35	-23.25002	28.85835	66	-22.96868	29.94395
36	-23.25857	28.86785	67	-22.92753	29.932
37	-23.26605	28.86938	68	-23.18855	30.08773
38	-23.2668	28.87483	69	-23.61493	29.96477
39	-23.26523	28.87315	70	-23.6047	30.00608
40	-23.26815	28.87362	71	-23.71718	30.15205
41	-23.26588	28.86957	72	-23.78613	30.29683
42	-23.2671	28.87025	73	-23.8017	30.27332
43	-23.27375	28.8685	74	-23.8021	30.2656
44	-23.27425	28.86915	75	-23.75247	30.11002
45	-23.27508	28.8718	76	-23.6326	30.08468
46	-23.27547	28.87248	77	-23.64832	30.08172
47	-23.2782	28.86103	78	-23.64767	30.0884
48	-23.22363	28.93787	79	-23.64835	30.08867
49	-23.63707	30.14962	80	-23.64932	30.0926
50	-23.66358	30.1652	81	-23.6514	30.09363
51	-23.59873	30.19453	82	-23.65213	30.09472
52	-23.48355	30.16018	83	-23.51928	29.49438
53	-23.48352	30.16018	84	-23.5191	29.49503
54	-23.551	30.09645	85	-23.519	29.49538
55	-23.55785	30.09725	86	-23.51887	29.4959
56	-23.55498	30.08915	87	-23.51792	29.49912
57	-23.55275	30.09513	88	-23.48137	29.52992
58	-23.56042	30.09147	89	-23.42985	29.56173

Waypoint	Latitude	Longitude	Waypoint	Latitude	Longitude
59	-23.5339	30.10513	90	-23.44517	29.5862
91	-23.46707	29.63355	122	-23.4769	29.14792
92	-23.47063	29.63482	123	-23.4947	29.19627
93	-23.47315	29.63575	124	-23.5111	29.25137
94	-23.29685	29.5469	125	-23.463	29.29023
95	-23.52085	29.64022	126	-23.4663	29.23182
96	-23.52005	29.64218	127	-23.4896	29.21462
97	-23.51702	29.64487	128	-23.5816	28.77537
98	-23.51567	29.64465	129	-23.5422	28.71507
99	-23.51257	29.64297	130	-23.7513	28.70443
100	-23.51008	29.6416	131	-23.5688	29.88088
101	-23.5056	29.6432	132	-23.5688	29.88088
102	-23.4374	29.44268	133	-23.5057	29.73122
103	-23.52172	29.35575	134	-23.5057	29.7312
104	-23.7277	29.40645	135	-23.5529	29.82422
105	-23.79685	29.35245	136	-23.6104	29.89075
106	-23.76512	29.30138	137	-23.5875	29.88523
107	-23.62653	29.28267	138	-23.555	29.88493
108	-23.61642	29.19882	139	-23.5255	29.90265
109	-23.67662	29.25878	140	-23.5256	29.90265
110	-23.6742	29.28118	141	-23.4506	29.90068
111	-23.66727	29.29983	142	-23.367	30.53257
112	-23.71253	29.27752	143	-23.4471	30.36273
113	-23.5451	29.11297	144	-23.4674	30.30353
114	-23.50502	29.06215	145	-23.4769	30.25368
115	-23.49067	28.99825	146	-23.4924	30.23017
116	-23.4998	28.9782	147	-23.5385	29.7192
117	-23.51298	28.92433	148	-23.5569	29.75663
118	-23.49335	28.91985	149	-23.5203	29.70848
119	-23.41987	28.88787	150	-23.5107	29.66693

Waypoint	Latitude	Longitude
120	-23.39633	28.9282
121	-23.41608	28.99165
166	-23.39977	30.12642
167	-23.50868	30.22278
168	-23.44255	30.15492
169	-23.41923	30.15883
170	-23.41753	30.15207
171	-23.39977	30.12642
172	-23.41672	30.24478
173	-23.41665	30.2444
174	-23.4164	30.24317
175	-23.41557	30.24307
176	-23.41382	30.24138
177	-23.418	30.24282
178	-23.41492	30.19688
164	-23.4013	30.13197
165	-23.3999	30.1262

ii. Poles to planes of joints in each 10’ x 10’ block:

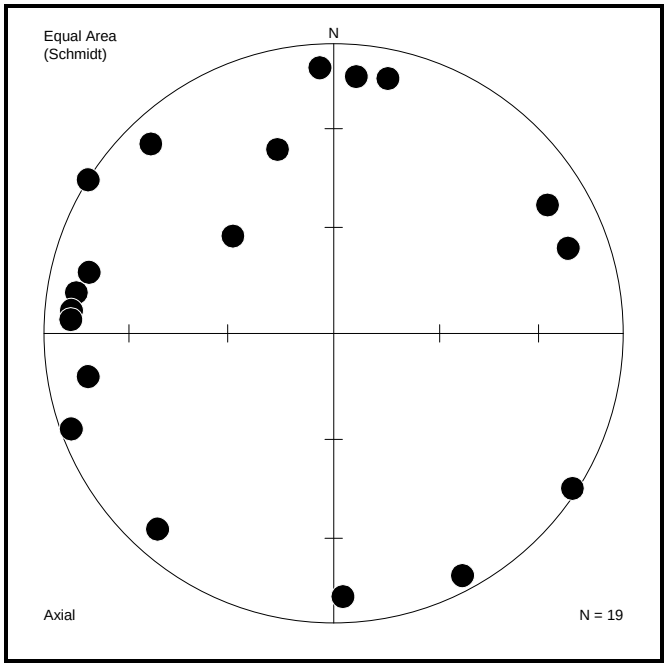

Figure 61: A summary of the poles to joint planes found in block S22° 50’ E29° 50’.

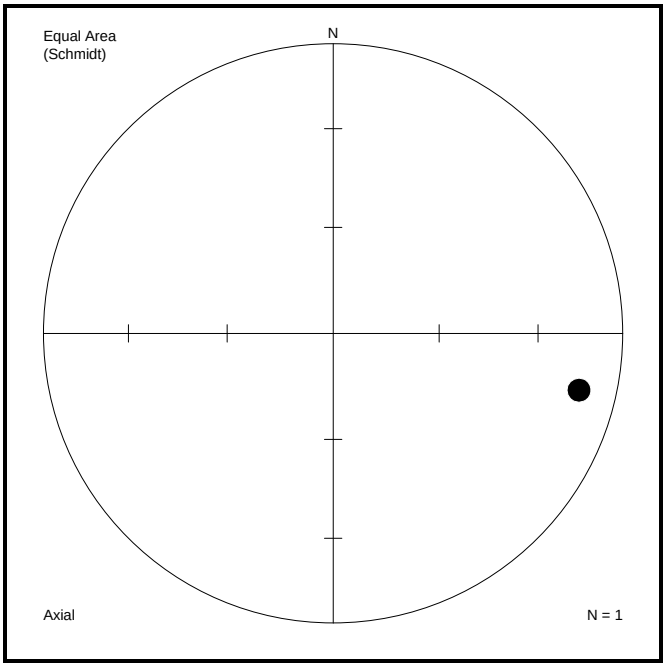

Figure 62: A summary of the poles to joint planes found in block S23° 10’ E29° 00’.

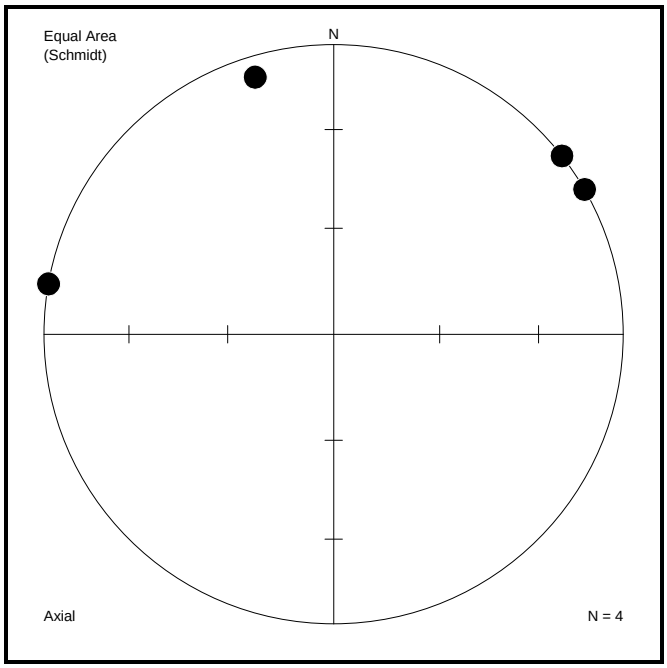

Figure 63: A summary of the poles to joint planes found in block S23° 10’ E29° 30’.

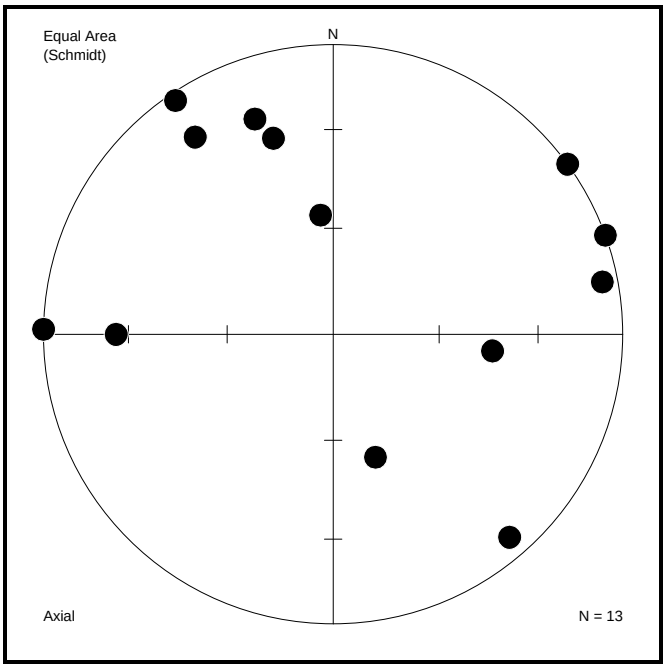

Figure 64: A summary of the poles to joint planes found in block S23° 10’ E30° 00’.

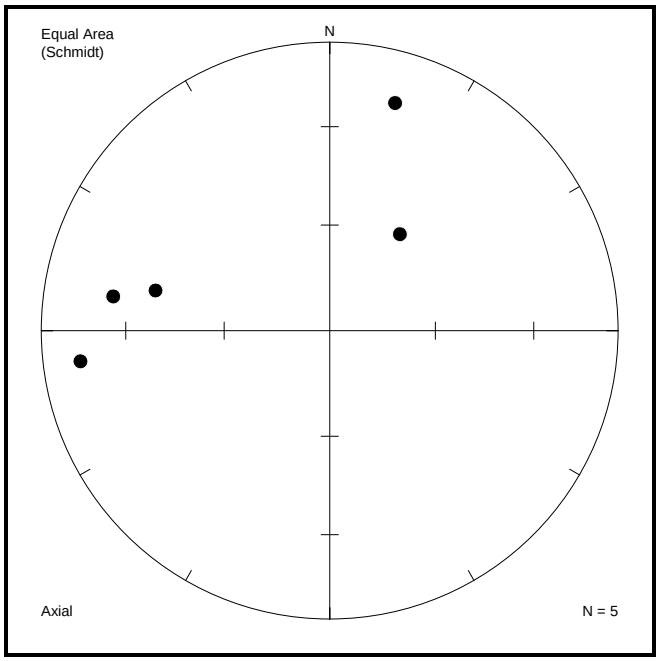

Figure 65: A summary of the poles to joint planes found in block S23° 20' E28° 50'.

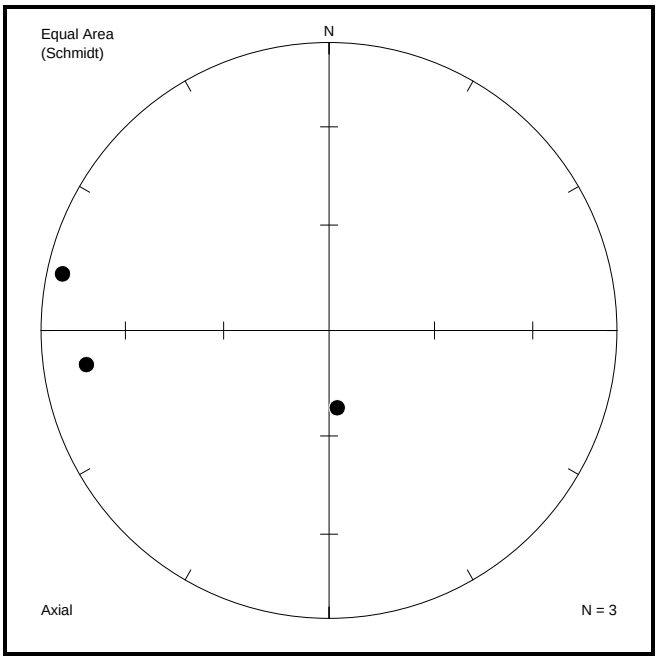

Figure 66: A summary of the poles to joint planes found in block S23° 20' E29° 00'.

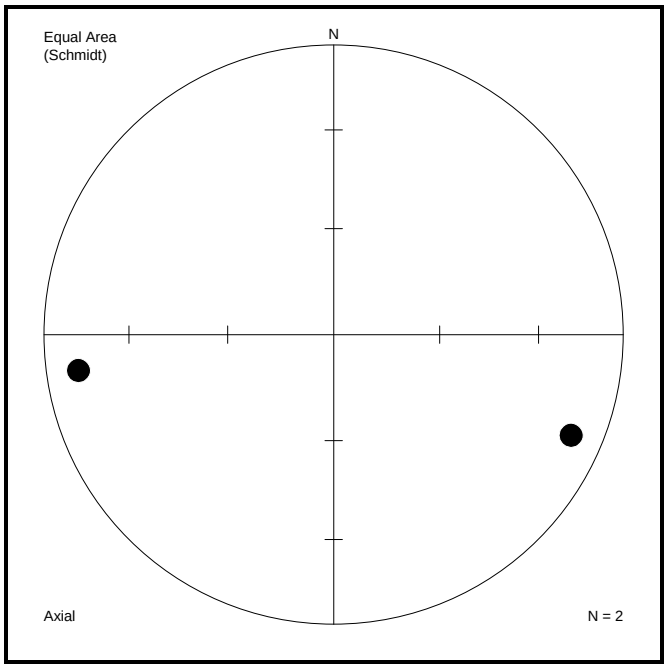

Figure 67: A summary of the poles to joint planes found in block S23° 20' E29° 10'.

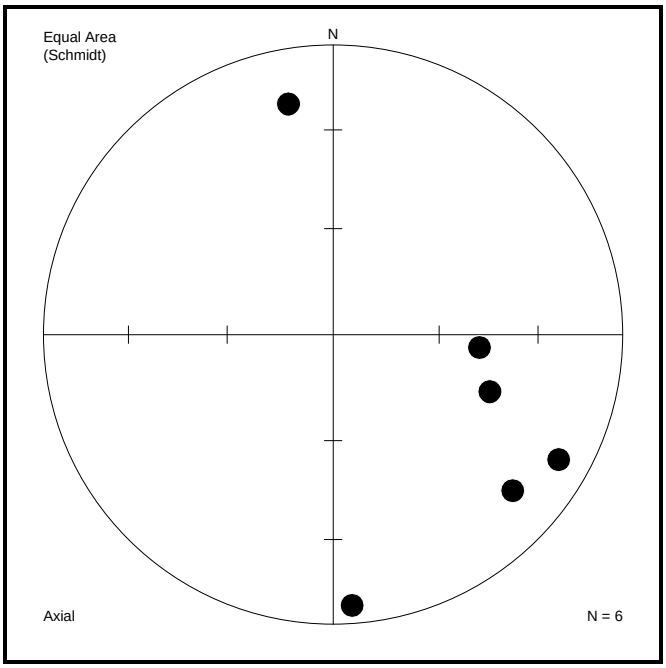

Figure 68: A summary of the poles to joint planes found in block S23° 20' E29° 20'.

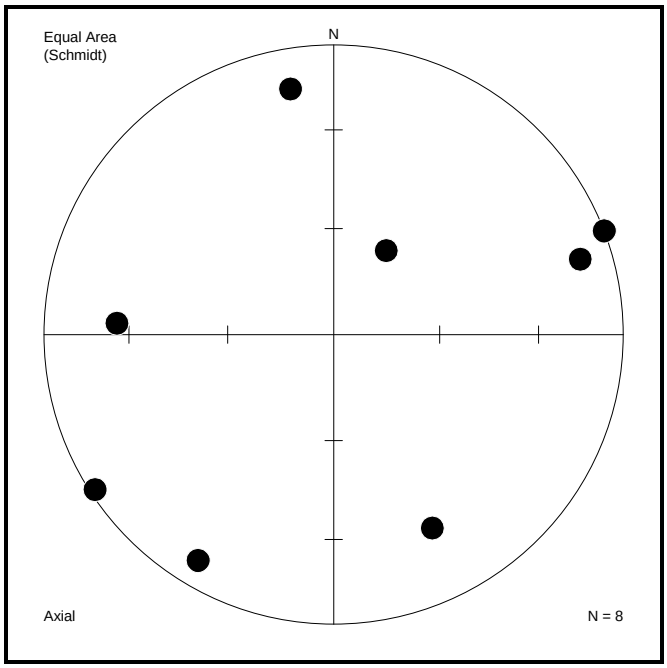

Figure 69: A summary of the poles to joint planes found in block S23° 20' E29° 30'.

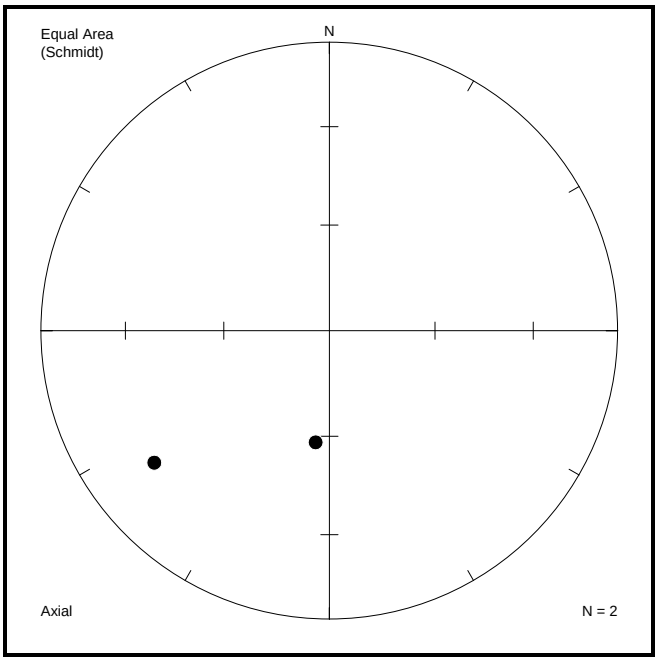

Figure 70: A summary of the poles to joint planes found in block S23° 20' E29° 50'.

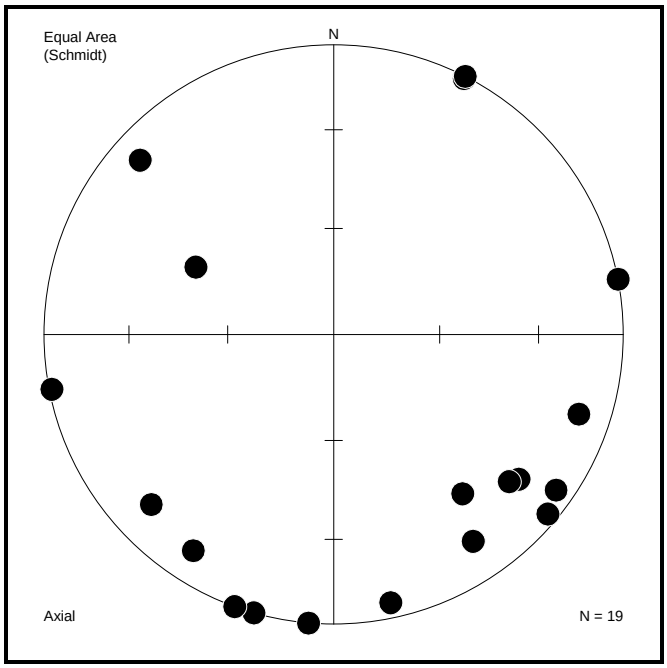

Figure 71: A summary of the poles to joint planes found in block S23° 20' E30° 00'.

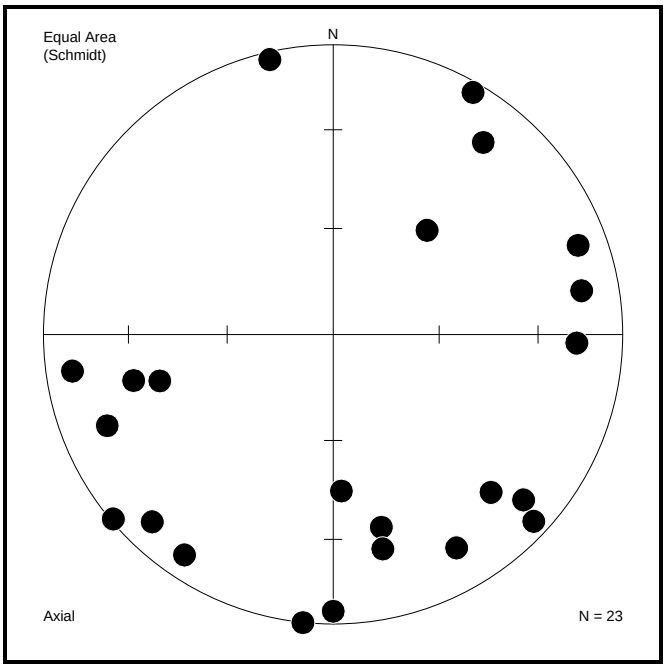

Figure 72: A summary of the poles to joint planes found in block S23° 20' E30° 10'.

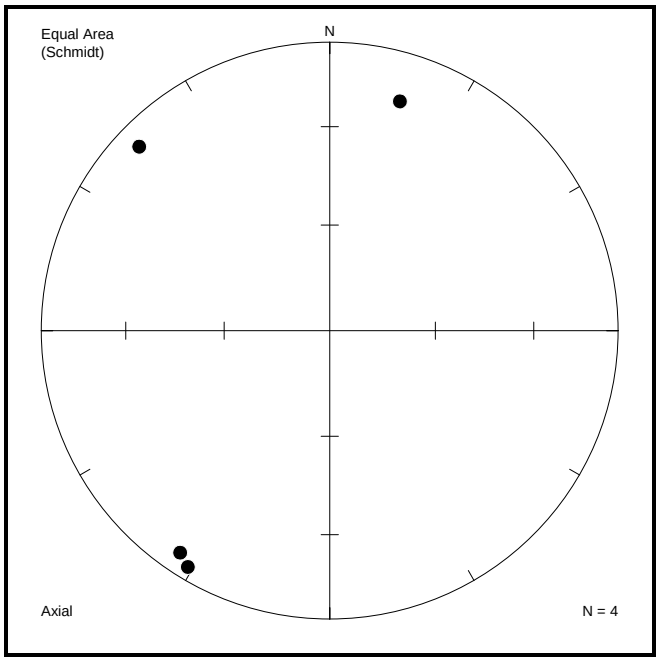

Figure 73: A summary of the poles to joint planes found in block S23° 20' E30° 20'.

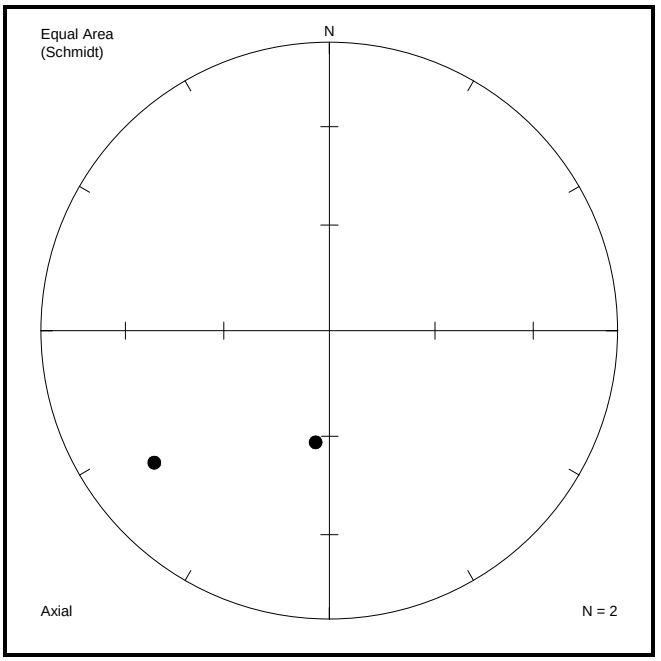

Figure 74: A summary of the poles to joint planes found in block S23° 20' E30° 30'.

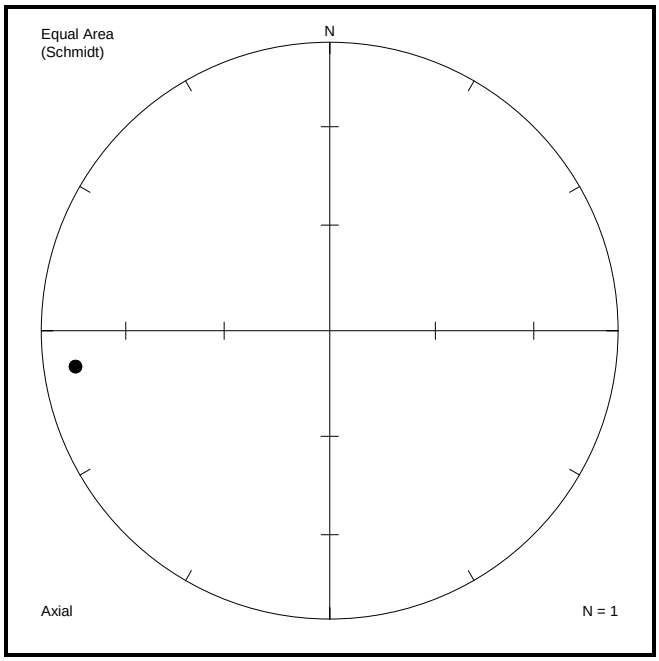

Figure 75: A summary of the poles to joint planes found in block S23° 30' E28° 40'.

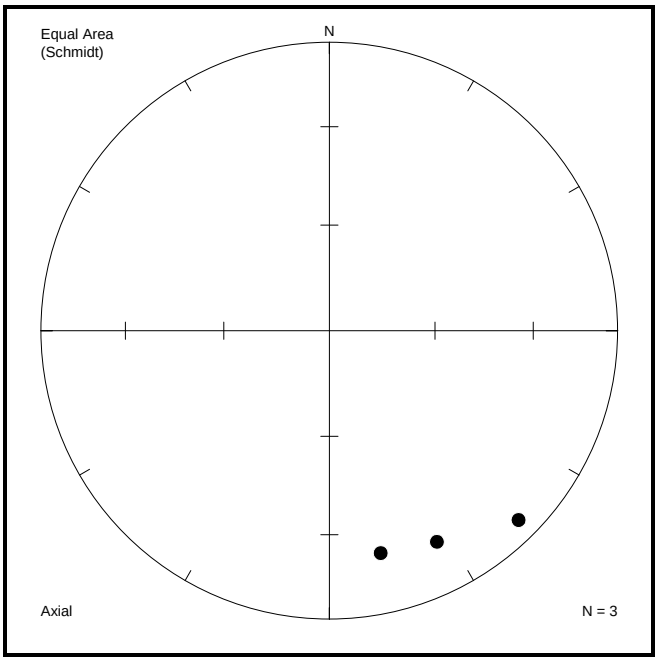

Figure 76: A summary of the poles to joint planes found in block S23° 30' E28° 50'.

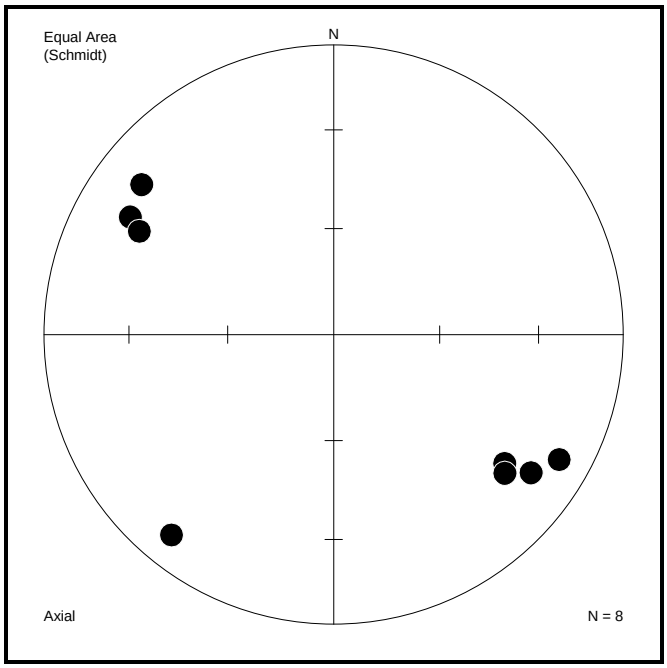

Figure 77: A summary of the poles to joint planes found in block S23° 30' E29° 20'.

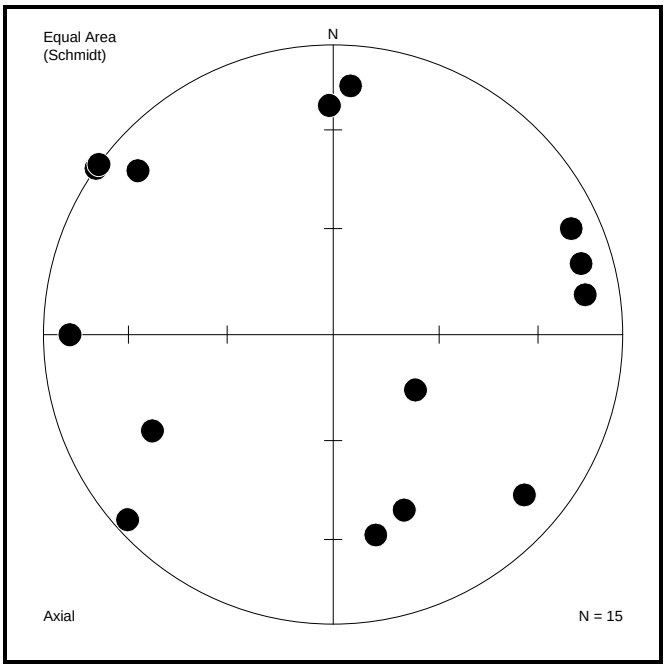

Figure 78: A summary of the poles to joint planes found in block S23° 30' E29° 30'.

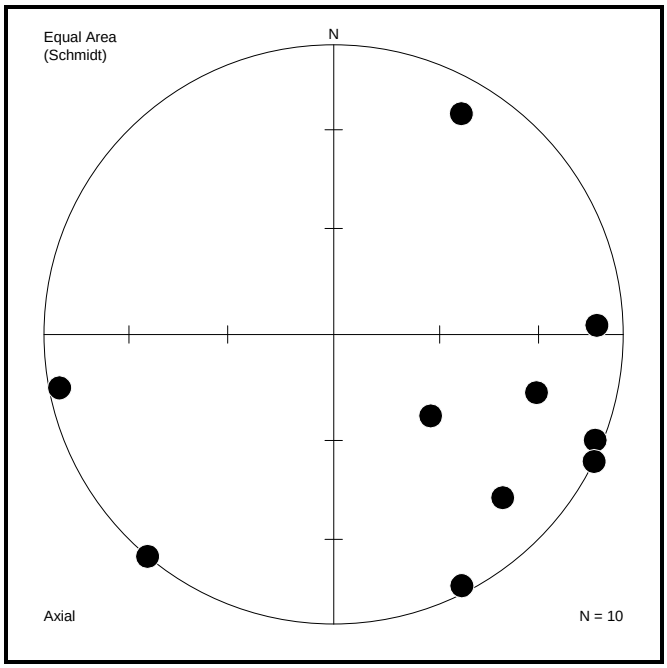

Figure 79: A summary of the poles to joint planes found in block S23° 30' E29° 40'.

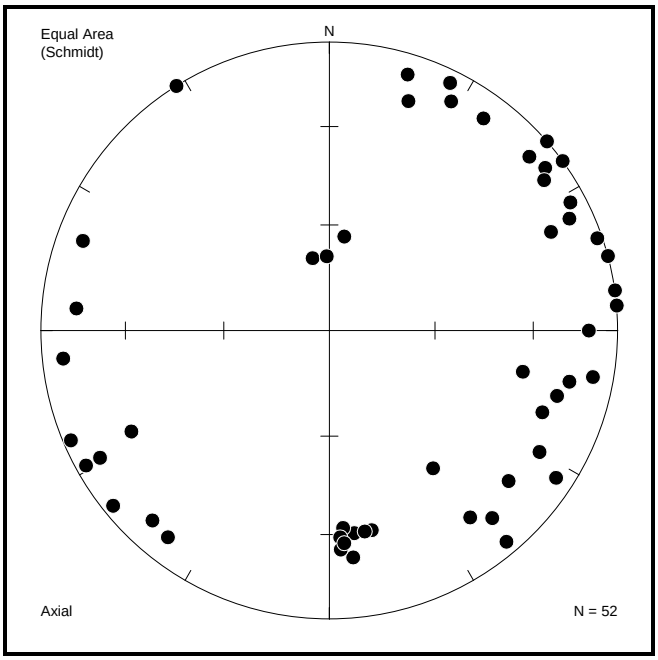

Figure 80: A summary of the poles to joint planes found in block S23° 30' E29° 50'.

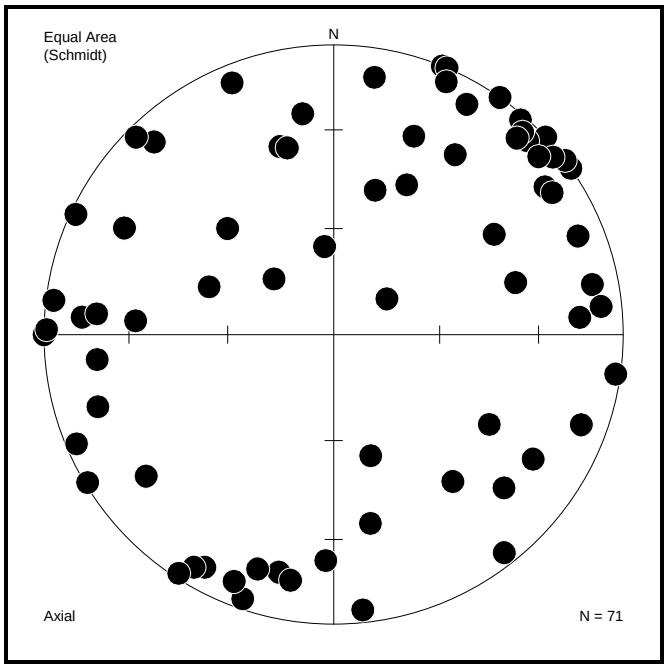

Figure 81: A summary of the poles to joint planes found in block S23° 30' E30° 00'.

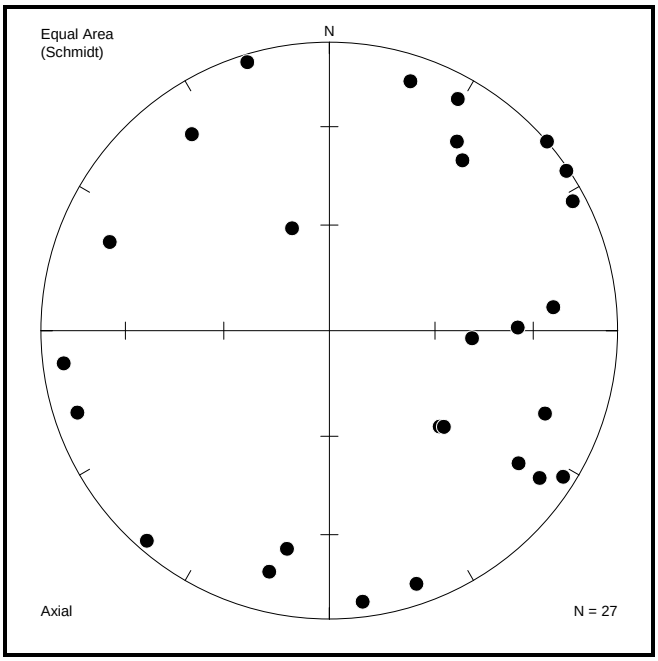

Figure 82: A summary of the poles to joint planes found in block S23° 40' E29° 00'.

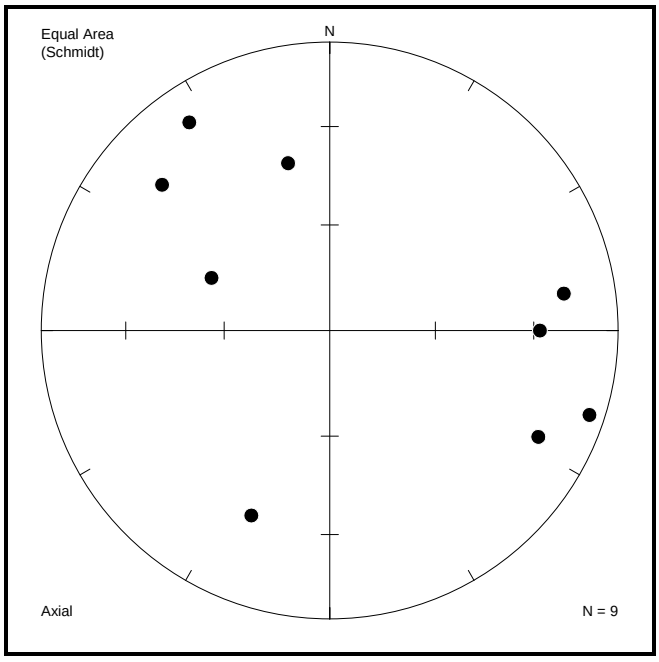

Figure 83: A summary of the poles to joint planes found in block S23° 40' E29° 10'.

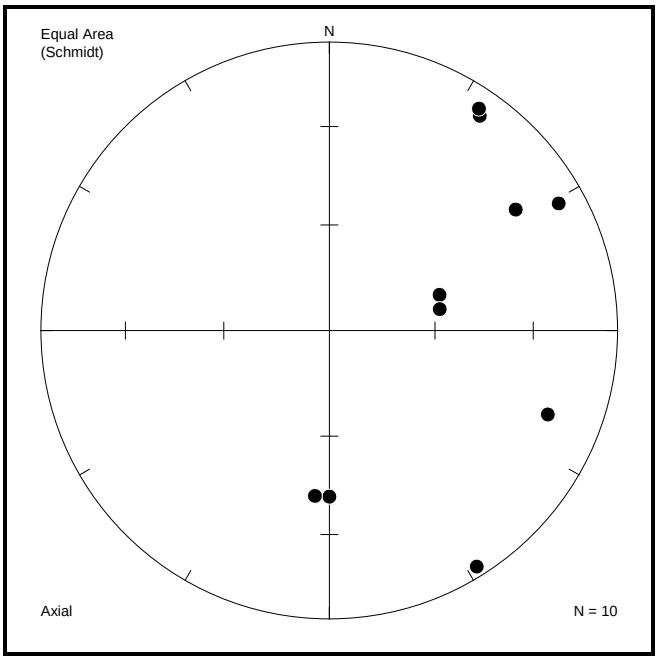

Figure 84: A summary of the poles to joint planes found in block S23° 40' E30° 00'.

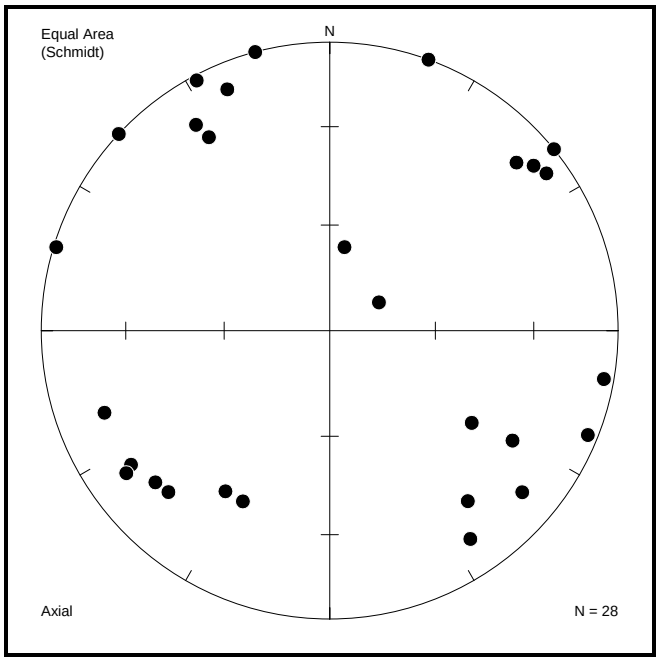

Figure 85: A summary of the poles to joint planes found in block S23° 40' E30° 10'.

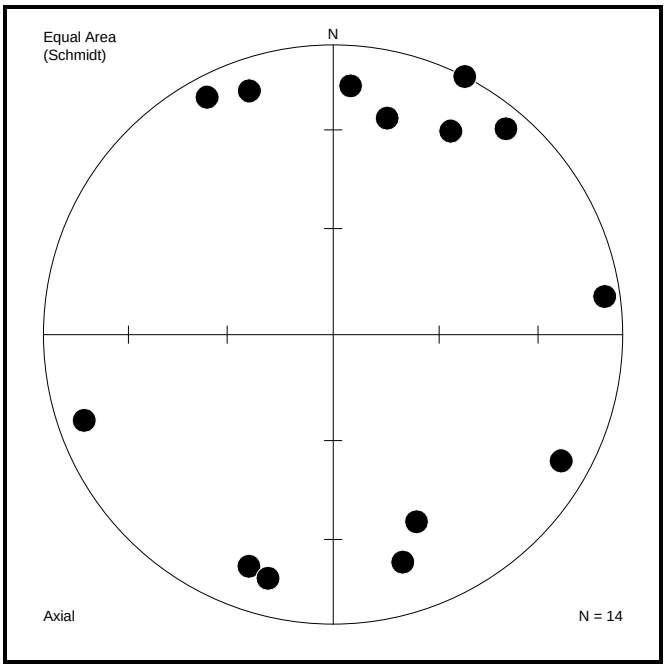

Figure 86: A summary of the poles to joint planes found in block S23° 50' E29° 00'.

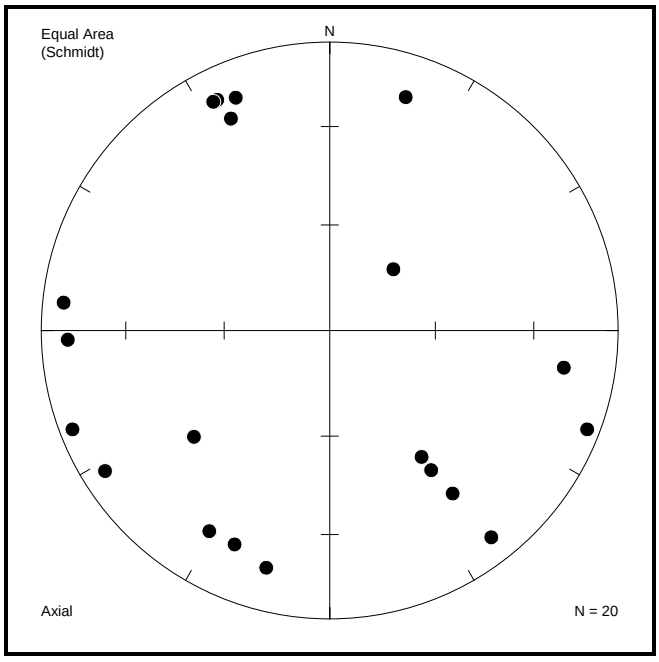

Figure 87: A summary of the poles to joint planes found in block S23° 50' E29° 10'.

iii. Rose diagrams indicating strikes of joints in each 10’ x 10’ block:

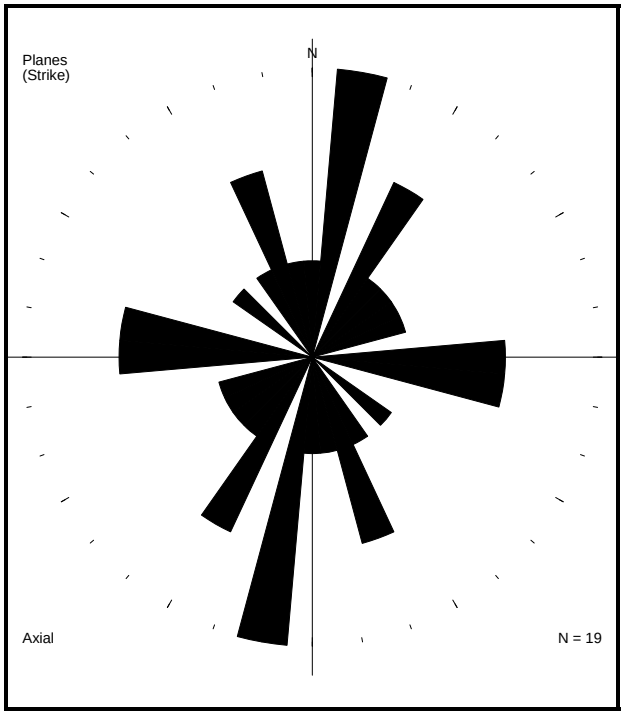

Figure 88: A summary of the joints' strike directions found in block S22° 50’ E29° 50’. (Ten degree intervals centred around 0°)

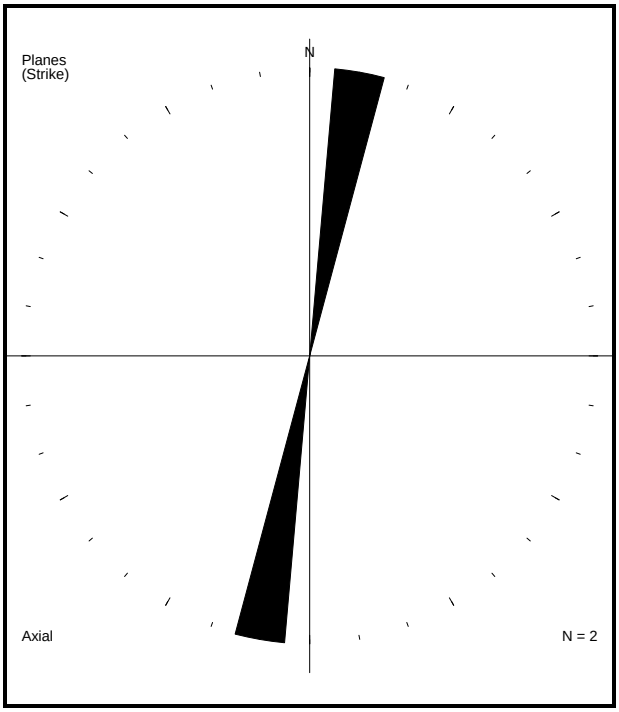

Figure 89: A summary of the joints' strike directions found in block S23° 10’ E29° 00’. (Ten degree intervals centred around 0°)

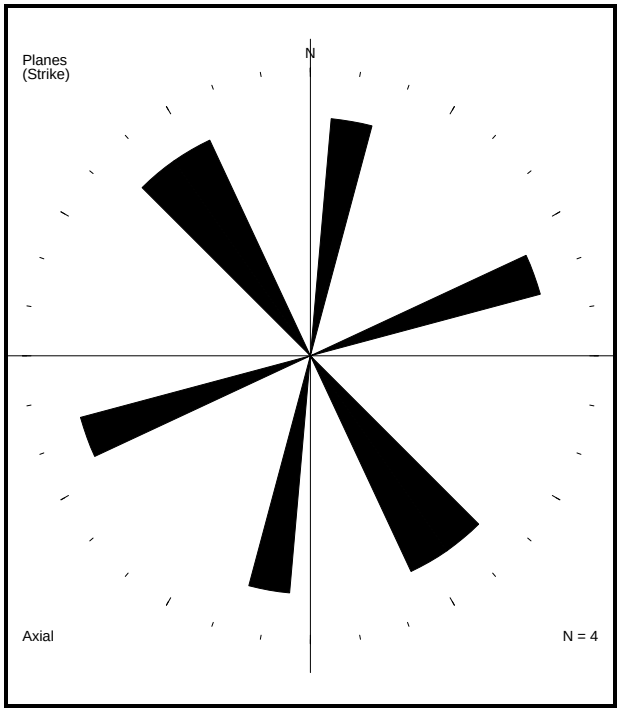

Figure 90: A summary of the joints' strike directions found in block S23° 10’ E29° 30’. (Ten degree intervals centred around 0°)

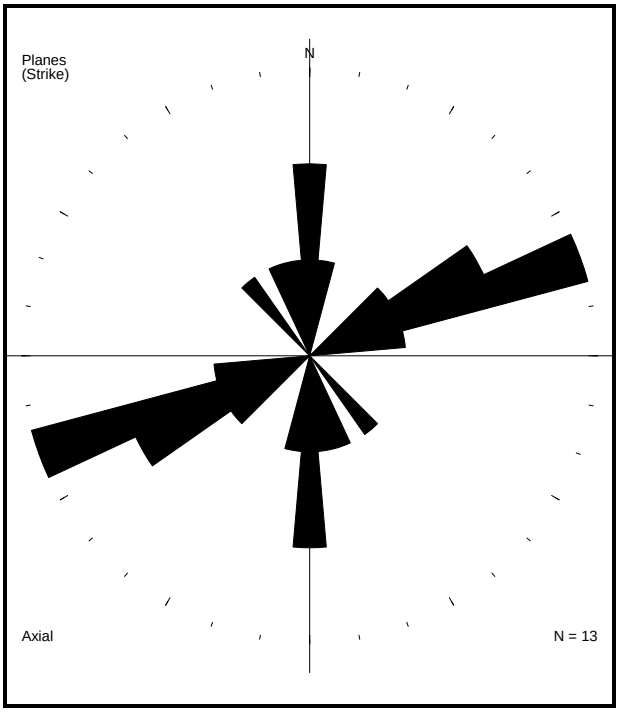

Figure 91: A summary of the joints' strike directions found in block S23° 10’ E30° 00’. (Ten degree intervals centred around 0°)

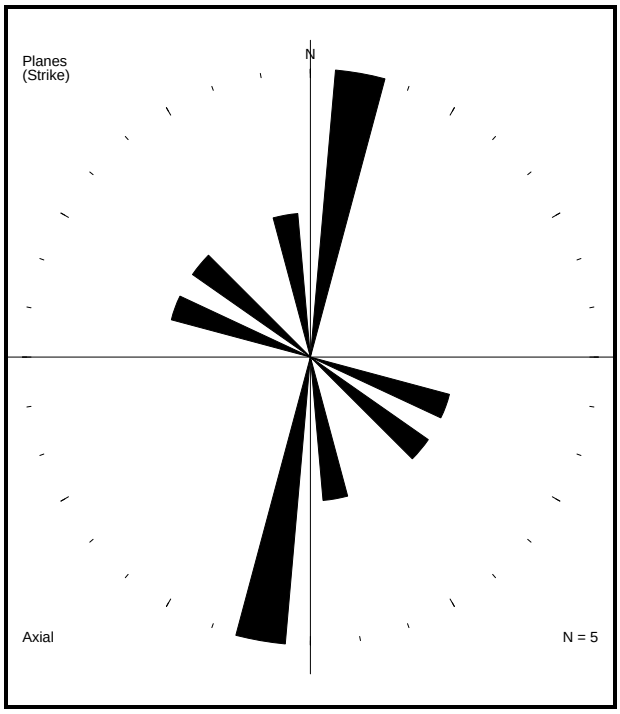

Figure 92: A summary of the joints' strike directions found in block S23° 20' E28° 50'. (Ten degree intervals centred around 0°)

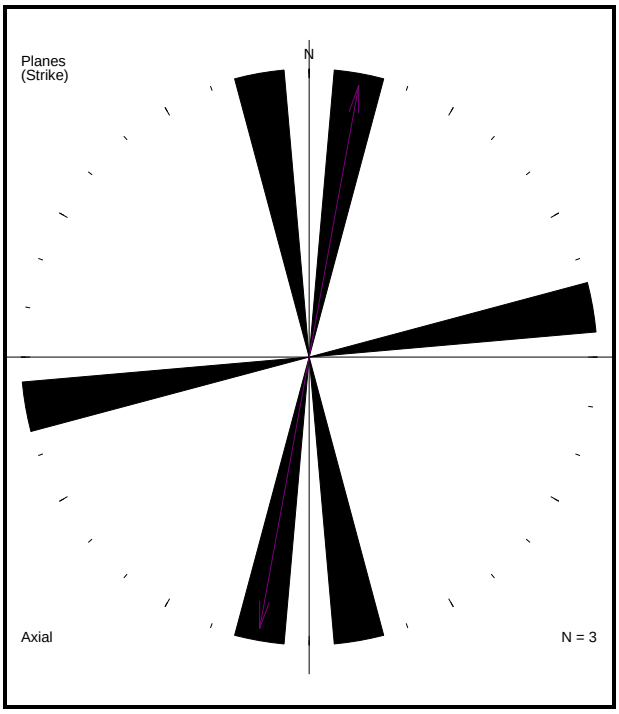

Figure 93: A summary of the joints' strike directions found in block S23° 20' E29° 00'. (Ten degree intervals centred around 0°)

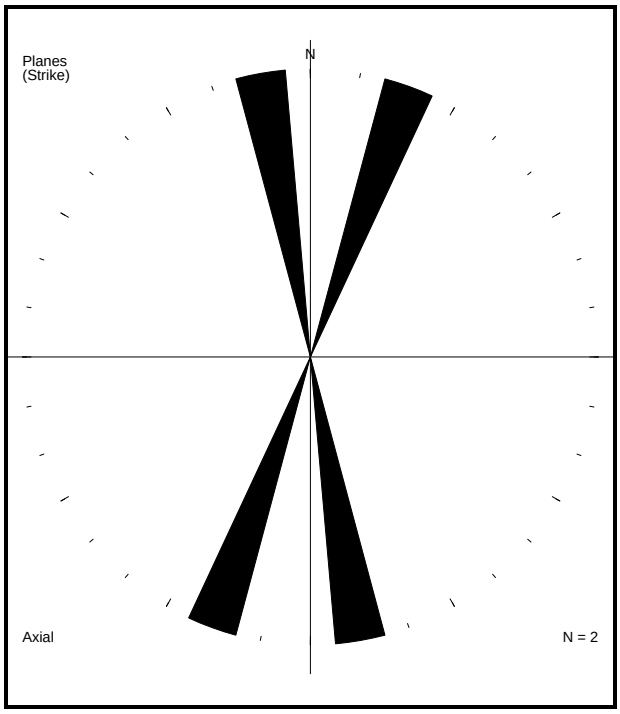

Figure 94: A summary of the joints' strike directions found in block S23° 20' E29° 10'. (Ten degree intervals centred around 0°)

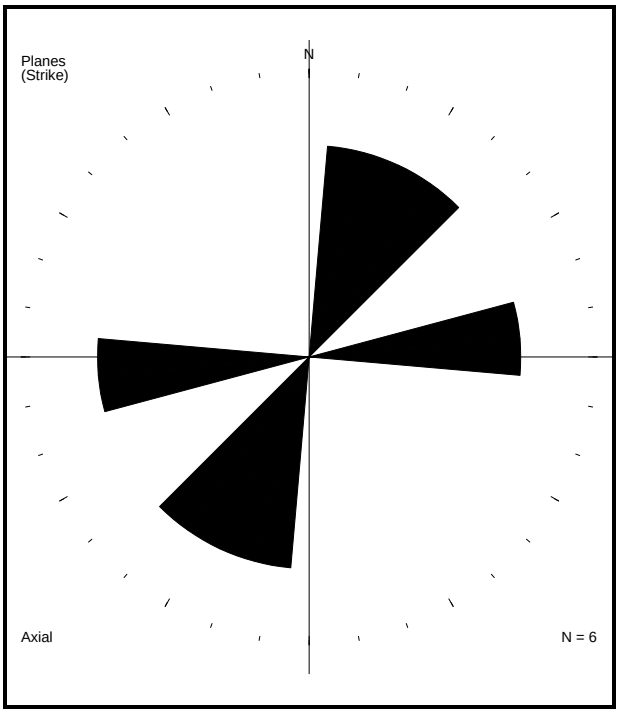

Figure 95: A summary of the joints' strike directions found in block S23° 20' E29° 20'. (Ten degree intervals centred around 0°)

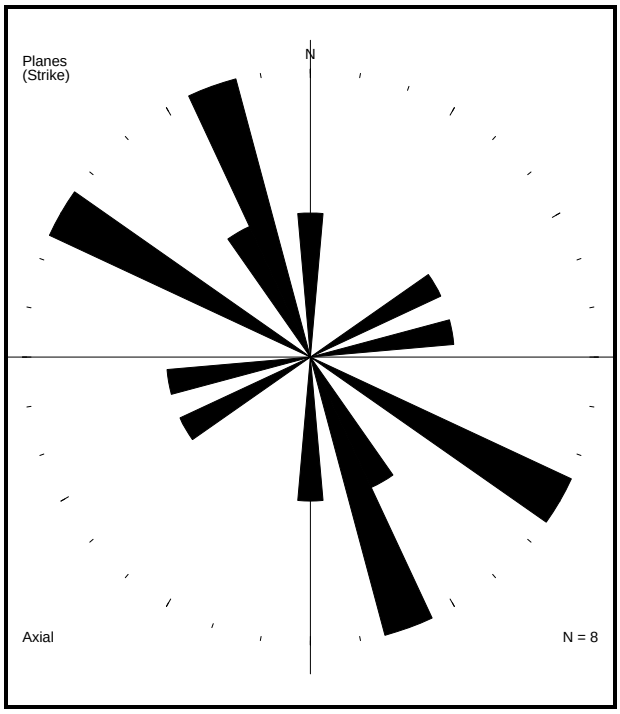

Figure 96: A summary of the joints' strike directions found in block S23° 20' E29° 30'. (Ten degree intervals centred around 0°)

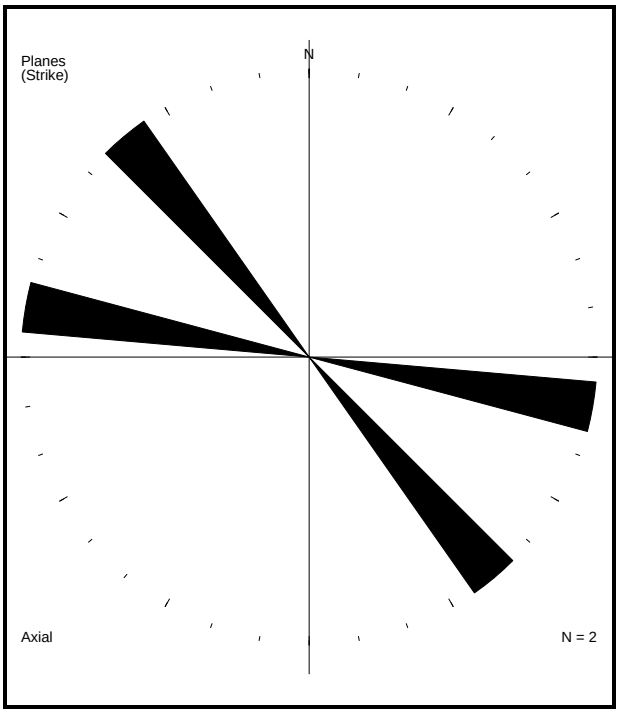

Figure 97: A summary of the joints' strike directions found in block S23° 20' E29° 50'. (Ten degree intervals centred around 0°)

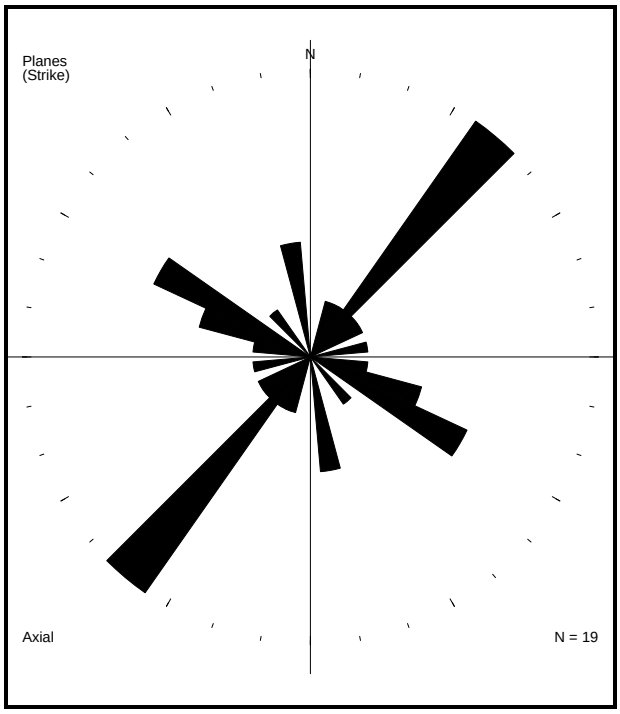

Figure 98: A summary of the joints' strike directions found in block S23° 20' E30° 00'. (Ten degree intervals centred around 0°)

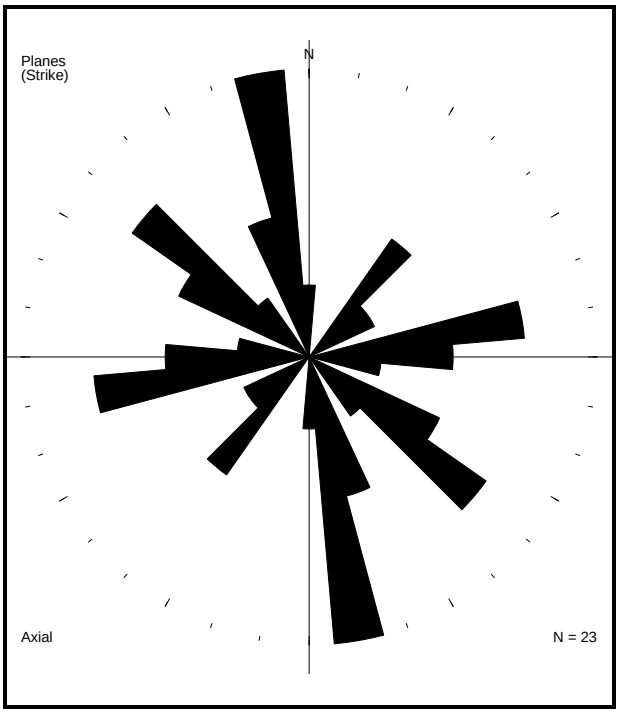

Figure 99: A summary of the joints' strike directions found in block S23° 20' E30° 10'. (Ten degree intervals centred around 0°)

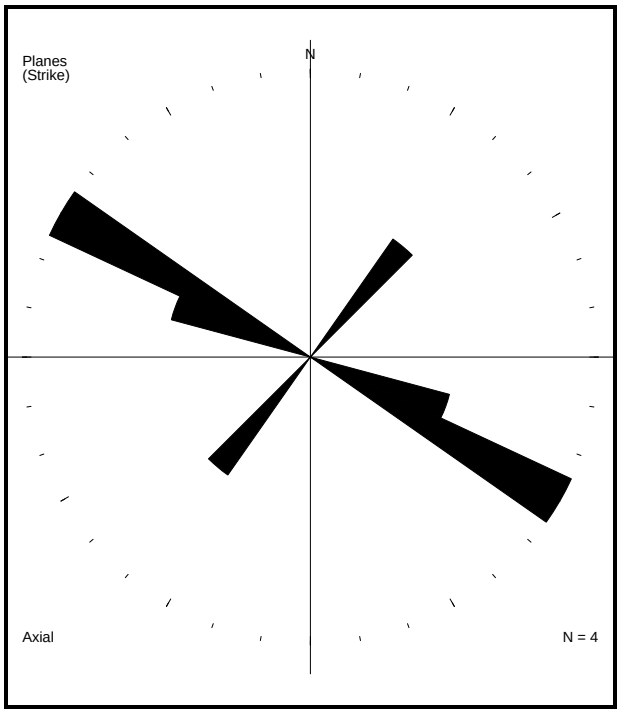

Figure 100: A summary of the joints' strike directions found in block S23° 20' E30° 20'. (Ten degree intervals centred around 0°)

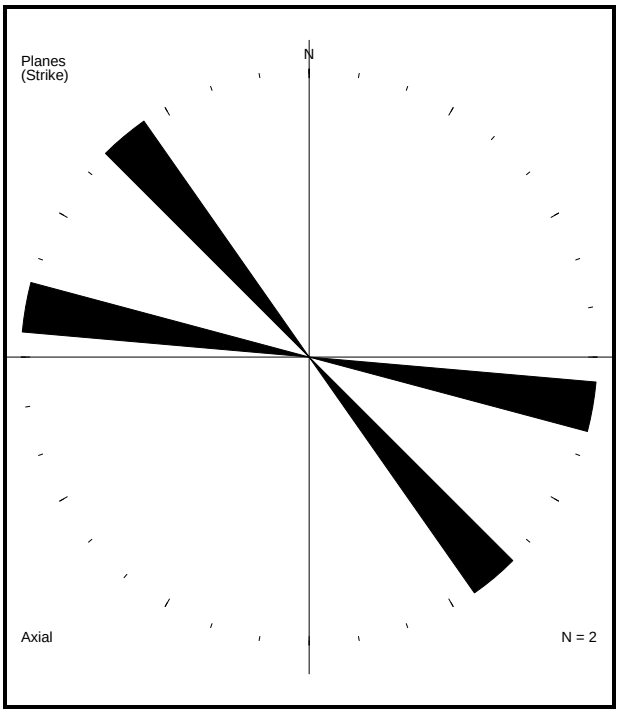

Figure 101: A summary of the joints' strike directions found in block S23° 20' E30° 30'. (Ten degree intervals centred around 0°)

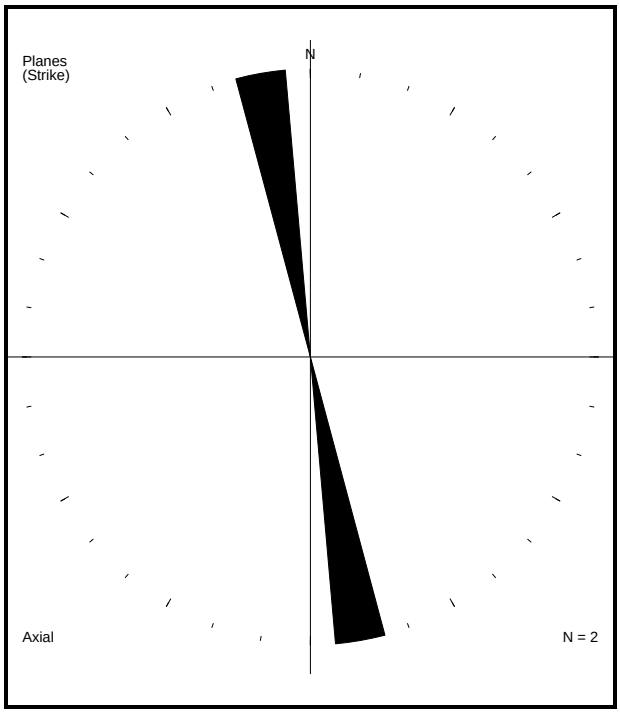

Figure 102: A summary of the joints' strike directions found in block S23° 30' E28° 40'. (Ten degree intervals centred around 0°)

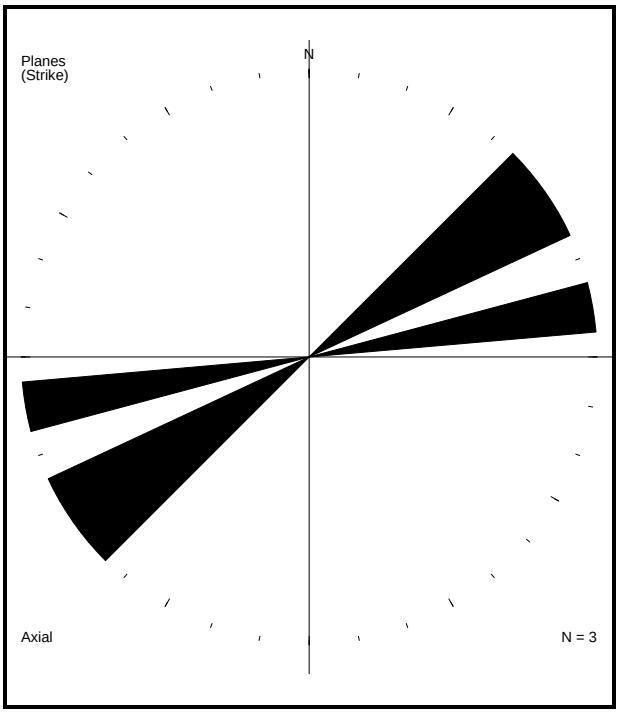

Figure 103: A summary of the joints' strike directions found in block S23° 30' E28° 50'. (Ten degree intervals centred around 0°)

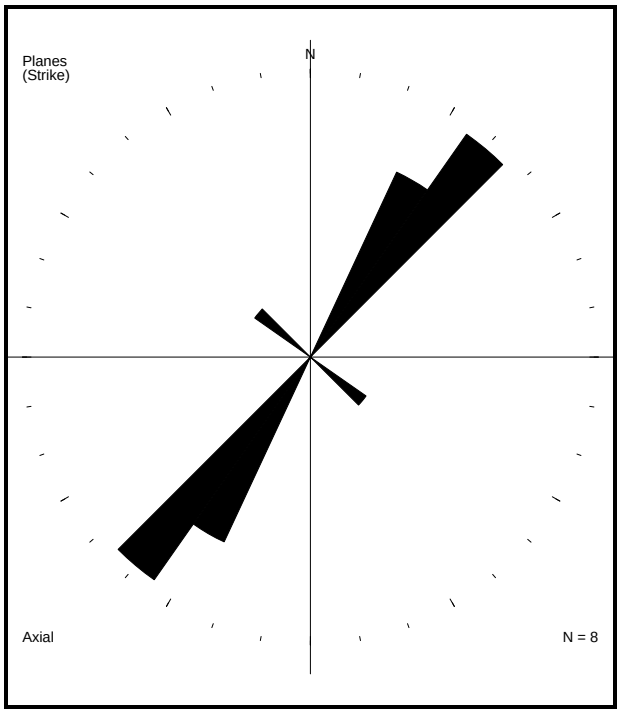

Figure 104: A summary of the joints' strike directions found in block S23° 30' E29° 20'. (Ten degree intervals centred around 0°)

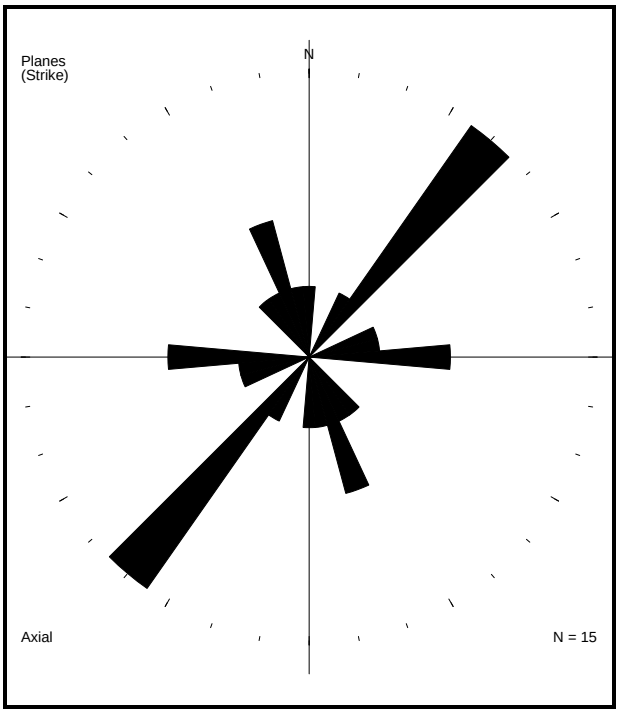

Figure 105: A summary of the joints' strike directions found in block S23° 30' E29° 30'. (Ten degree intervals centred around 0°)

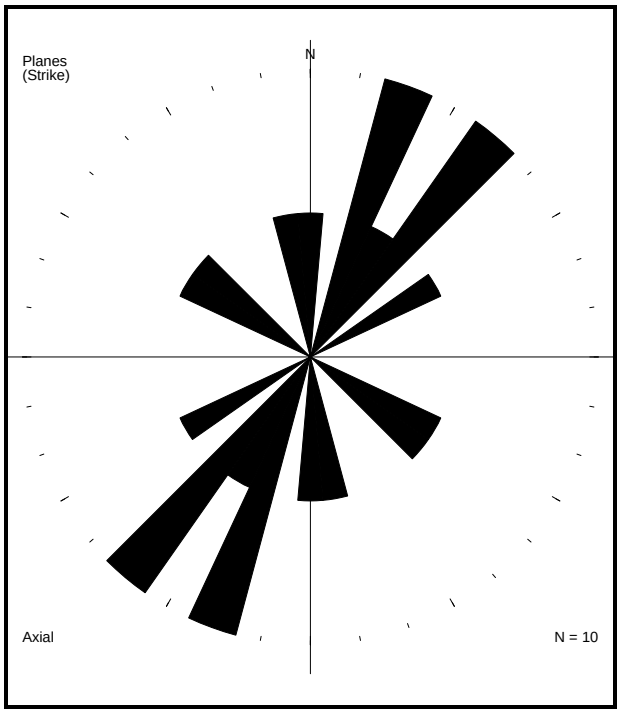

Figure 106: A summary of the joints' strike directions found in block S23° 30' E29° 40'. (Ten degree intervals centred around 0°)

Figure 107: A summary of the joints' strike directions found in block S23° 30' E29° 50'. (Ten degree intervals centred around 0°)

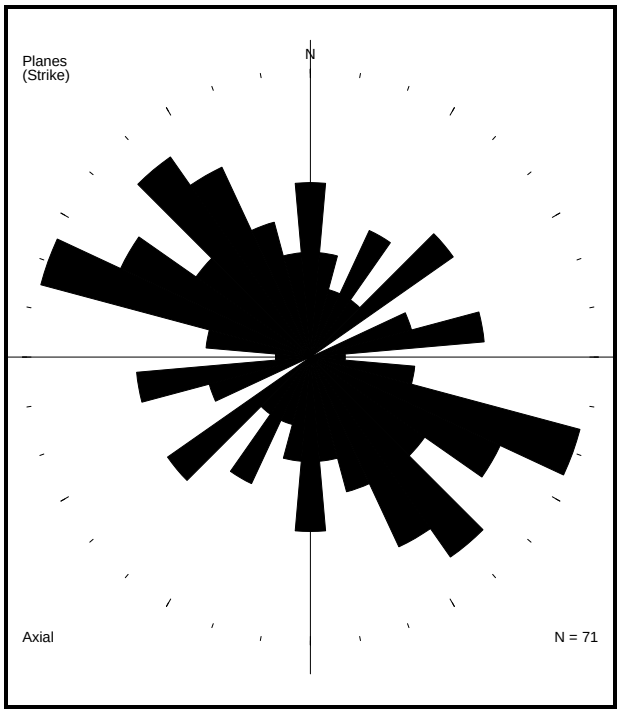

Figure 108: A summary of the joints' strike directions found in block S23° 30' E30° 30'. (Ten degree intervals centred around 0°)

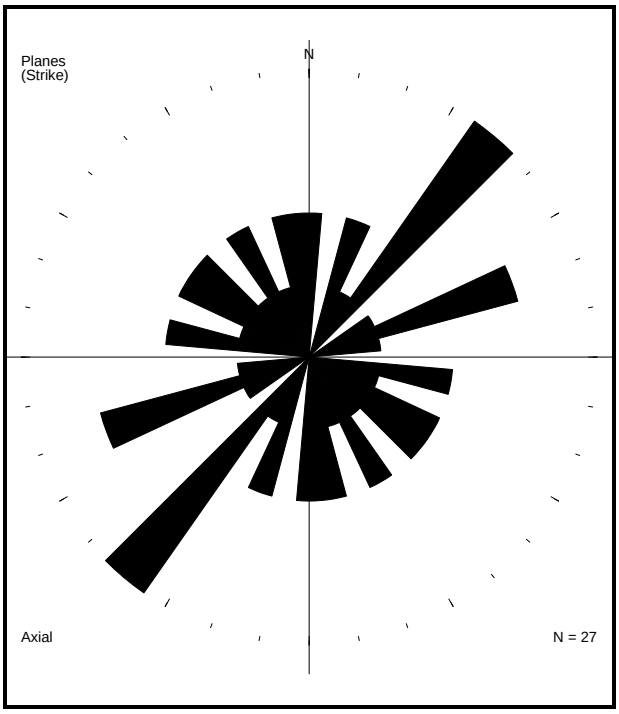

Figure 109: A summary of the joints' strike directions found in block S23° 40' E29° 00'. (Ten degree intervals centred around 0°)

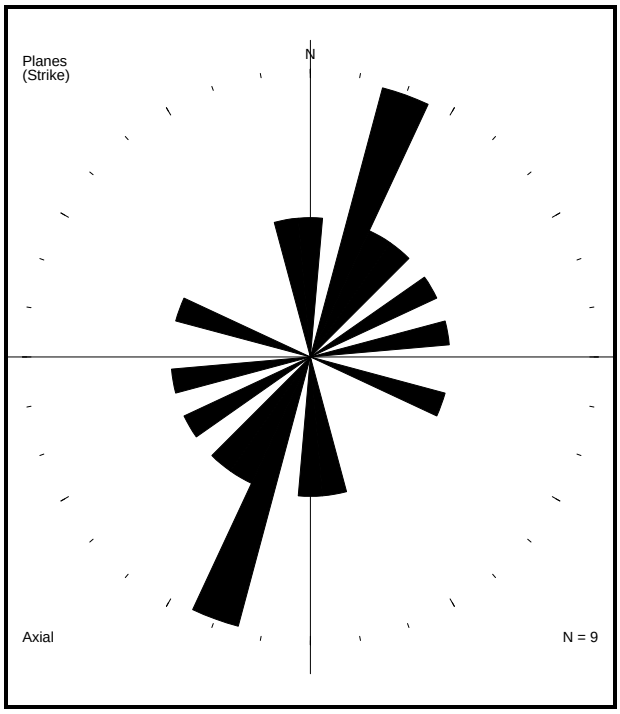

Figure 110: A summary of the joints' strike directions found in block S23° 40' E29° 10'. (Ten degree intervals centred around 0°)

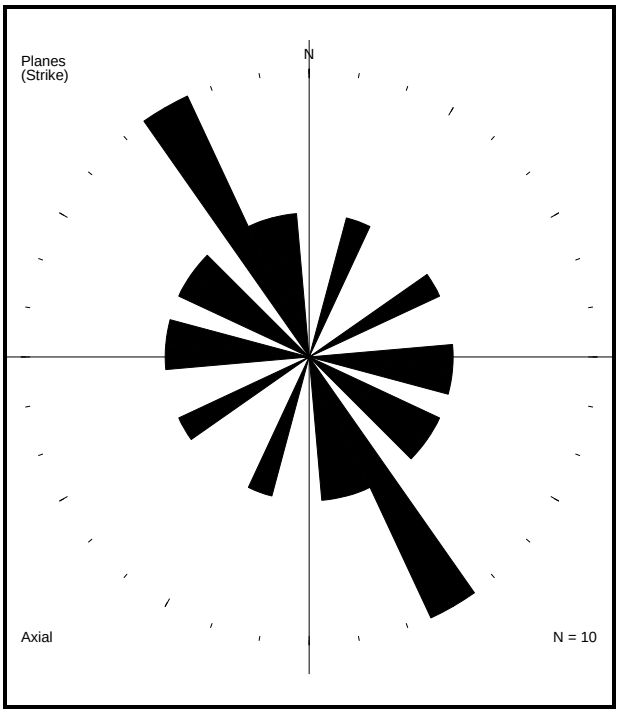

Figure 111: A summary of the joints' strike directions found in block S23° 40' E30° 00'. (Ten degree intervals centred around 0°)

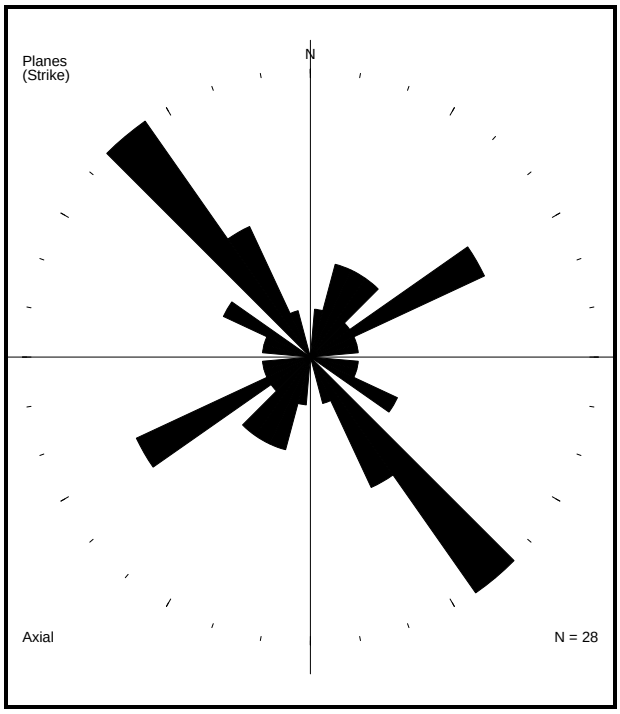

Figure 112: A summary of the joints' strike directions found in block S23° 40' E30° 10'. (Ten degree intervals centred around 0°)

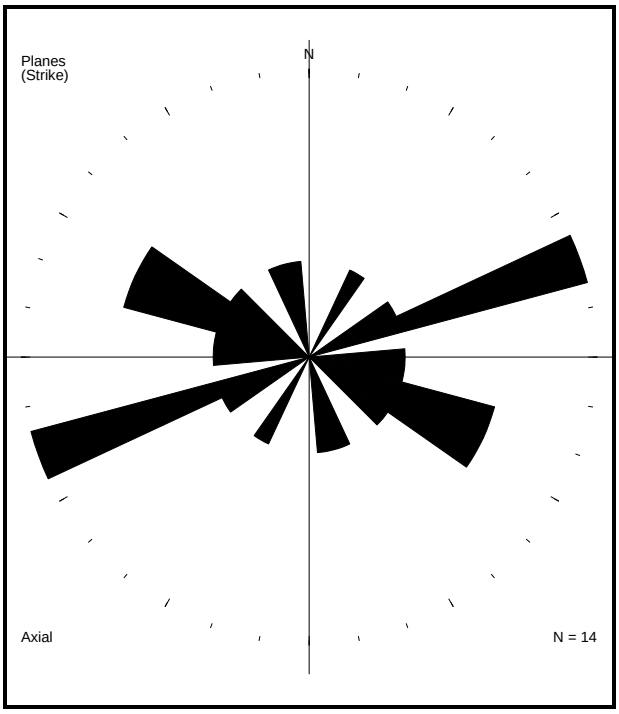

Figure 113: A summary of the joints' strike directions found in block S23° 50' E29° 00'. (Ten degree intervals centred around 0°)

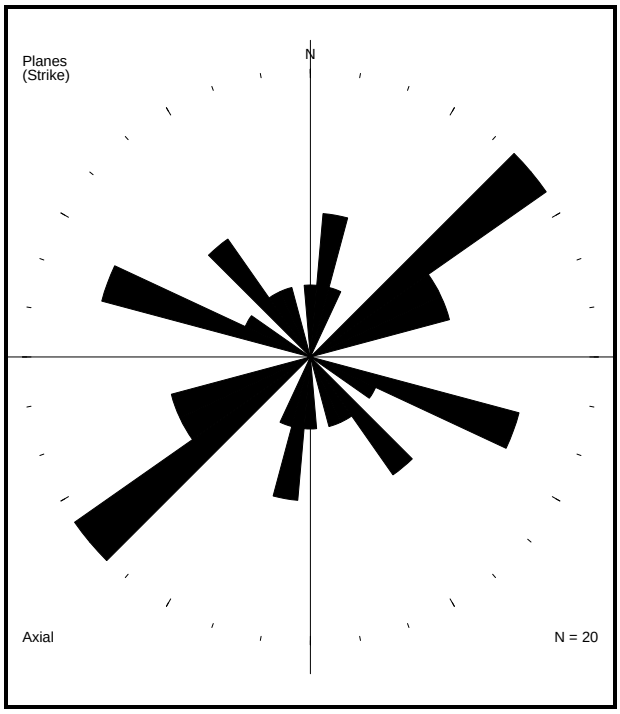

Figure 114: A summary of the joints' strike directions found in block S23° 50' E29° 10'. (Ten degree intervals centred around 0°)

iv. Density distribution intersection lineations of joints in each 10’ x 10’ block (refer to section 4.1):

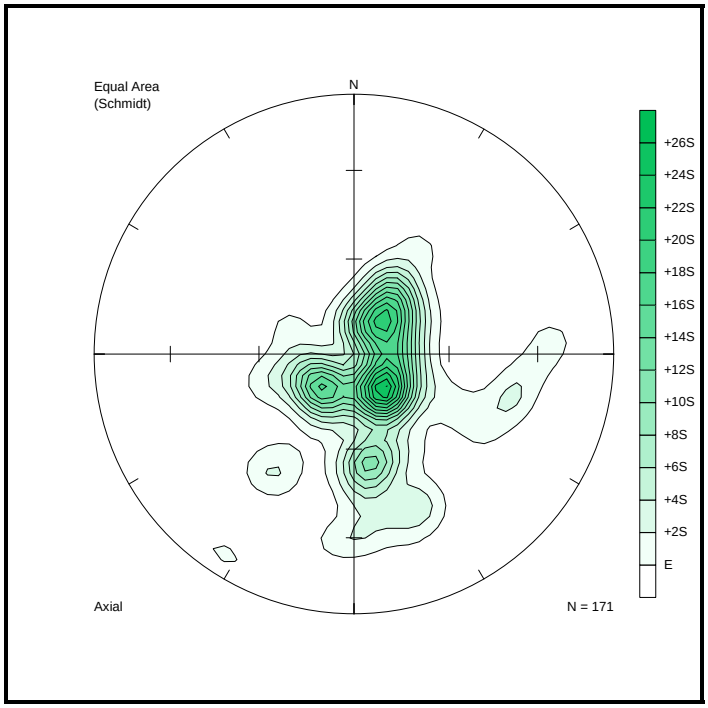

Figure 115: Density distribution of the lineations created by the intercepts of joints in block S22° 50’ E29° 50’.

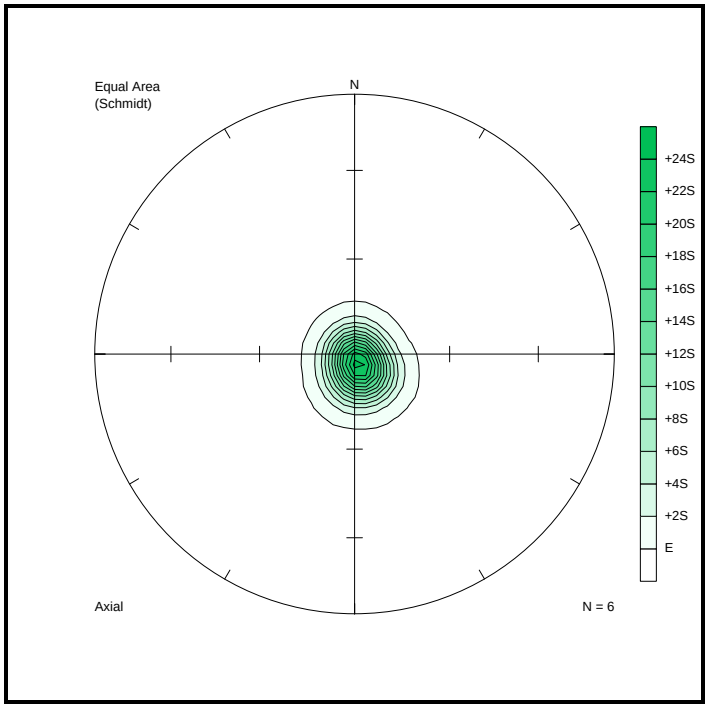

Figure 116: Density distribution of the lineations created by the intercepts of joints in block S23° 10’ E29° 30’.

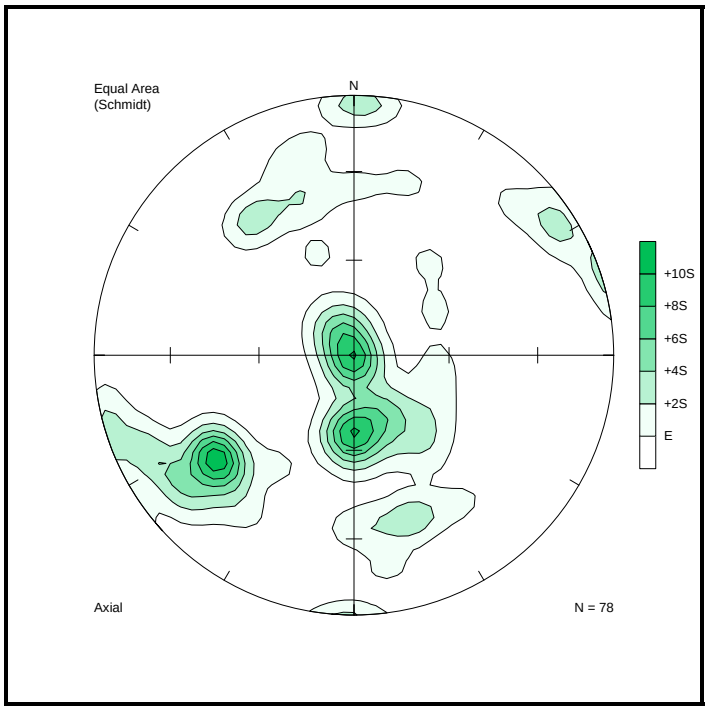

Figure 117: Density distribution of the lineations created by the intercepts of joints in block S23° 10’ E30° 00’.

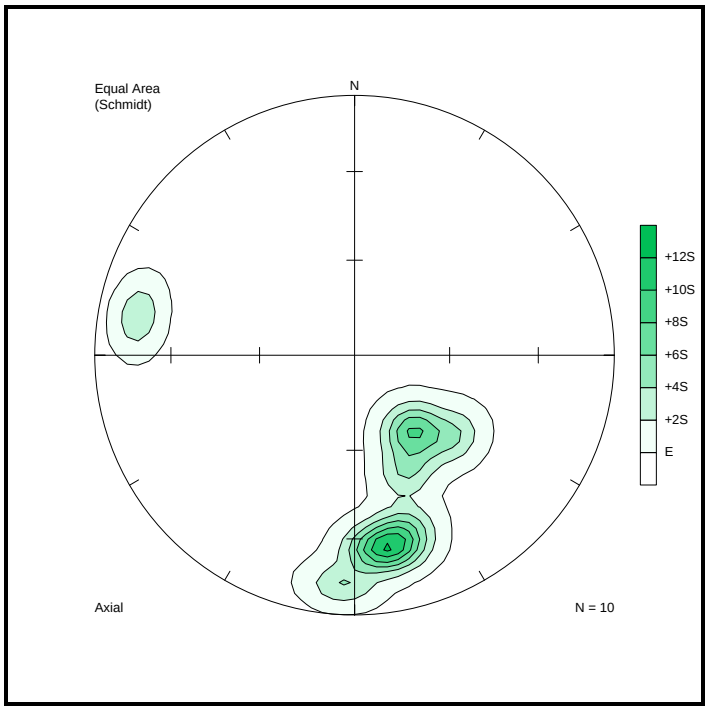

Figure 118: Density distribution of the lineations created by the intercepts of joints in block S23° 20’ E28° 50’.

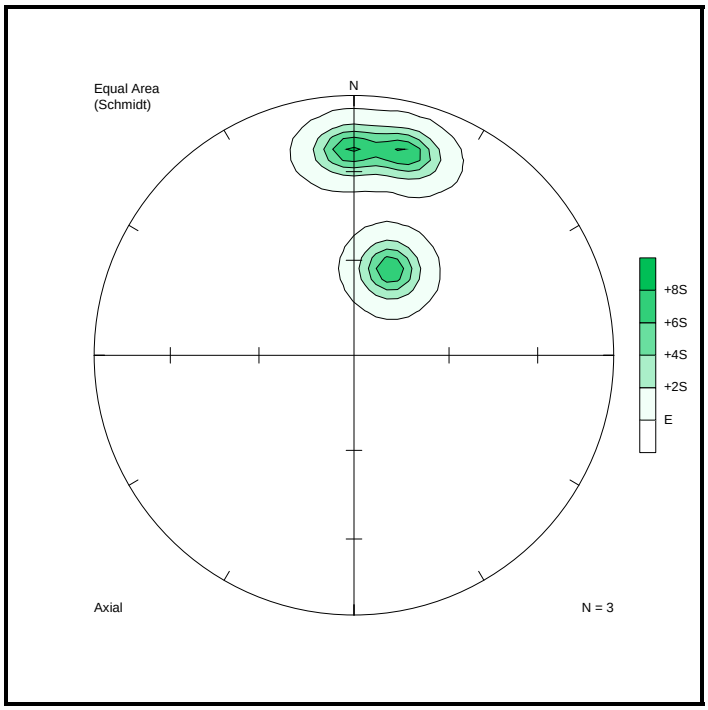

Figure 119: Density distribution of the lineations created by the intercepts of joints in block S23° 20' E29° 00'.

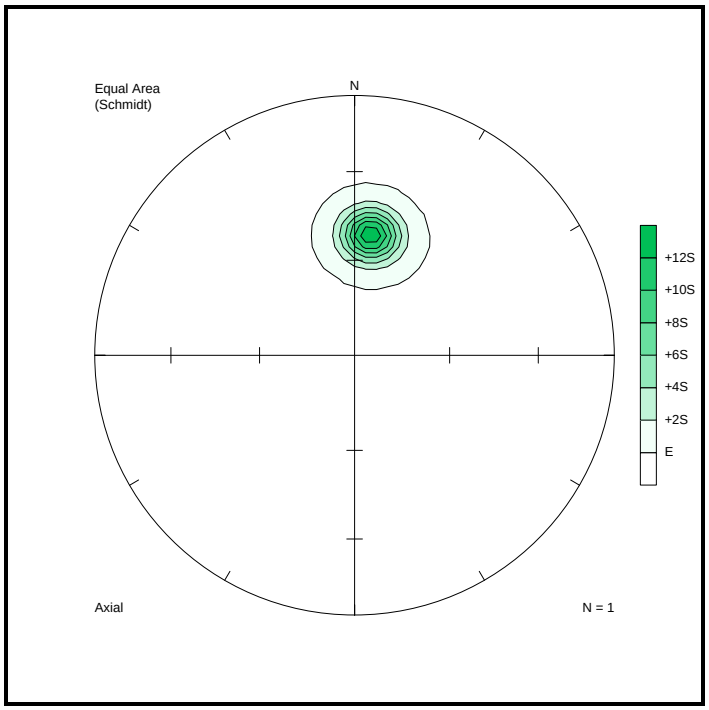

Figure 120: Density distribution of the lineations created by the intercepts of joints in block S23° 20' E29° 10'.

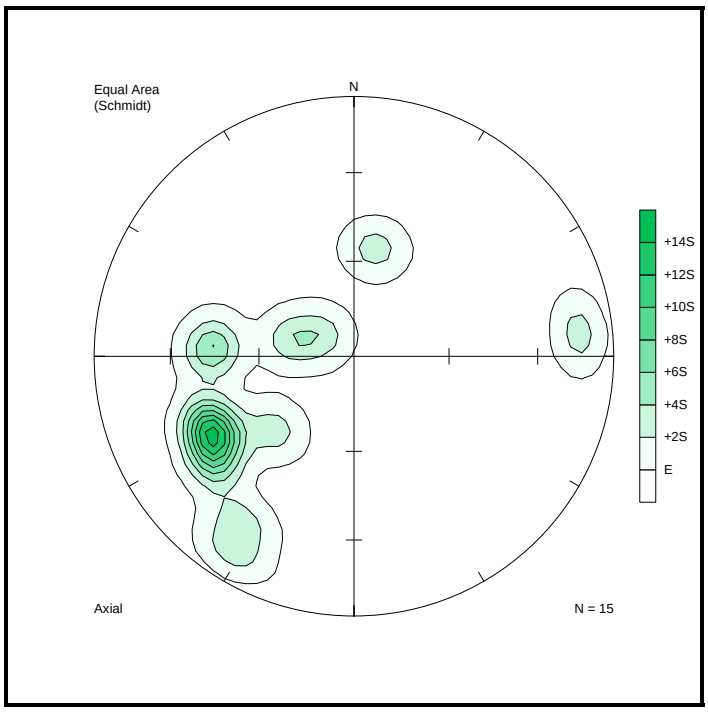

Figure 121: Density distribution of the lineations created by the intercepts of joints in block S23° 20' E29° 20'.

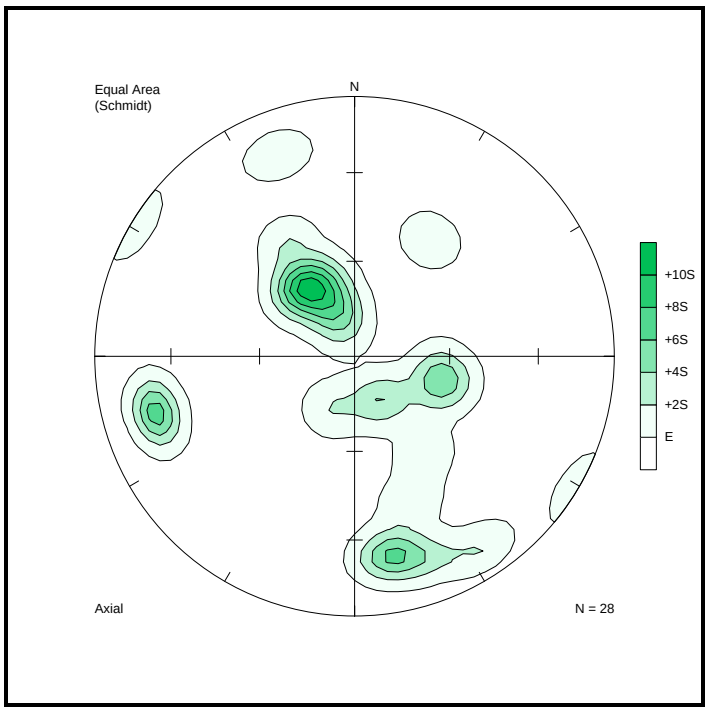

Figure 122: Density distribution of the lineations created by the intercepts of joints in block S23° 20' E29° 30'.

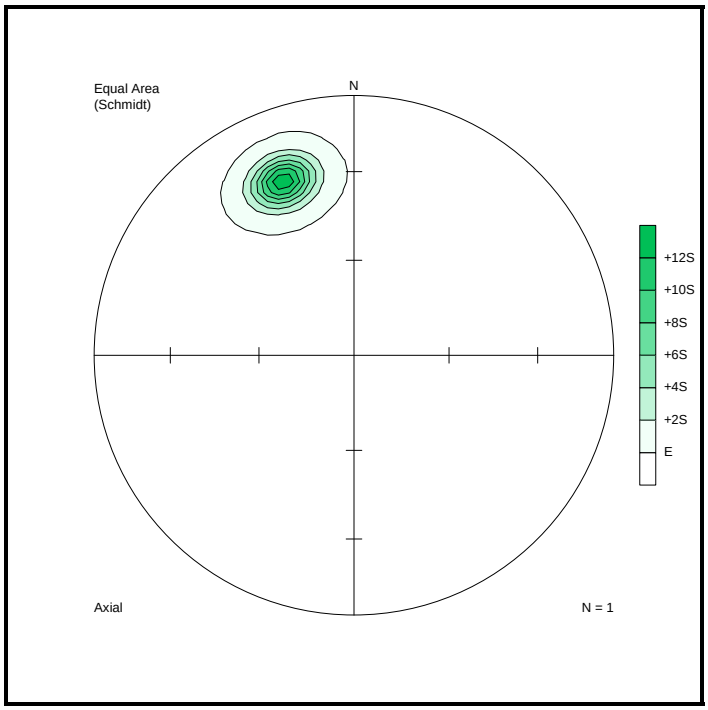

Figure 123: Density distribution of the lineations created by the intercepts of joints in block S23° 20' E29° 50'.

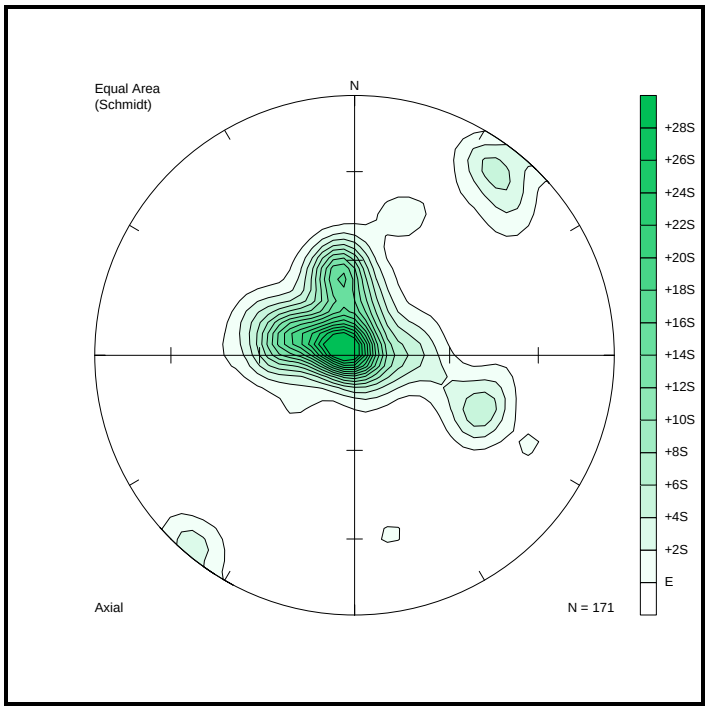

Figure 124: Density distribution of the lineations created by the intercepts of joints in block S23° 20' E30° 00'.

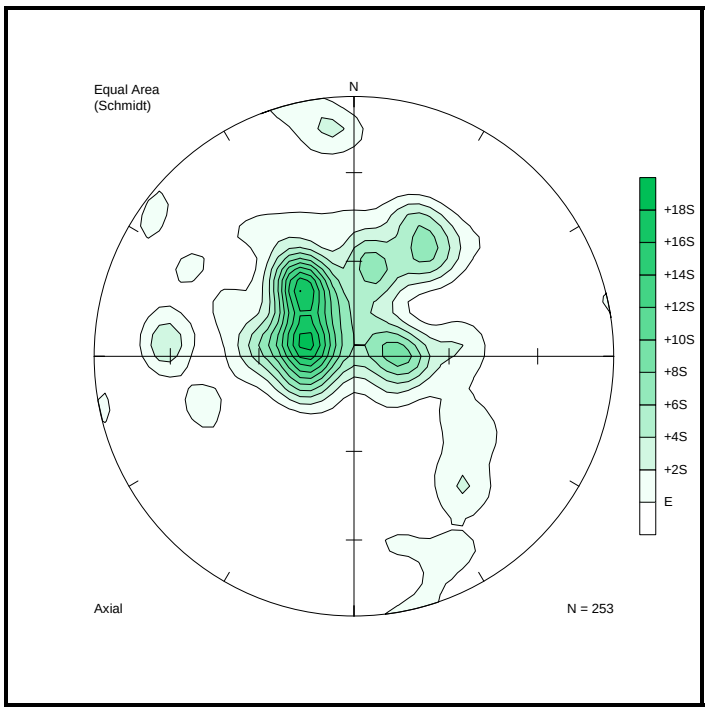

Figure 125: Density distribution of the lineations created by the intercepts of joints in block S23° 20' E30° 10'.

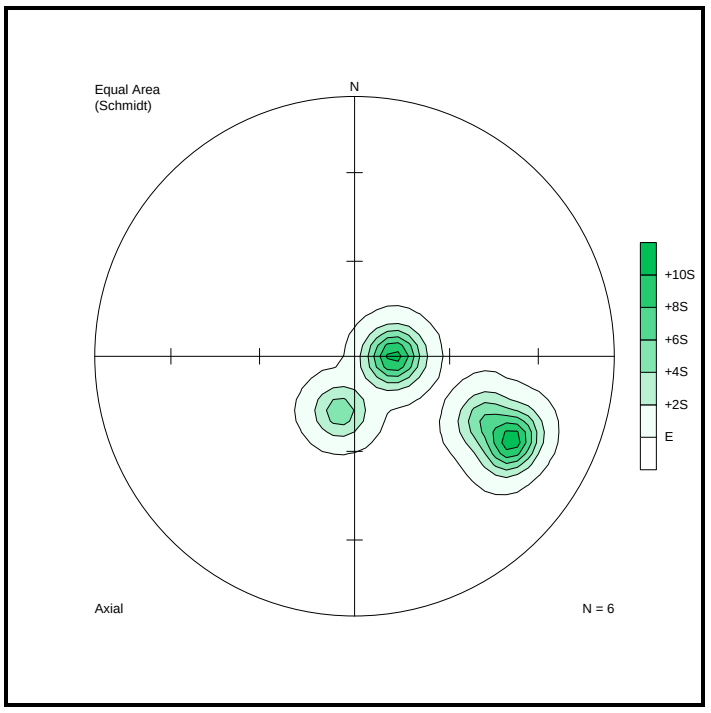

Figure 126: Density distribution of the lineations created by the intercepts of joints in block S23° 20' E30° 20'.

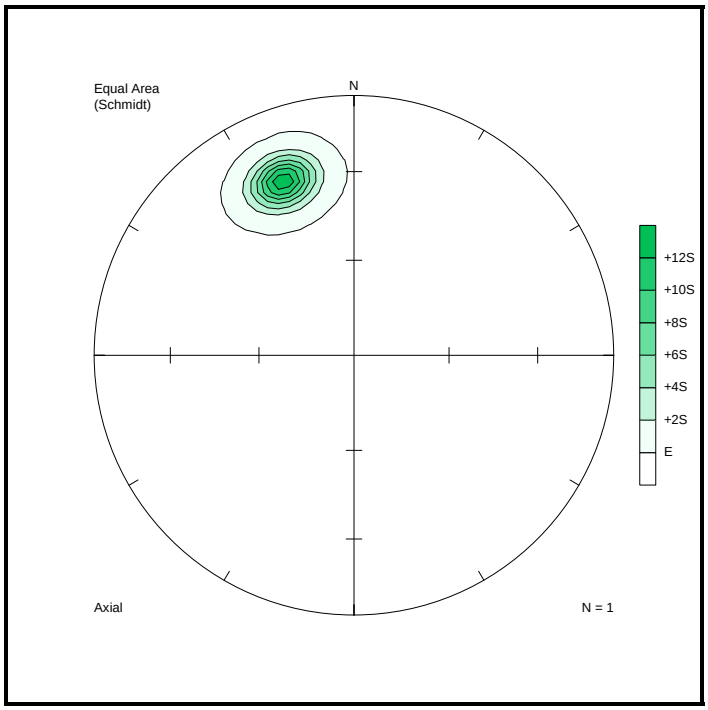

Figure 127: Density distribution of the lineations created by the intercepts of joints in block S23° 20' E30° 30'.

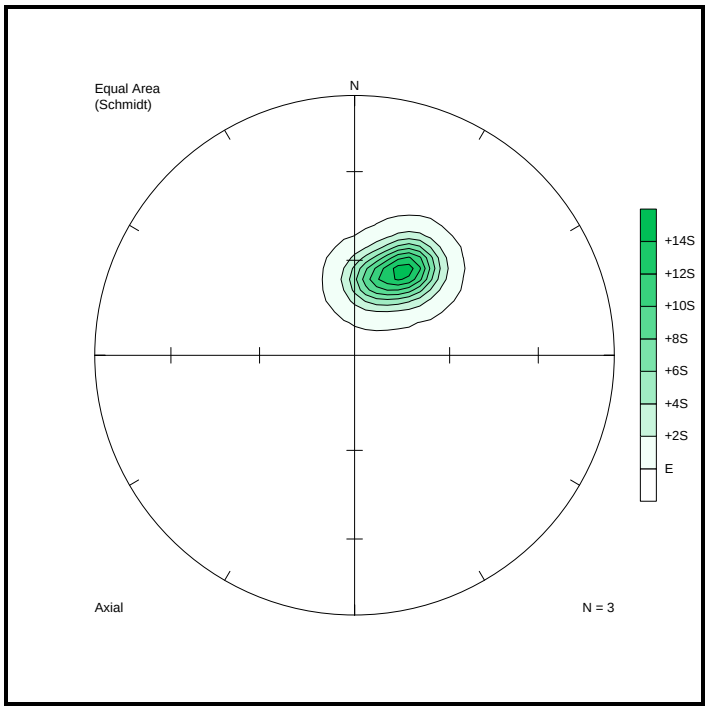

Figure 128: Density distribution of the lineations created by the intercepts of joints in block S23° 30' E28° 50'.

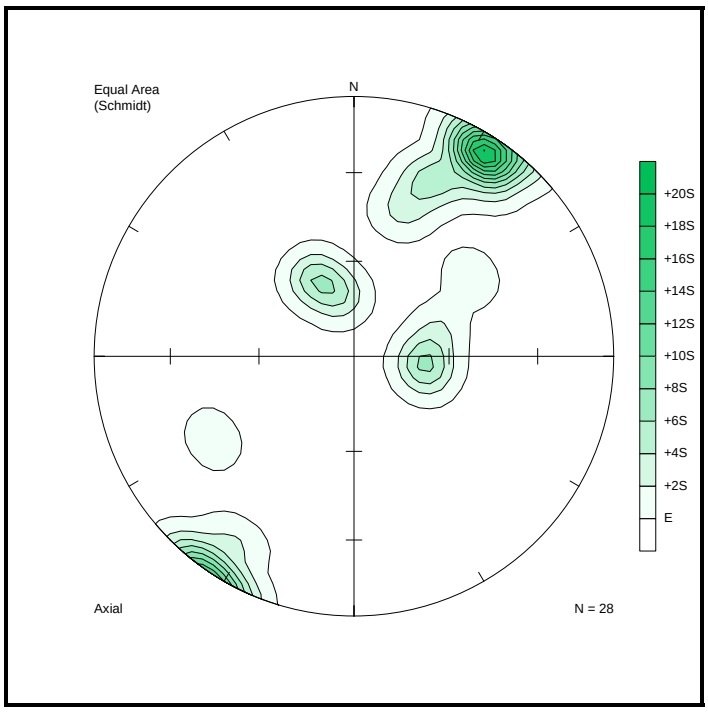

Figure 129: Density distribution of the lineations created by the intercepts of joints in block S23° 30' E29° 20'.

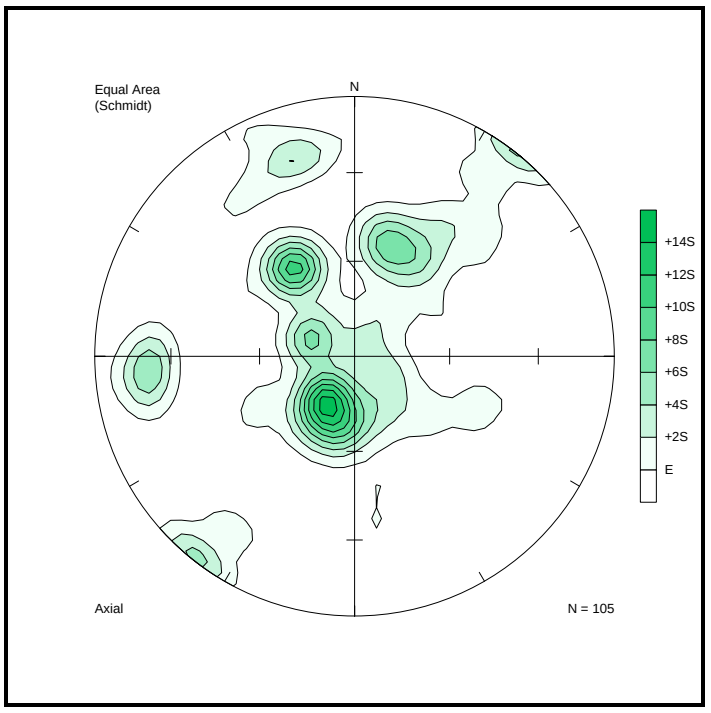

Figure 130: Density distribution of the lineations created by the intercepts of joints in block S23° 30' E29° 30'.

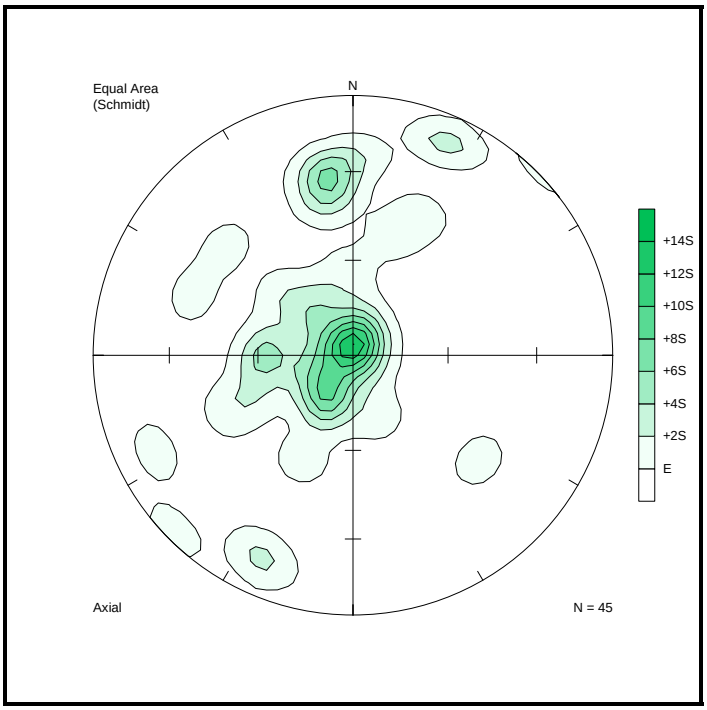

Figure 131: Density distribution of the lineations created by the intercepts of joints in block S23° 30' E29° 40'.

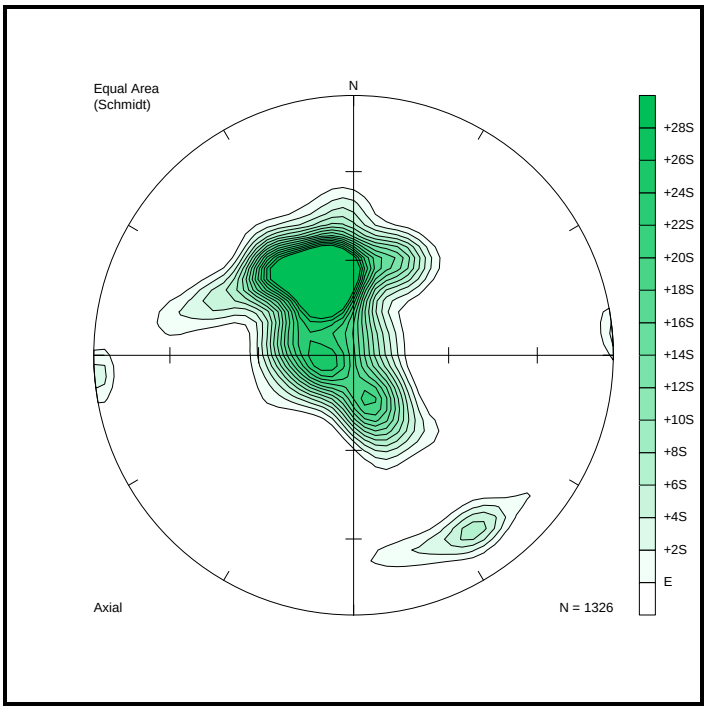

Figure 132: Density distribution of the lineations created by the intercepts of joints in block S23° 30' E29° 50'.

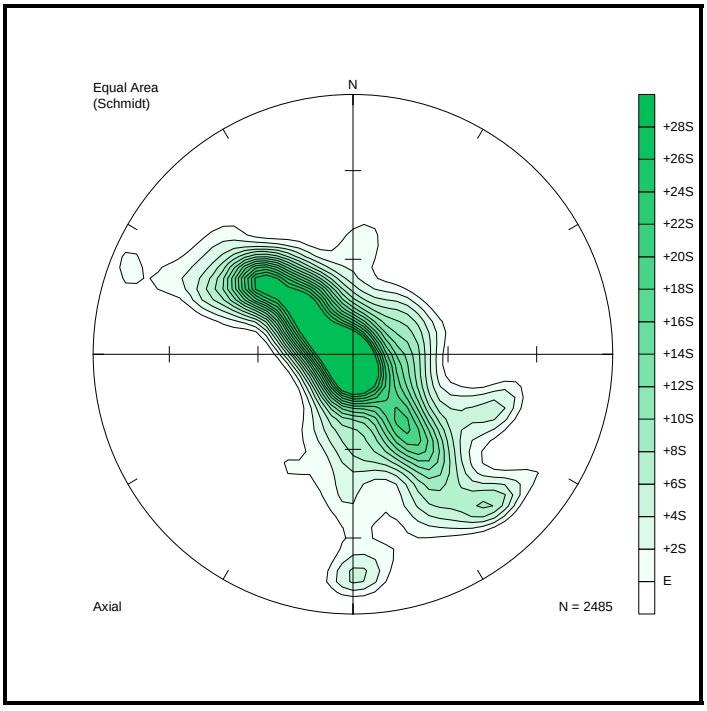

Figure 133: Density distribution of the lineations created by the intercepts of joints in block S23° 30' E30° 00'.

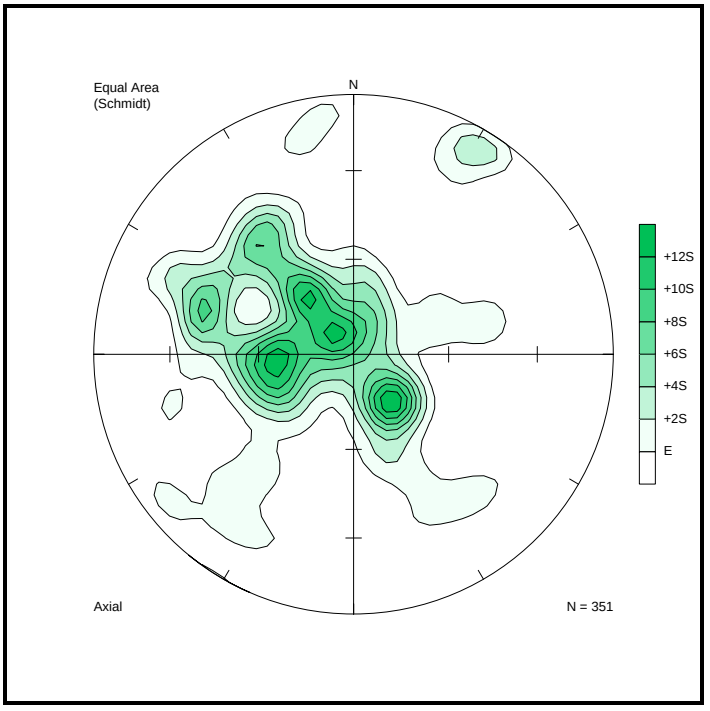

Figure 134: Density distribution of the lineations created by the intercepts of joints in block S23° 40' E29° 00'.

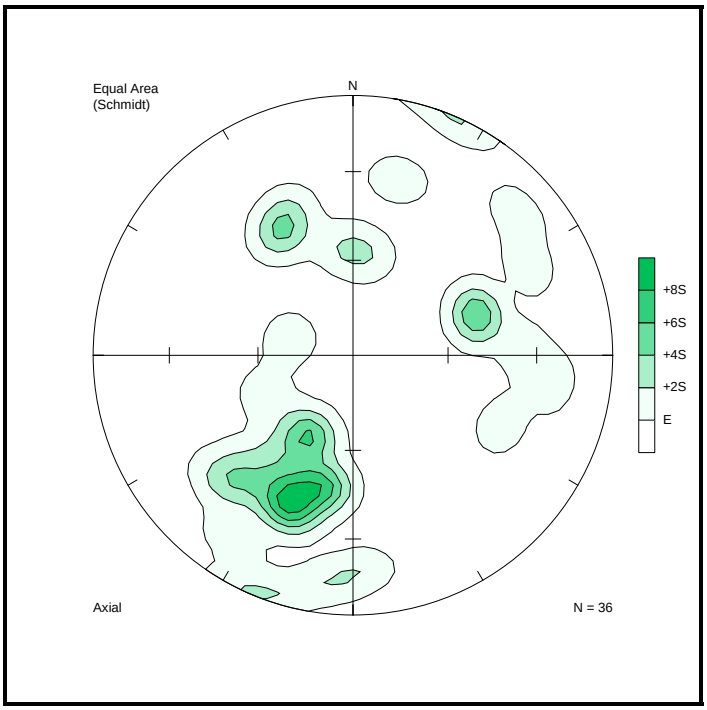

Figure 135: Density distribution of the lineations created by the intercepts of joints in block S23° 40' E29° 10'.

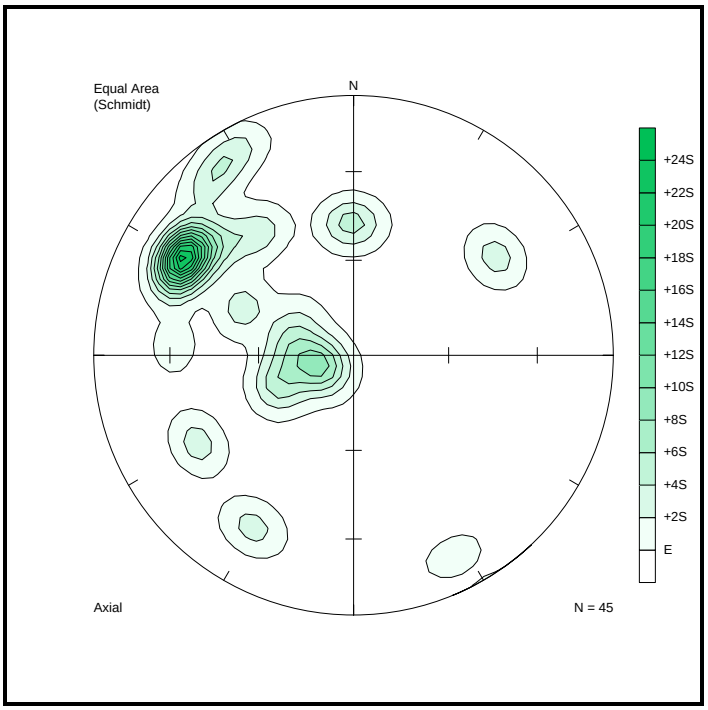

Figure 136: Density distribution of the lineations created by the intercepts of joints in block S23° 40' E30° 00'.

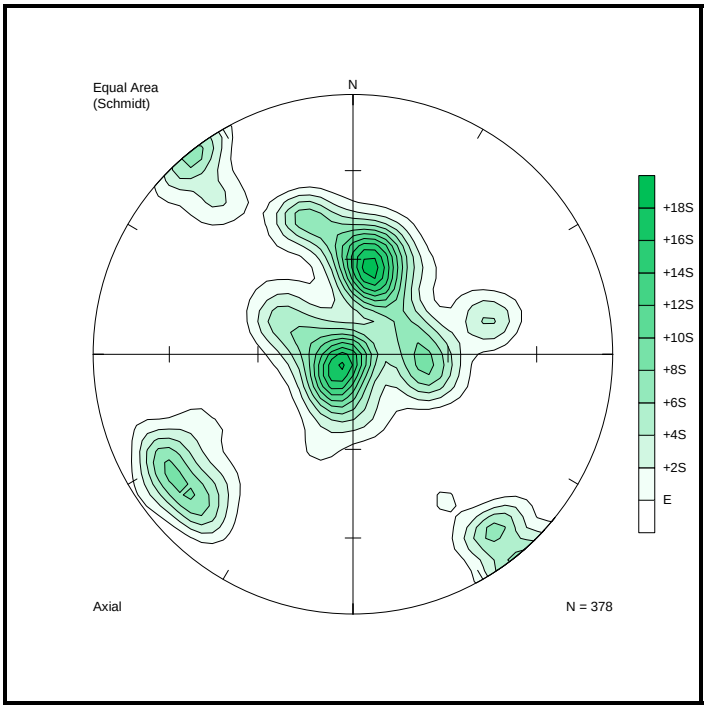

Figure 137: Density distribution of the lineations created by the intercepts of joints in block S23° 40' E30° 10'.

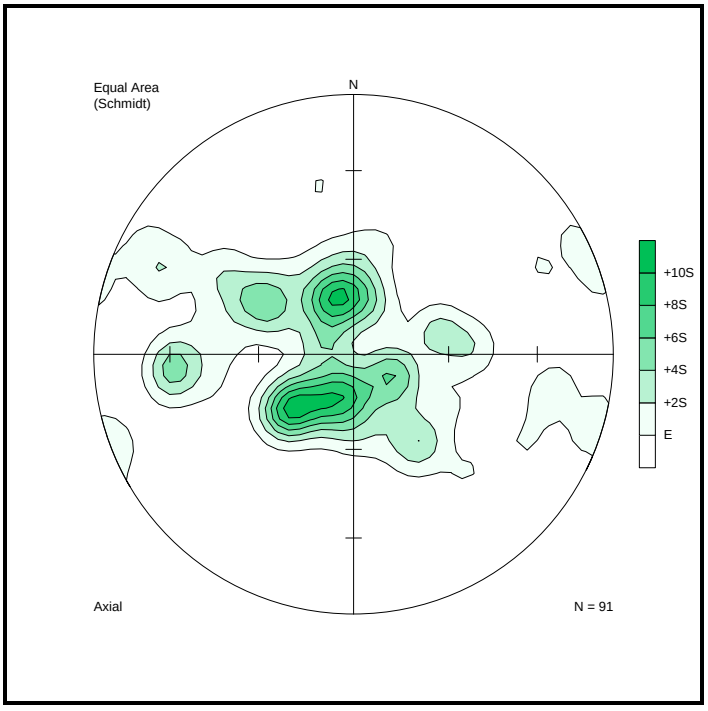

Figure 138: Density distribution of the lineations created by the intercepts of joints in block S23° 50' E29° 00'.

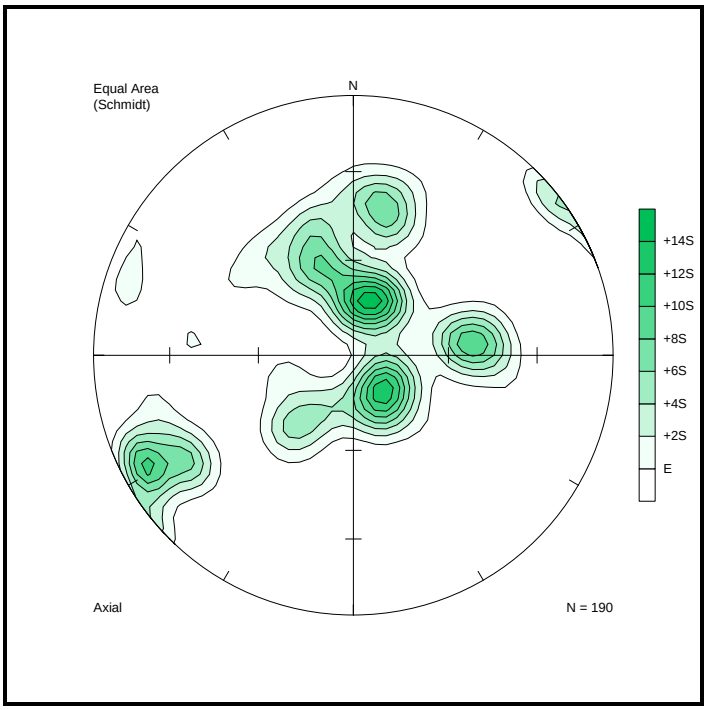

Figure 139: Density distribution of the lineations created by the intercepts of joints in block S23° 50' E29° 10'.

v. An explanation of inverse distance weighting from Wikipedia (Available from: http:/en.wikipedia.org/wiki/Inverse_distance_weighting):

Inverse distance weighting (IDW) is a method for multivariate interpolation, a process of assigning values to unknown points by using values from usually scattered set of known points.

A general form of finding an interpolated value u for a given point $\mathbf{x}$ using IDW is an interpolating function:

$$u(\mathbf{x}) = \frac{\sum_{k=0}^{N} w_k(\mathbf{x}) u_k}{\sum_{k=0}^{N} w_k(\mathbf{x})},$$

where:

$$w_k(\mathbf{x}) = \frac{1}{d(\mathbf{x}, \mathbf{x}_k)^p},$$

is a simple IDW weighting function, as defined by Shepard[1], $\mathbf{x}$ denotes an interpolated (arbitrary) point, $\mathbf{x}_k$ is an interpolating (known) point, d is a given distance (metric operator) from the known point $\mathbf{x}_k$ to the unknown point $\mathbf{x}$, N is the total number of known points used in interpolation and p is a positive real number, called the power parameter. Here weight decreases as distance increases from the interpolated points. Greater values of p assign greater influence to values closest to the interpolated point. For $0 < p < 1$ $u(\mathbf{x})$ has sharp peaks over the interpolated points $\mathbf{x}_k$, while for $p > 1$ the peaks are smooth. The most common value of p is 2.

The *Shepard's method* is a consequence of minimization of a functional related to a measure of deviations between tuples of interpolating points $\{\mathbf{x}, u\}$ and k tuples of interpolated points $\{\mathbf{x}_k, u_k\}$, defined as:

$$\phi(\mathbf{x}, u) = \left(\sum_{k=0}^{N} \frac{(u - u_k)^2}{d(\mathbf{x}, \mathbf{x}_k)^p} \right)^{\frac{1}{p}},$$

derived from the minimizing condition:

$$\frac{\partial \phi(\mathbf{x}, u)}{\partial u} = 0.$$

The method can easily be extended to higher dimensional space and it is in fact a generalization of Lagrange approximation into a multidimensional spaces. A modified version of the algorithm designed for trivariate interpolation was developed by Robert J. Renka and is available in Netlib as algorithm 661 in the Toms Library.